

DELFT UNIVERSITY OF TECHNOLOGY

LASER SWARM

MID TERM REVIEW

DESIGN SYNTHESIS EXERCISE

Authors:

S. BILLEMONT
L.S. BOERSMA
B. BUYENS
S.R. FINCK
J.P. FLORIJN
T.C. GOOSSENS
N.S. OBORIN
A.J. VOROBIEV
G.J. VAN DER WEL
Z. ZHOU

Tutor:

BEN GORTE

Coaches:

PREM SUNDARAMOORTHY
MATHIEU WILLAERT

May 18, 2010

Preface

The first month of this project has already passed, and this mid term report indicates an important milestone. We're not there yet, but we are getting on with it.

We did not, however, do everything by ourselves, and this is a good place to thank those who have been so kind as to give us some of their precious time.

First I want to mention professor Edoardo Charbon, who kindly explained and showed to us the workings of his Single Photon Avalanche Diode (SPAD)¹: without his help we would be hopelessly in the dark on these fascinating devices. From this place I also want to thank professor Kourosh Khoshelham for helping us to some valuable material on remote sensing. I also want to thank Jasper Bouwmeester, who provided us with some helpful information on solar panel pricing.

And finally I thank our tutor, professor Ben Gorte, who was very generous to us with his time and has been very supportive of the entire project.

I hope you will have as much fun reading this report, as we had in making it!

Yours sincerely,

Co Florijn,
Chairman

¹See [Niclass(2008), 98-105], [M. Gersbach and Charbon(2009)] and [David Stoppa and Charbon(2009)]

Contents

Preface	i
Contents	ii
List of Figures	viii
List of Tables	xii
List of Acronyms	xiii
1 Introduction	1
2 Technical Design Development	2
2.1 Project Approach Description	2
2.1.1 Group Procedures	2
2.1.2 Reporting	2
2.1.3 Project Outline	3
2.2 Work Flow Diagram	3
2.3 Work Breakdown Structure	3
2.4 Gantt chart	8
3 Risk Management	9
3.1 Market Analysis	9
3.2 Technical Resource Contingencies	9
3.3 Technical Risk Assessment	12
3.3.1 Ground Segment	12

3.3.2	During Mission	13
3.3.3	Measurement Protocol	16
3.3.4	Post-Mission	18
3.3.5	Risk Control	18
4	Design Options	20
4.1	Attitude Determination and Control Subsystem	20
4.1.1	Attitude Determination	20
4.1.2	Attitude Control	20
4.1.3	Note on Receiver Pointing	21
4.2	Communications	21
4.2.1	Tracking	21
4.2.2	Swarm Satellites Crosslink Frequency	21
4.2.3	D/L and U/L Frequency	21
4.2.4	Antenna Configuration	22
4.2.5	Data Storage	22
4.2.6	Communications Architecture	22
4.3	Electrical Power System	22
4.4	Orbit Architecture	23
4.5	Optical Emitting Payload	24
4.5.1	Introduction	24
4.5.2	Laser Types	24
4.6	Optical Receiving Payload	24
4.6.1	Introduction	24
4.6.2	Types of Optical Receiving Devices	25
4.6.3	Important Parameters for Optical Receiving Devices	25
5	N^2 Chart	26
6	Tradeoff	28
6.1	Attitude and Orbit Determination and Control Subsystem	28

6.1.1	Pruning the Attitude Determination and Control Subsystem design option tree	28
6.1.2	Attitude Determination Subsystem	28
6.1.2.1	Trade method	30
6.1.2.2	Trade criteria	30
6.1.2.3	Weight factors	30
6.1.2.4	Trade-off	31
6.1.3	Attitude Control Subsystem	31
6.1.3.1	Trade method	32
6.1.3.2	Trade criteria	32
6.1.3.3	Weight factors	32
6.1.3.4	Trade-off	33
6.1.4	Orbit Determination Subsystem	33
6.1.5	Orbit Control Subsystem	33
6.2	Communications	34
6.2.1	Trade off communication architecture	34
6.2.2	Trade off D/L and U/L frequency	35
6.2.3	Trade off crosslink frequency	35
6.2.4	Trade off antenna configuration	35
6.2.5	Trade off tracking method	35
6.3	Trade-off for the Electrical Power System	36
6.3.1	Pruning of the EPS design option structure	36
6.3.1.1	Power Source	36
6.3.1.2	Power Storage	36
6.3.1.3	Power Distribution, Regulation and Control	36
6.3.2	Trade method rationale and organization	38
6.3.2.1	Multijunction solar cells	40
6.3.2.2	Thin film solar cells	42
6.3.2.3	Trade off method and rationale	43
6.3.3	Trade-off summary	43
6.4	Orbit Analysis	45

6.4.1	Eliminating the obvious losers	45
6.4.2	Analysis of the remaining options	45
6.4.2.1	Polar orbit	45
6.4.2.2	Sun Synchronous orbit	45
6.4.2.3	Repeating ground track orbit	46
6.4.2.4	Frozen orbit	46
6.4.3	Preliminary Orbit Parameters	46
6.5	Orbit Altitude	47
6.5.1	Earth Oblateness	47
6.5.2	Perturbations due to other Celestial bodies	48
6.5.3	Solar Radiation Pressure	48
6.5.4	Atmospheric Drag	48
6.5.5	Exposure to Particle Radiation	50
6.5.6	Final Orbit Parameters	51
6.6	Satellite Formation Design	64
6.6.1	Orbital Parameters	64
6.6.2	Stationkeeping	67
6.6.3	Collision Avoidance	70
6.7	Optical Sensing	73
6.7.1	Introduction	73
6.7.2	Atmospheric and Oceanic Effect	73
6.7.2.1	Atmospheric Transmission	73
6.7.2.2	Ocean scattering	75
6.7.3	Optical Receiver Device	75
6.7.3.1	General Introduction to Photon Detection	76
6.7.3.2	Wavelength estimation	76
6.7.3.3	Receiver Prune	78
6.7.3.4	Trade Method	79
6.7.3.5	Trade Criteria	80
6.7.3.6	Weight Factor	80

6.7.3.7	Trade summary	80
6.7.4	Optical Emitting Payload	80
6.7.4.1	Optical Transition	81
6.7.4.2	Exciton Dynamics	81
6.7.4.3	Laser Geometry	82
6.7.4.4	Efficiency	82
6.7.4.5	Pulsed vs Continuous Waves	82
6.7.4.6	Blue Laser Types	83
6.7.4.7	Trade-off Criteria	83
6.7.4.8	Trade-off Summary	85
6.7.5	Laser Thermal Control	85
6.7.5.1	Thermal Physics	85
6.7.5.2	Theoretical Thermal Limits For Lasers	86
6.7.5.3	Thermal Control	87
6.8	Receiver Pointing	87
6.8.1	Trade Method	87
6.8.2	Trade Criteria	87
6.8.3	Weight Factors	87
6.8.4	Trade-off	88
6.9	Final Preliminary Design	89
7	Operations and Logistics	95
8	Stability & Control	97
8.1	Stability	97
8.2	Control	98
9	Sustainable Development Strategy	100
9.1	Production and Logistics	100
9.2	Operations	100
9.3	End of Life	101

10 Simulation	102
10.1 Simulation	102
10.1.1 Orbit	102
10.1.2 Earth Model	103
10.1.2.1 Digital Elevation Model	103
10.1.2.2 Scattering Model	103
10.1.3 Signal Path	104
10.1.4 Noise	105
10.2 Data Analysis	106
10.2.1 Altitude Determination	106
10.2.2 Bidirectional Reflection Density Function Determination	106
10.3 Simulations	107
10.3.1 Variation of Photon Density with Altitude	107
10.3.2 Solar Photons Fraction	108
A Design Option Diagrams	111
B Subsystem Budget Overview	123
C Gantt Chart	125

List of Figures

2.1	Updated work flow diagram for the mid-term report	4
2.2	Updated work flow diagram for the final report	5
2.3	Updated work break-down structure for the mid-term report	6
2.4	Updated work break-down structure for the final report	7
3.1	Market Breakdown Diagram with different data sets [Mar(2008)]	10
3.2	Relative reliability of passive ADCS subsystems.	14
3.3	Relative reliability of active ADCS subsystems.	15
3.4	Technical Risk Map	19
5.1	N^2 chart of the Laser Swarm mission	27
6.1	Pruned design option tree for the ADCS	29
6.2	ADS design concepts	30
6.3	ADS design concepts	32
6.4	The pruned design option tree for the power source	37
6.5	The pruned design option tree for the power storage	38
6.6	The design option tree for the power distribution and regulation and control	39
6.7	Schematic representation of a triple-junction solar cell	41
6.8	Spectral irradiance of a triple-junction solar cell in function of the wavelength	41
6.9	Schematic layout of a thinfilm CIGS solar cell	42
6.10	Pruned design option tree for the orbit characteristics	52
6.11	$d\omega/dt$ for a range of altitudes and several different inclinations.	52
6.12	Acceleration due to solar radiation pressure vs. area normal to the sun, for different satellite masses.	53

6.13 Acceleration due to solar radiation pressure vs. mass, for different areas.	53
6.14 Acceleration due to solar radiation pressure vs. Area/Mass ratio.	54
6.15 The solar cycle, clearly showing the solar maxima at 11 year intervals. Data after 2007 is projected. <i>Source: NASA</i>	54
6.16 Air density vs. orbit altitude for different solar cycle stages.	55
6.17 Orbit decay for a satellite with $C_D = 4$, $A = 2.5 \text{ m}^2$ and $m = 119 \text{ kg}$. Estimates for initial orbital altitudes of 300, 400 and 500 km at solar maximum (- -), solar minimum (-) and time average (- - -).	56
6.18 Orbit decay for a satellite with $C_D = 4$, $A = 0.2 \text{ m}^2$ and $m = 10.7 \text{ kg}$. Estimates for initial orbital altitudes of 300, 400 and 500 km at solar maximum (- -), solar minimum (-) and time average (- - -).	57
6.19 Total ΔV for a satellite with $C_D = 4$, $A = 2.5 \text{ m}^2$ and $m = 119 \text{ kg}$. Estimates for a range of orbit altitudes and different solar cycle stages.	58
6.20 Total ΔV for a satellite with $C_D = 4$, $A = 0.2 \text{ m}^2$ and $m = 10.7 \text{ kg}$. Estimates for a range of orbit altitudes and different solar cycle stages.	59
6.21 AP-8 Proton Flux Model (energy $> 100 \text{ MeV}$) at solar maximum (a) and solar minimum (b) as a function of distance in mean Earth radii.	60
6.22 AE-8 Electron Flux Model (energy $> 0.5 \text{ MeV}$) at solar maximum (a) and solar minimum (b) as a function of distance in mean Earth radii.	61
6.23 3D view of the base orbit.	62
6.24 Ground track of the base orbit.	63
6.25 The relative motion of co-altitude satellites in circular orbits. Relative inclination and relative phase are shown. <i>Source: [et al.(2001)]</i>	65
6.26 Intersection of two orbits with the same inclination. <i>Source: [et al.(2001)]</i>	65
6.27 Geometry of angular separation. <i>Source: [et al.(2001)]</i>	66
6.28 i_R and ϕ_R vs. equatorial angular separation. Orbit inclination of 85°	67
6.29 Minimum and maximum angular separation vs. equatorial angular separation. Orbit inclination of 85°	68
6.30 Orbit separation geometry.	68
6.31 Debris field evolution, (a) immediately after impact, (b) spreading out after some time and eventually settling into the orbit (c) and decaying. <i>Source: [et al.(2001)]</i>	71
6.32 A schematic summary illustrating how absorption by various constituents in the atmosphere influences the propagation of light and divides the spectrum into distinct bands.	74
6.33 Atmospheric Absorption Bands	74

6.34 Light penetration ocean depth with different wavelength	75
6.35 Classification of state-of-the-art optical Time Of Flying (TOF) image sensors.	77
6.36 SPAD cross-section diagram.	77
6.37 SPAD photon detection probability as a function of wavelength for two values of excess bias voltage	78
6.38 MPD photon detection probability as a function of wavelength	78
6.39 Ratio of atmospheric transmittance versus photon detection efficiency	79
6.40 The pruned design option tree for the Laser receivers	90
6.41 The diagram of the parabolic mirror	91
6.42 The diagram receiver assembly micro lenses	91
6.43 The diagram receiver assembly faceted mirror	92
6.44 Left: individual energy quantum energy levels occupied with individual wave equation. Optical transitions given in random electron orbit; emission and absorption could take place at any energy level. Right: Einstein coefficients for optical transmission. 'J' represents the photon density in \mathbf{k} -space. Spontaneous emission is independent on photon density.	92
6.45 General layout of a laser. laser cavity with fully reflecting mirror (left) and partially reflected mirror (right). Under the stimulation of population inversion lasing action occurs due to optical reflection.	93
6.46 Three possible laser level system. Left: Three-level system. Middle and right: Four-level system with equal pump power level. The difference is the bandgap between energy level one and two. Hence, the efficiency of the four-level system in the middle is higher, since the effective lasing action energy quantity is higher with equal pump power	93
6.47 Refractive index as function of radial position, where the Sellmeier coefficients A, B, C, D, E, and F are constants dependent on gain material, c and b are temperature dependent, T is the temperature in degrees centigrade, and l is the wavelength in micrometers.	93
6.48 Transverse pump intensity distribution (red) and thermal profile (blue). The temperature profile is approximately parabolic only near the center of the crystal.	94
6.49 Design options for the pointing mechanism	94
7.1 Hierarchy of the operations for the laser swarm mission.	96
10.1 Example of a Bidirectional Reflection Density Function (BRDF)	104
10.2 Signal path representation	105

10.3 Height variation effect in the # received photons	108
A.1 Design option tree for the Attitude Determination and Control Subsystem (ADCS) .	112
A.2 Design option tree for the communication systems	113
A.3 Design option tree for the power source	114
A.4 Design option tree for the power storage	115
A.5 Definitions of the inclination i , the right ascension of the ascending node Ω , the argument of perigee ω and the true anomaly ν . <i>source: http://reentrynews.aero.org</i> .	116
A.6 Design option tree for the orbit architecture of LEO and MEO	117
A.7 Design option tree for the orbit architecture of Geosynchronous Earth Orbit (GEO)	117
A.8 Design option tree for the orbit architecture of High Earth Orbit (HEO)	118
A.9 Design option tree for the distribution and regulation and control of the Electrical Power System (EPS)	119
A.10 Design option tree of laser emitter. Numbers indicate typical values.	120
A.11 Photomultiplier tube configuration and working mechanism	121
A.12 Single photon detection using quantum dot configuration	121
A.13 Design option tree for laser receiver. Numbers represent typical values.	122

List of Tables

3.1	The mass contingency allowance	11
3.2	The power contingency allowance	11
6.1	Trade-off attitude determination	31
6.2	Trade-off attitude control	33
6.3	Trade-off table for the power source	44
6.4	Mass and area estimates	48
6.5	Required ΔV for various orbit altitudes for a 5 year mission. In m/s	50
6.6	Parameters of the base orbit for the emitter satellite.	51
6.7	Height and width of the relative motion analemma for two co-altitude satellites in a 500 km orbit with an inclination of 85 degrees.	67
6.8	Recommended methods of handling the principle perturbations in LEO. Source: [et al.(2001)]	69
6.9	Inter-satellite collision estimations for a formation of 5 and 9 satellites. Probability values based on extrapolation of values given in [et al.(2001)].	72
6.10	Receiver tradeoff table.	81
6.11	Emitter tradeoff table.	84
6.12	Trade-off pointing mechanism	88
10.1	Simulation results for varying altitude	107

List of Acronyms

ACS	Attitude Control Subsystem
ADCS	Attitude Determination and Control Subsystem
ADS	Attitude Determination Subsystem
AOCS	Attitude and Orbit Control Subsystem
AODCS	Attitude and Orbit Determination and Control Subsystem
ASTER	Advanced Spaceborne Thermal Emission and Reflection Radiometer
BRDF	Bidirectional Reflection Density Function
CCD	Charge-Coupled Device
CIGS	Copper Indium Gallium Selenide
CMG	Control Moment Gyro
CMOS	Complementary Metal Oxide Semiconductor
COTS	Commercial Of The Shelf
DEM	Digital Elevation Model
ECEF	Earth-Centered, Earth-Fixed
EOL	End-of-Life
EPS	Electrical Power System
FOV	Field Of View
GDEM	Global Digital Elevation Model
GEO	Geosynchronous Earth Orbit
GLAS	Geoscience Laser Altimeter System
GPS	Global Positioning System
GSO	Geostationary Orbit
HEIO	Highly Elliptical Orbit
HEO	High Earth Orbit
IAQC	Integrated Active Quenching Circuits
IR	Infra Red
ISIS	Innovative Solutions In Space
JAT	Java Astrodynamics Toolkit
laser	Light Amplification by Stimulated Emission of Radiation
LEO	Low Earth Orbit
LiDAR	Light Detection And Ranging
LWIR	Long Wave Infrared
MANS	Microcosm Autonomous Navigation System
MEO	Medium Earth Orbit

MPD	Micro Photon Device
MTR	Mid Term Review
MWIR	Mid Wave Infrared
NIR	Near Infrared
OED	Optical Emitting Device
OFOV	Optical Field of View
OCS	Orbit Control Subsystem
ODS	Orbit Determination Subsystem
ORD	Optical Receiving Device
OEP	Optical Emitting Payload
ORP	Optical Receiving Payload
ROIC	Read-Out Integrated Circuit
SILAT	Stereo Imaging Laser Altimeter
SPAD	Single Photon Avalanche Diode
SWIR	Short Wave Near Infrared
TDRS	Tracking and Data Relay Satellite
TOD	True Of Date
TOF	Time Of Flying
TRL	Technology Readiness Level
WBS	Work Breakdown Structure
UV	Ultra Violet
WFD	Work Flow Diagram
WGS84	World Geodetic System 1984

Abstract

In February 2010 the ICESat mission ended after 7 years of measuring ice sheet mass balance, cloud and aerosol heights, as well as land topography and vegetation characteristics using a space based Light Detection And Ranging (LiDAR) system. ICESat used only one of the possible approaches for LiDAR, namely the use of a high energy laser and a large receiver telescope. The other approach is using a high frequency, low energy laser and a single photon detector. The advantage of the latter approach is that it has a much lower mass, but it is uncertain if even a single photon per pulse reaches the receiver. One possible solution could be to use a swarm of satellites around the emitter, each equipped with a single photon detector. However, the technical feasibility of this concept has not yet been proven.

This report briefly highlights different ways in which such a mission could be accomplished, and then decides what way will be the most likely to succeed.

Chapter 1

Introduction

In February 2010 the ICESat mission ended after 7 years of measuring ice sheet mass balance, cloud and aerosol heights, as well as land topography and vegetation characteristics. To do all this, ICESat had only one instrument on board: a space based LiDAR system (Geoscience Laser Altimeter System (GLAS)), allowing for an unprecedented 3D view of the Earth's surface and atmosphere. The laser lifetimes, however, were severely limited because of manufacturing errors in one of the laser components.

ICESat followed only one of the possible approaches for LiDAR, namely the use of a high energy laser and a large receiver telescope. The other approach is using a high frequency, low energy laser and a single photon detector. The advantage of the latter approach is that it has a much lower mass, but it is uncertain if even a single photon per pulse reaches the receiver. One possible solution could be the use of a swarm of satellites around the emitter, each equipped with a single photon detector. However the technical feasibility of this concept has not yet been proven.

In this mid term review some options for this concept are proposed and traded off so as to find the best fit for the mission. This tradeoff is what the bulk of this report is about. Also described are the workings and results from the simulator, as well as the project and risk management. Chapters on operation and logistics, stability and control and sustainability are included too.

Chapter 2

Technical Design Development

In this chapter an update is given on the Technical Design Development as given in the Project Plan. All charts and documents have been updated. First the project approach description is updated in section 2.1. Work Flow Diagrams and Work Breakdown Structures are updated in sections 2.2 and 2.3, whereas the Gantt chart is revisited in section 2.4.

2.1 Project Approach Description

2.1.1 Group Procedures

The DSE project is approached by first establishing specific roles for the group members, so that every group member is assigned a clearly defined managerial and technical function. After this the group operational procedures are defined. They are as follows:

1. The Chairman will lead a 'scrum' meeting every morning upon arrival of all members to establish what everyone has done the day before and what they will be doing the day of the meeting. This is done in order to keep all members up-to-date with all aspects of the project. The meeting concludes with updates on any external communications (with organizations and teaching staff) as well as any other points relevant at that time.
2. When done, groups responsible for certain design tasks will present their results to the rest of the team.
3. The team meets with tutor and coaches at least once a week.
4. Everyone is present at The Fellowship between 09:00 and 17:00 every workday, except for a 45 minute lunch break.
5. Upon completion of a deliverable, a meeting is conducted to establish a plan for the next deliverable.

2.1.2 Reporting

The reporting is done in L^AT_EX. There is a main report file which contains the layout of the report and the references to other files that contain the chapters, sections, figures, tables and other documents required for the report. When the file is compiled and printed it will show the entire report.

This has the advantage that work can be easily divided among group members, and any change made to a file will not influence the rest of the report. The file sharing is performed using Subversion (SVN). SVN not only allows file sharing, but it automatically assigns versions to a document and keeps track of changes. The repository is hosted with GoogleTMCode.

2.1.3 Project Outline

The official start of the DSE project is the establishment of the Mission Need Statement. At this point all members should be aware of the main goal of the assignment.

The design process is started by defining the tasks in the project plan, then finding the requirements and functions. From the requirements, a set of design options will be created for the Mid Term Review (MTR). In the MTR a trade-off will be made based on an extensive functional and risk assessment. After the MTR, work on the detailed design can begin. At this stage all subsystems will be given a careful consideration in terms of cost, mass and power budgets. Final decisions on detailed parameters and variables will be made. Leading up to the Final Review (FR), the feasibility study can be concluded.

Parallel to the design phase, the simulator software will be developed by a team of 3 to 4 people, depending on workload and time available. This software should be able to perform calculations accurate enough to aid the trade-off scheduled before the MTR. In this chapter the project planning will be revised. More specifically the Work Flow Diagrams (WFDs) and Work Breakdown Structures (WBSs) of the midterm and final reports and the Gantt chart. These have been updated because now it is more clear as to which tasks have to be performed for the remainder of the project. Also, the work flow for the simulator has been added to the charts. In sections 2.2 the revised Work Flow Diagram will be shown. This is followed by section 2.3, which shows the updated Work Flow Diagram. The final section gives the Gantt chart, our timeline for this project.

2.2 Work Flow Diagram

The tasks to be done on the simulator have been updated and presented in more detail. Some tasks have also been changed in the WFDs: they now start earlier or later so as to better describe the work flow of the project. The tasks in the green and blue boxes respectively describe the simulator design finalization and tradeoff execution in more detail. Red boxes are tasks which are explicitly needed for the Mid Term Review (MTR). The updated WFD of the MTR is given in figure 2.1, page 4.

The WFDs of the final report have also been updated. In retrospect, a very important part if the final report was not present in the WFDs: perfecting the design and the feasibility determination. Now these tasks have been added to the diagram to make it complete. As with the WFD of the MTR, all boxes in red are explicitly required for the final report. The diagram can be seen in figure 2.4, page 7.

2.3 Work Breakdown Structure

The WBSs have been updated like the work flow diagrams. Some extra and other more detailed tasks defined in the WFDs have also been added to these structures. Also, the layout has been changed somewhat to improve readability and correctness. The updated WBSs can be seen in figures 2.3 and 2.4, starting on page 6.

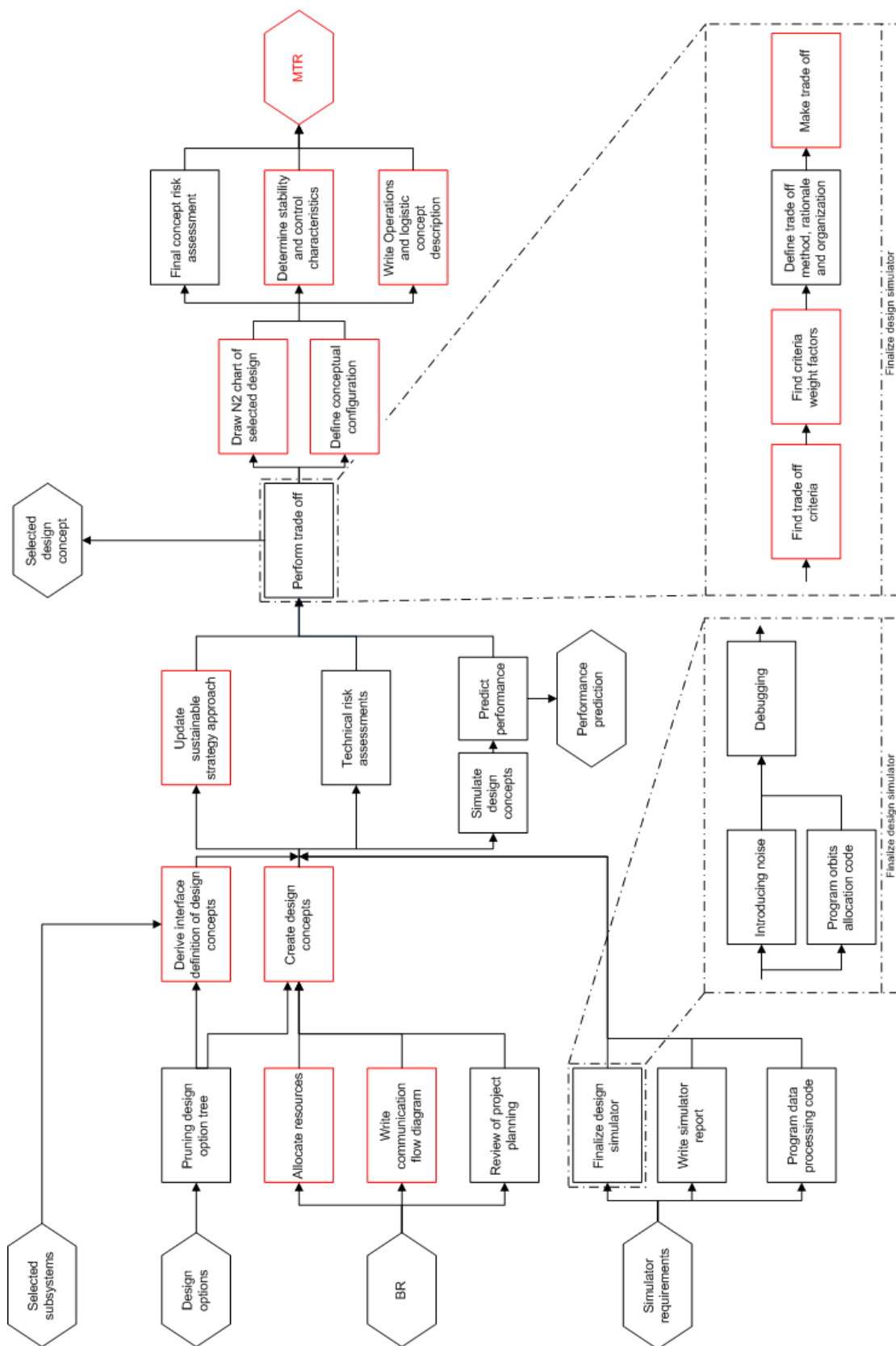


Figure 2.1: Updated work flow diagram for the mid-term report

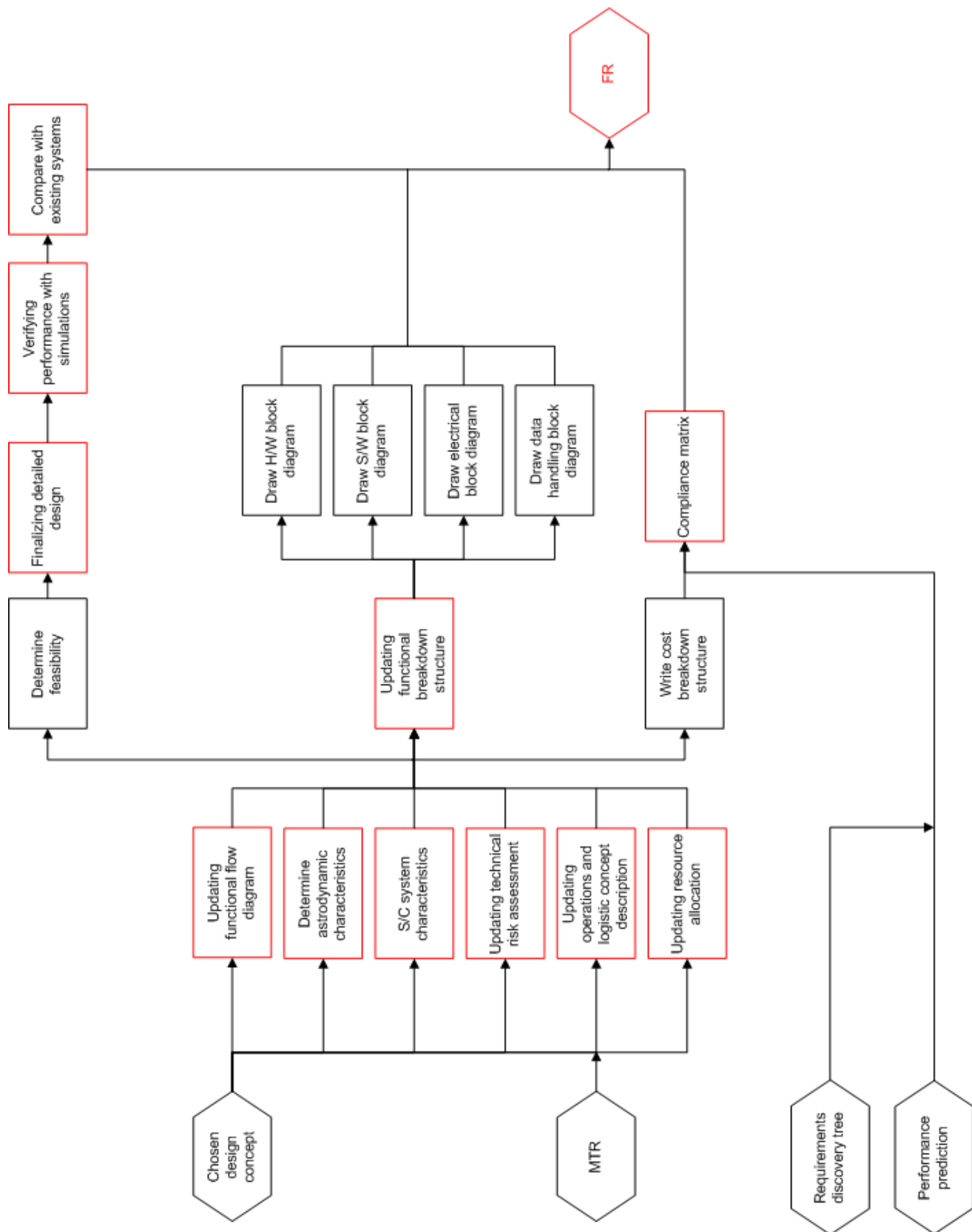


Figure 2.2: Updated work flow diagram for the final report

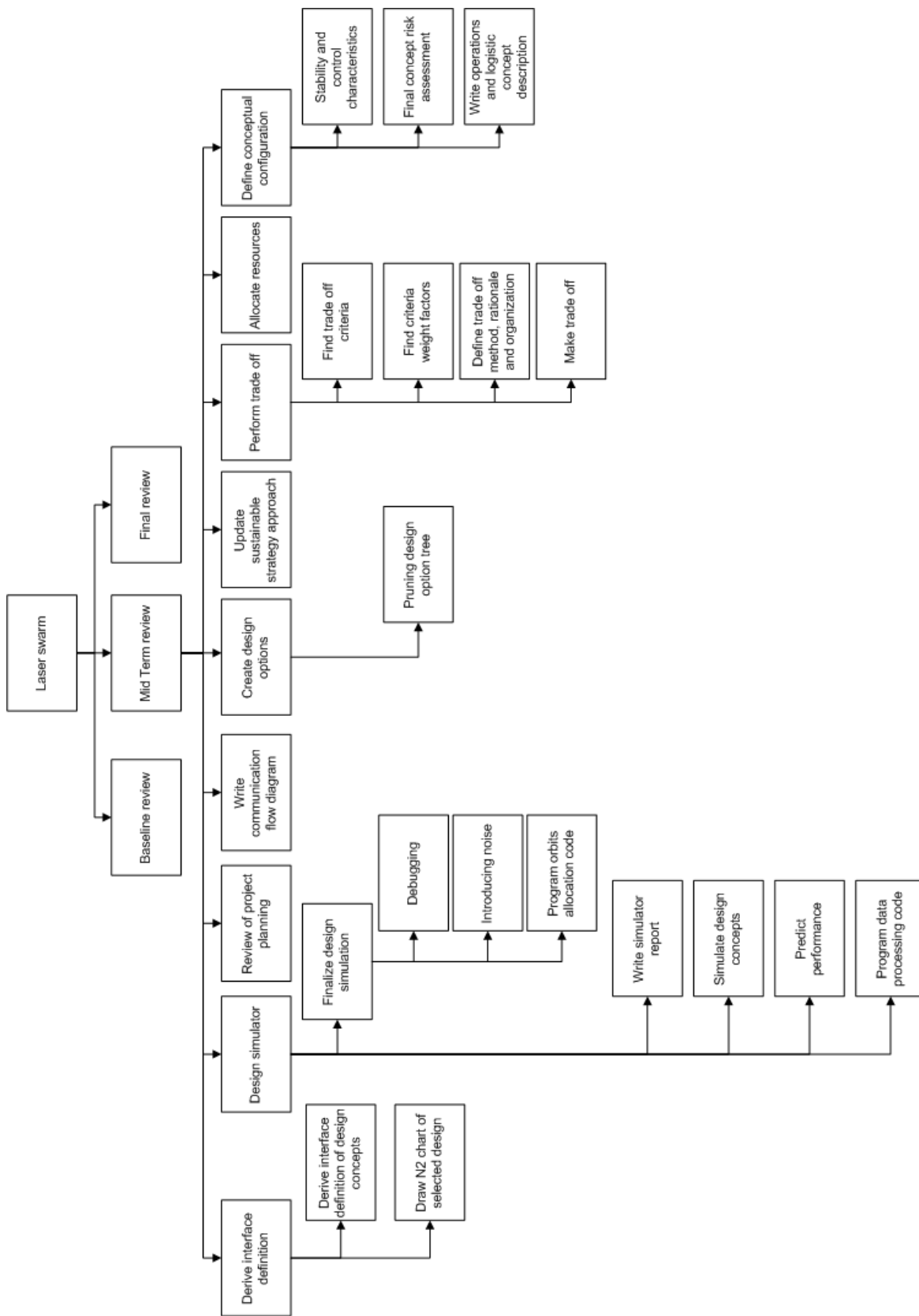


Figure 2.3: Updated work break-down structure for the mid-term report

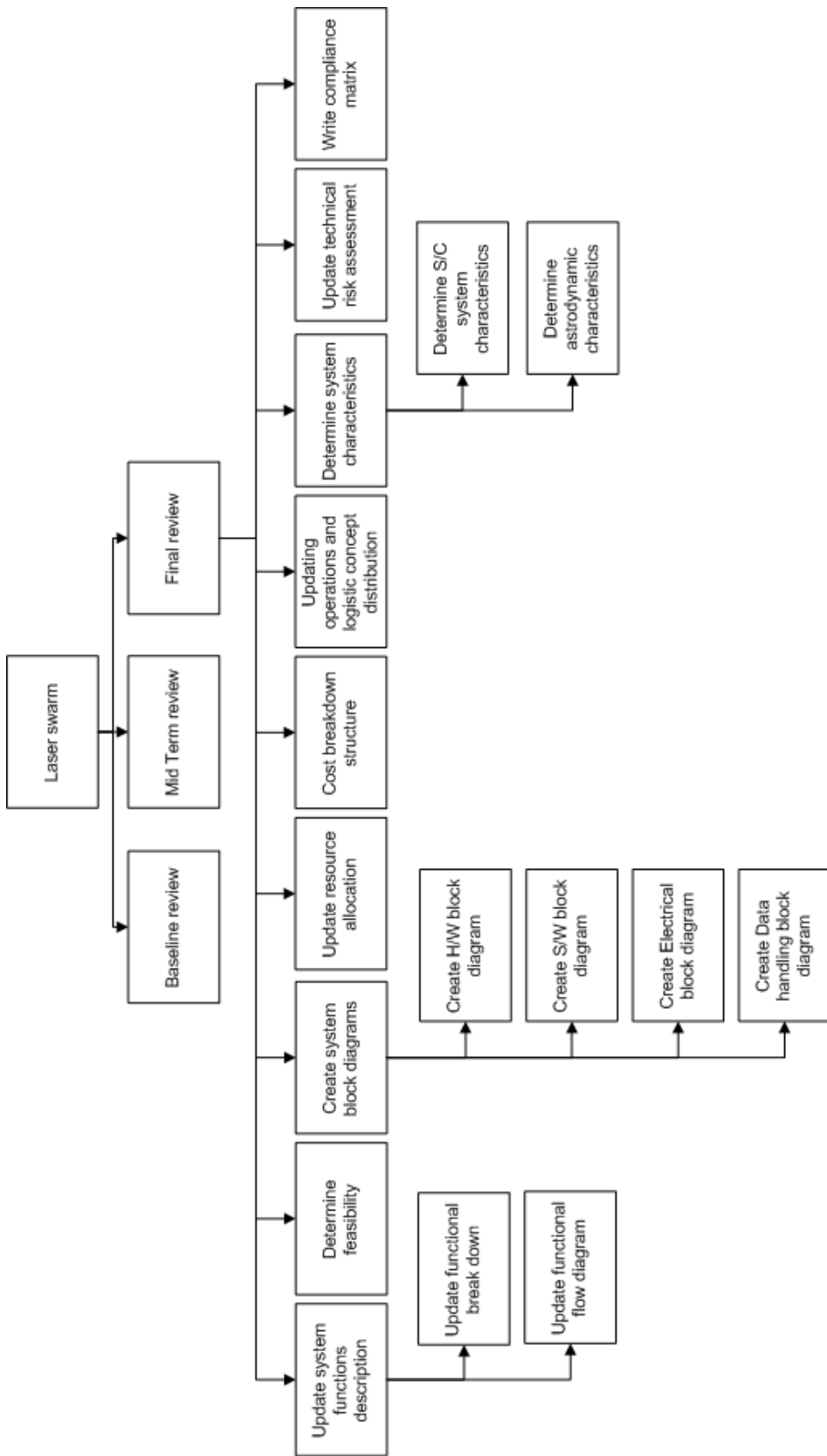


Figure 2.4: Updated work break-down structure for the final report

2.4 Gantt chart

As the WFDs and the WBSs have been updated, so the Gantt chart has also been updated. Now that the project is further along, it is easier to estimate which tasks need to be done for the mid-term and final reports. The duration of these tasks also was much easier to estimate. The Gantt chart has been updated to contain all tasks set in the WFDs. Special care was taken to make sure the Gantt chart is consistent with the WFDs and the WBSs.

This time the simulator tasks were not separated from the rest of the project because the simulator is more involved with the rest of the project for the mid-term and final reports.

The updated Gantt chart can be found in appendix C, page 125.

Chapter 3

Risk Management

All projects, whether big or small, innovative or mundane, are bound to fail under certain circumstances. It is, therefore, in the interest of the team to foresee possible causes of failure and to try to account for them. This is why the risk analysis is performed - it aids in determining and evaluating the gravity of potential failures and helps minimize the damage.

First and foremost is the risk of technical failure which will render the system inoperational or malfunctioning. This risk accounts for the failure of one of the subsystems and is addressed in subsection 3.3.5.

Another risk is that the system will not meet market demands by either being too expensive or having a very narrow range of application. This risk is addressed in subsection 3.1.

In order to distribute the risks associated with the design process, contingency is introduced. This is discussed in section 3.2.

3.1 Market Analysis

Market analysis determines the main potential users and is mainly dependent on the quality and quantity of the obtained data. There are four types of the measurement data sets and it is convenient to analyze them separately. Figure 3.1 on page 10 gives the market diagram with the different data sets.

In the Market Breakdown Diagram, each data type has both science and commercial potential users. For example, in the science field the oceanographic data can be used for climate research. Scientists can study the evolution of weather patterns from the ocean system by modeling changes in the heat distribution of the ocean. On the other hand, in the commercial field maps of currents, eddies and vector winds are used in commercial shipping and recreational yachting to optimize routes. All the blocks in the diagram could be potential return on investment on short or long term.

3.2 Technical Resource Contingencies

Now that the design has started, the contingencies enter the picture. As the design matures, they become less and less, eventually dropping to zero. For the moment the design stage is still on “Conceptual Estimate”. In this stage, the contingencies are still quite large. For the mass contingency, see table 3.1, the contingencies are between 15% and 20%. From table 3.2 it can be seen that the contingencies are between 15% and 45%.

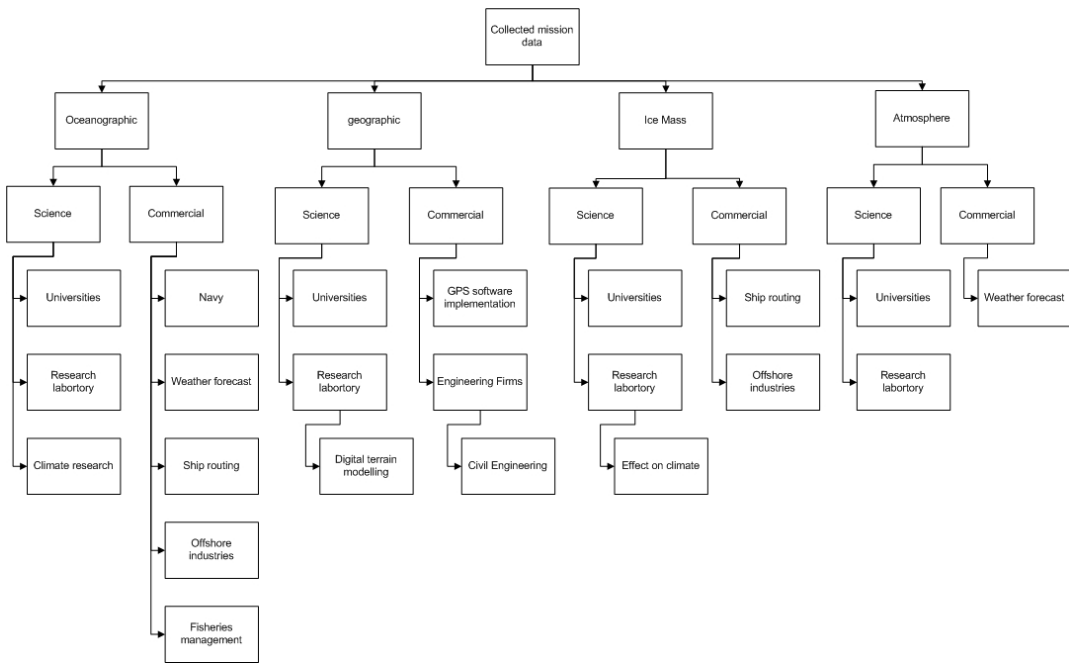


Figure 3.1: Market Breakdown Diagram with different data sets [Mar(2008)]

As the design gets finalized, these will drop to the range of 10% to 25%.

Design maturity	Contingencies [%]						
	Propulsion	ADCS	C&DH	Thermal	Power	Structures & Mechanisms	Payload
Conceptual estimate	20	20	25	20	15	20	20
Layout calculation	15	15	20	15	10	15	15
Pre-released drawings	5	5	10	10	5	5	5
Released drawings	3	3	5	5	5	3	3
Specifications (vendor/subcontractor)	5	5	5	5	5	5	5
Actual measurement qualification hardware	1	1	1	1	1	1	1
Actual measurement flight hardware	0	0	0	0	0	0	0

Table 3.1: The mass contingency allowance

Design maturity	Contingencies [%]			
	ADCS	C&DH	Power	Payload
Conceptual estimate	20	20	15	30
Layout calculation	15	15	10	20
Pre-released drawings	5	5	5	10
Released drawings	3	3	5	5
Specifications (vendor/subcontractor)	5	5	5	5
Actual measurement qualification hardware	1	1	1	1
Actual measurement flight hardware	0	0	0	0

Table 3.2: The power contingency allowance

3.3 Technical Risk Assessment

The main objective of the technical risk assessment is to determine the reliability compared to the possible (functional or financial) consequences per specific event. To be able to determine any of these reliabilities, a definition of reliability should be stated. In this case, reliability is formulated as:

The probability that a specific (part of a) subsystem will function without endangering the top level requirements over the expected lifetime.

Next to formulating the definition of reliability, it should be noted that the determined reliabilities in this section are relative reliabilities, i.e. the probability that a particular subsystem outperforms another subsystem with the same core function in terms of reliability. Hence, no absolute values of reliability are determined in this section. The relative reliabilities allow for comparison material during the trade-off between multiple design options. The risk assessment analysis is divided into four main sections:

- I Ground segment (before vehicle leaves Earth's atmosphere)
- II During mission
- III Measurement protocol
- IV Post-mission

The possible events, with their respective reliability, are outlined in these sections and after that the expected consequences are shortly explained.

3.3.1 Ground Segment

A *Financial*

A1. Insufficient funds or low market-demand

The approximate costs are determined in the cost budget. The mission data and the final results can be very interesting for a vast number of commercial parties and research or educational facilities. Every space mission is created for at least one specific (user-demanded) requirement set by a user. This third party is responsible for covering the cost. Since the space mission is developed after this request is set, the probability that there will be insufficient funds is low (especially when more than one company can be considered as the user). However, the consequence can be severe if the funds are not enough to start or continue the development.

B *Technological readiness*

B1. Technology for level zero requirements are not available

If the technology for measuring, detecting or processing the level zero requirements is not available at present, the requirements cannot be met and alternatives should be devised, or the mission should be terminated. In our case, the technical readiness level of the payload is relatively high and hence has a high reliability. If, however, the specific payload would have a low technical readiness level, the mission should be terminated or delayed. Therefore, it has important consequences to the mission.

C *Launch*

C1. Total launch failure

Total failure indicates complete failure of the launch vehicle and all laser swarm constellation components. Needless to say, the reliability is relatively low; however, the consequences of this event are catastrophic.

C2. Partial launch failure

Partial launch failure indicates non-complete failure of laser swarm constellation components, i.e. some of the satellites (more receivers and one emitter) can still perform core tasks. Considering historical launch data, the reliability that no partial failure will occur during launch is relatively high. The consequence can be very different, depending on which part (or what fraction) of the constellation cannot perform its core task. If one of the receivers will be destroyed, the level zero requirements might still be achievable. However, if the emitter is (partially) destroyed, the mission will surely be endangered.

C3. Delayed vehicle launch

Delaying the vehicle launch is not particularly a problem from the technological side of the mission; however, it will affect the financial situation. Next to the fact that the data and results are delayed, extra costs will be imposed due to an increase in launch vehicle pad costs, extra personnel costs and others. The reliability of this event is actual not that high, since it is dependent on a lot of criteria like third-party companies, the weather, and atmospheric properties. The consequences are mainly financial.

3.3.2 During Mission

D *Orbit accuracy*

D1. One or more satellites are in a wrong orbit.

After launch and orbit initializing, it is possible one or more of the satellites are in a wrong orbit. If this deviation from the desired orbit is relatively small, the ADCS subsystem should be able to cope with this minor error and adjust the orbit. If the altitude error is large, major altitude changes should be imposed. Assuming a low to moderate error, the consequence is not really severe if the ADCS system is working properly. The chance of actually putting a satellite in the wrong orbit is also relatively small.

In the next section, the reliability of the ADCS subsystems is compared. Assuming a non-hybrid spacecraft, i.e. a spacecraft which uses one of the ADCS subsystems considered in the design option tree, the consequences of failure are equal for all subsystems and thus shall not be inspected individually. The consequences are severe considering not only the loss of pointing accuracy, but also a decrease in vehicle stability and the total failure of controllable altitude control.

E *Altitude and control determination*

E1. *Passive systems*

E1a. Gravity-gradient.

The gravity gradient technique is only dependent on gravity fluctuation in nadir direction, which makes it relatively reliable.

E1b. Passive magnetic.

The passive magnetic technique is only dependent on magnetic fluctuation near a celestial body. Since this is the only dependency, the technique is really reliable.

E1c. Zero momentum.

The zero-momentum technique uses a momentum-bias wheel, initially with no angular velocity. Like with all mechanical systems, the presence of (angular) motion will decrease the reliability (due to possible mechanical failure like static failure, fatigue etc.). The reliability however is pretty high, but lower relative to passive magnetic and gravity gradient.

E1d. Momentum-bias wheel.

The momentum-bias wheel technique uses, like the name already predicts, momentum wheels to dump and correct torques. In that sense it has the same reliability as the zero-momentum subsystem. However, since these momentum wheels are constantly spinning, the reliability is slightly lower than the previous mentioned subsystem.

E1e. Spin stabilization.

Spin stabilization can be achieved using rotation about one principal axis (single-spin) or two principal axes (dual-spin). Next to the fact that due to external torques (debris collision, aerodynamic drag) the spacecraft can become unstable, i.e. this subsystem has more dependencies, making it relatively unreliable.

Figure 3.2 demonstrates relative reliabilities of different passive ADCS systems.

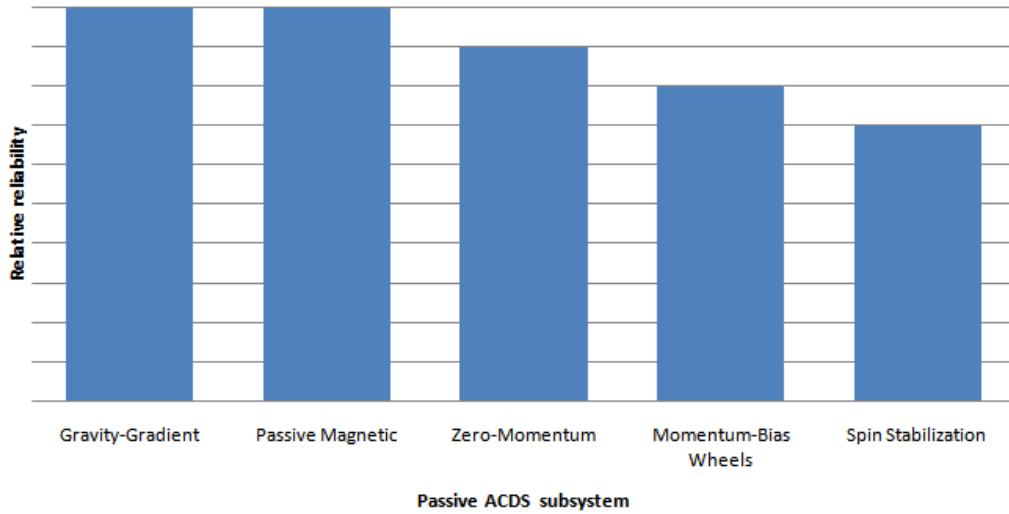


Figure 3.2: Relative reliability of passive ADCS subsystems.

F Active systems

F1. Actuator

F1a. Thrusters (hot and cold gas).

Multiple-axes thruster systems are very efficient ways for controlling attitude and stability. The system is dependent on fuel consumption, combustion and mechanical properties. Each of these dependencies decreases the reliability.

F1b. Reaction and momentum wheels.

Mechanical reliability is an import aspect for using active reaction and momentum wheels.

F1c. Control Moment gyros.

A control-moment-gyro system consists of a spinning rotor and one or more motorized gimbals that tilt the rotor's angular momentum. Mechanical reliability is an important aspect for using this. Since it is also dependent on the motorized gimbals, the reliability is slightly lower than the reaction and momentum wheels.

F1d. Magnetic torquers

The magnetic torquers interact with the Earth's magnetic field, creating compensating torques to induce stability. Reliability is high due to the fact that the magnetic field is known and the system is dependent on a low number of parameters.

F2. Sensors

Assuming a high technical readiness level of the sensors, the reliability is considered high. Also, the consequences of failure are high as the continuation of the mission may be impaired.

Figure 3.3 demonstrates relative reliabilities of different active ADCS systems.

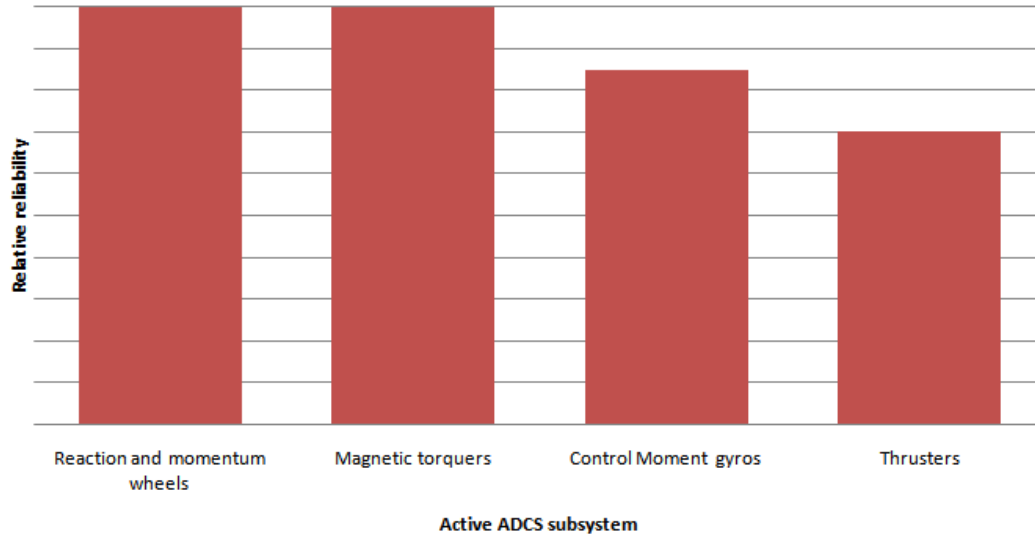


Figure 3.3: Relative reliability of active ADCS subsystems.

G *Electric Power System (EPS)*

G1. *Solar Panels*

G1a. Solar panel deflection error or mechanical failure.

During launch, the solar panels are retracted to achieve the lowest volume possible. During the initializing of the mission (assuming the spacecraft is in the right orbit), the solar panels need to be deployed. Errors can occur due to mechanical reasons or external disturbances. The probability of this is pretty low. The consequence can be however that the effective solar panel is decreased and hence a decrease in available electrical power will occur. This makes the consequences pretty severe. Any other mechanical failure (broken joints, internal PN-junction failure, or a loss of an entire solar panel) will have severe consequences as well.

G1b. Solar panel characteristics reliability (degradation).

Degradation of solar panels should always be considered during mission development. Since this (should be) known upfront, the consequences are relatively low. The probability of this actually happening is nearly 100%.

G1c. Severe degradation (due to external phenomenon)

Atomic oxygen, hazardous radiation, debris collision and other external factors can influence the performance of the solar panels. Since these are not known from the start, it is difficult to cope with them. The probability of this happening is pretty small, but will have pretty severe consequences.

G2. *Batteries*

G2a. Initial internal failure

Considering a high level of technical readiness level, the internal reliability is high. The consequences do alter the functional capacity of the mission, since no energy can be stored if the energy capacity system would completely fail, meaning that during eclipse no energy can be used.

G2b. Decrease in capacity

Considering a high level of technical readiness level, the reliability is high. Consequences are low, because they are known and should be part of the mission analysis.

3.3.3 Measurement Protocol

Since actual measurements are an important level zero requirement, the consequence of the items in the measurement protocol are all really severe. Unless stated otherwise, the consequences in the following section can thus be stated in this way.

Measurement

H Emitter

H1. Laser pulses cannot be sent/ no photon generation

Considering a high level of technical readiness level, the reliability is high.

H2. Pointing towards nadir

This is dependent on ADCS risks.

H3. Laser notifies receiver (time adjustment)

Considering a high level of technical readiness level, the reliability is high.

H4. Laser degradation

Laser degradation is dependent on multiple parameters: thermal properties, input power interval, external factors and internal mechanical errors (manufacturing or design errors). However, due to extensive research and development concerning laser technology, the probability of severe laser degradation within the lifetime is relatively low.

I Receiver

I1. Point towards target

This is dependent on ADCS risks.

I2. Receive and detect photons

Considering multiple satellite receivers, the probability of total failure to receive and detect photons using advanced single photon receiving devices (like SILAT, GLAS or photon-receiving modules) is negligible.

I3. Turn photon into electrical signal

Considering a high level of technical readiness level, the reliability is high.

Communication

J Inter satellite communication

J1. Determine relative position receiver and emitter

Considering a high technical readiness level, the reliability is high.

J2. Time differences

Considering a high technical readiness level, the reliability is high.

K Data handling

K1. Store data/ make data package

Considering a high level of technical readiness level, the reliability is high.

K2. Transmit package

Considering a high level of technical readiness level and relative low-tech technology, the reliability is high.

K3. Interpreted results

Historical data comparisons for the interpretation of altimetry missions are sufficient, but not elaborate. However, the reliability is still pretty high.

K4. Reproduce terrain model

Historical data comparisons for the interpretation of altimetry missions are sufficient, but not elaborate. However, the reliability is still pretty high.

L Housekeeping/ Ground communication*L1. Housekeeping data from ground station to satellite*

Considering a high level of technical readiness level, the reliability is high.

L2. Adjusting space segment characteristics

Considering a high level of technical readiness level, the reliability is high.

M Structural*M1. Joints*

Considering a high level of technical readiness level, the reliability is high.

M2. Connection points

Considering a high level of technical readiness level, the reliability is high.

M3. Thermal limits

Thermal limits will alter the characteristics of pretty much all subsystems. However, thermal will be excluded in this analysis, because this is not a part of the project.

M4. Fatigue

High-cycle loading is usually not present (except for momentum wheels) and should therefore only play a minor role. The probability is low. The consequences are medium to high if high-cycle loading will lead to fatigue and hence partial failure.

M5. Electrical overlay failure

This event is dependent on the reliability of the EPS.

M6. Launch loads

Due to large forces and vibrations during launch the structure of the satellite can fail. Since the launch loads are well known the reliability is low, the consequences can be severe.

N External*N1. Debris collision*

Unknown external phenomenon. The probability of this event causing total failure, which is a function of multiple parameters like orbit and celestial position, is low to medium.

N2. Dangerous radiation

Unknown external phenomenon. The probability of this event causing total failure, which is a function of multiple parameters like orbit and celestial position, is low to medium.

N3. Charged particles collision

Unknown external phenomenon. The probability of this event causing total failure, which is a function of multiple parameters like orbit and celestial position, is low to medium.

N5. Politics or international influence

Political decisions or international influences can alter the space mission considerably. With altimetry missions, the probability of these external influences causing a delayed or complete stop of the mission is negligible. The consequences, however, could be very severe.

N6. Classified information (military)

Some parts of the measurement are considered classified information, for example military ground stations or governmental classified areas. The government and/ or military can pressure the vehicle engineers to

keep certain information classified. However, if this is the case, most of the measurements still can be taken and analyzed. So where the probability is medium, the consequences are very low.

3.3.4 Post-Mission

O *Satellite decommission*

O1. *Decommission LEO*

At the end of life the satellites have to be decommissioned to allow new mission to take their place. To decommission satellites in Low Earth Orbit (LEO) one could just wait a couple of years and air drag will cause the satellites orbit to degrade to the point when they can burn up in the atmosphere, so the consequences are low. However, it is desirable to have the satellites burn up faster, so as to remove the risks of satellite collision. The probability to no longer be able to eject the satellite from orbit depends on whether or not its propulsion system is still working; as such this probability is low.

O2. *Decommission GEO*

Satellites in GEO can not be placed in an orbit that will cause them to burn up in the atmosphere because they will cross paths with too many other satellites. Because risk is so high these satellites are instead decommissioned by ejecting them from orbit further into space. This way, new GEO satellites can take the place of the swarm. If this is not done, then the dead satellites will continue orbiting the Earth, wasting space that can be used by other satellites, as a result the consequence of failure is high. Being able to reposition a satellite depends on the ADCS systems; as such the probability of this event is low.

3.3.5 Risk Control

Sometimes it is possible to decrease the failure probability. For example, A1, F1a and H4 could be the top 3 risk segment. Failure probability of A1 can be pulled down by doing detailed market analysis. In case of F1a, safe combustion performance as well as fuel consumption can be tested and modified in a laboratory environment to increase the thrusters' reliability. Laser degradation (H4) is crucial in the system, and reliable energy source should be used to prevent failure. Meanwhile, thermal control can be performed to achieve high reliability of the laser emitter.

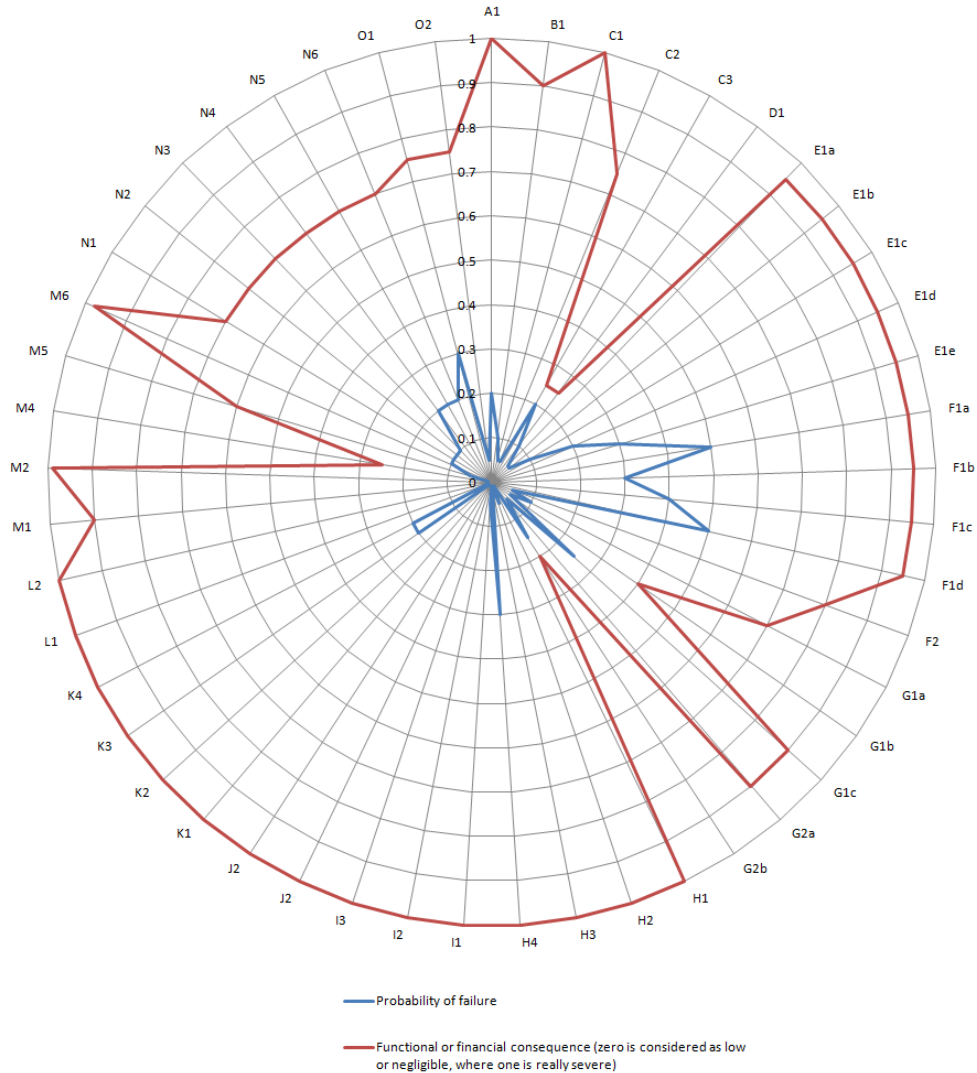


Figure 3.4: Technical Risk Map

Chapter 4

Design Options

In this chapter the design options are repeated from the baseline report. This is done so that the reader gets the whole picture from options to the design finally chosen. This is done for the ADCS, the telecommunications subsystem, the EPS, the orbits, the Optical Emitting Payload (OEP) and the Optical Receiving Payload (ORP), in sections 4.1 to 4.6. The full text has not been included, and the diagrams have been moved to appendix A.

4.1 Attitude Determination and Control Subsystem

The design of the ADCS is twofold: on one side there is the attitude determination, on the other the attitude control. If the state of the satellite is not as it should be the attitude control part adapts the attitude.

A design option tree for the ADCS can be found in figure A.1 on page 112. The chart displays a few properties of each design option for a quick comparison.

4.1.1 Attitude Determination

For attitude determination a number of different techniques can be used. First of all there are inertial measurement units like gyroscopes and accelerometers. Then there are Sun sensors, Earth scanners and star trackers to determine the attitude of the satellite. A recent technique to determine the attitude is using accurate relative Global Positioning System (GPS) measurements with multiple antennas on the satellite body.

4.1.2 Attitude Control

The attitude control is able to change the attitude of the satellite. Thrusters exert gases and momentum wheels spin up to give a momentum to the satellite. In magnetic torquers a current through a coil produces a Lorentz force, using the magnetic field of the Earth. Control Moment Gyro (CMG)s have a constant speed, but the angle in which the force vector is directed is adapted by a single or double set of gimbals.

Passive means of attitude control include gravity gradient, spin stabilization and passive magnetic.

4.1.3 Note on Receiver Pointing

It is important to acknowledge the fact that the receiver payload does not necessarily need to be pointed with the use of ADCS. Also actuators and optics can be used for the pointing.

4.2 Communications

For the communications subsystem 5 different topics were investigated:

- Tracking
- Swarm satellites crosslink frequency
- D/L and U/L frequency
- Antenna configuration
- Communications architecture

4.2.1 Tracking

For tracking there are the following design options:

- Microcosm Autonomous Navigation System (MANS)
- GPS
- Tracking and Data Relay Satellite (TDRS)
- Satellite crosslinks
- Ground tracking

Details for these tracking methods can be found in [Wertz(2006)], p. 502-507.

4.2.2 Swarm Satellites Crosslink Frequency

The frequency band normally used for inter satellite communications are the V-band frequency. This band lies around 60 GHz and has no limit on the power flux density.

4.2.3 D/L and U/L Frequency

Frequency bands available for upload and download of scientific data are:

- C-Band
- X-Band
- Ku-Band
- Ka-Band
- SHF/EHF-band

Details for all frequency bands can be found in [Wertz(2006)], p. 566.

4.2.4 Antenna Configuration

The following antennas, suitable for beamwidths of less than 20 degrees, producing gains above 15dB, are considered:

- Parabolic reflector center-feed
- Parabolic reflector cassegrain
- Parabolic reflector off-set feed
- Phased array
- Lens with switched-feed array
- Parabolic reflector off-set shaped subreflector with feed array for scanning

Drawings and descriptions of these antennas can be found in [Wertz(2006)], p. 573.

4.2.5 Data Storage

Today Dynamic RAM is almost exclusively used by satellites for mass data storage because they allow very large capacities of 1000 Gbits and more. Typically, they do not have external addressing to each RAM location but operate on a block or file basis. The block may be of the order of 1000 bytes or sometimes it will correspond to one source packet. Dynamic RAM has a simple structure: only one transistor and a capacitor are required per bit, compared to six transistors in Static RAM. This allows Dynamic RAM to reach a very high density [et al.(2007)].

Since this technology has recommended itself as the best around, there is no logical reason to design or trade-off other options. For this reason it is not included in the design option tree.

4.2.6 Communications Architecture

In this subsection we will discuss the possible communications architectures and the transmission power and bandwidth required for the communication subsystem in each satellite:

- Centralized architecture
- Decentralized architecture
- Extremely decentralized architecture

A detailed description of these architecture can be found in the baseline review [et al.(2010)]. The design option tree for communications subsystem is shown in figure A.2 on page 113.

4.3 Electrical Power System

The electrical power system (EPS) is divided in to four parts: the power source, the energy storage, the power regulation and control and the power distribution. These are also the four main branches in the EPS design options structure. Figures A.3, A.4 and A.9 (pp. 114-119) show the complete design option tree for the EPS.

Figure A.3 shows the complete design option structure of the power source. There are five possibilities: photovoltaics, primary batteries, fuel cells, a static power source and a dynamic power source. Primary batteries and fuel cells give a lot of power but only have a short lifetime. Static and dynamic power sources are expensive but have a long lifetime and can deliver a lot of power. Photovoltaics are the main source used for missions relatively near to Earth. They are light, cheap in comparison with static and dynamic power sources and have been used extensively in the past, giving a large database of information and a lot of experience.

The design options for power storage can be seen in figure A.4. There are two types of batteries: primary and secondary. Primary batteries can be used to store power only for short missions, up to a couple of days in the case of high power usage and up to a couple of months for payloads which have a low power usage. Secondary batteries are rechargeable, making them absolute favorites for long term missions around Earth. They provide power for satellites using photovoltaics as power source during eclipse and are recharged between eclipse periods.

The power regulation and control and the power distribution can be seen in A.9. The power regulation and control is the subsystem which handles battery charging and discharging, the interaction between the power source and the bus and determines how regulated the bus is. This subsystem can be a general design or can be tailor-designed for each mission. The power distribution is highly entwined with the power regulation and control subsystem. Unregulated buses follow from a decentralized power distribution, while quasi- and fully regulated buses have a centralized distribution. Depending on the power load profile, alternating or direct current can be used. Also some sort of fault protection is necessary to the system does not short-circuit. This can be done with fuses, extra current carrying cables or extra power storage. Usually a mix of the three is used.

4.4 Orbit Architecture

In this section the design options in the orbit architecture tree as seen in figures A.6, A.7 and A.8 (pp. 117-117), are described.

The orbits are divided in four categories: LEO, Medium Earth Orbit (MEO), GEO and HEO. Some orbits like hyperbolic and parabolic trajectories are not included as they are not relevant for the mission.

After the main categories there are subdivisions, which can in turn have subdivisions as well. These subdivisions list the special orbits types that are possible, sometimes there is also a block called “other”. This is because special orbit types have special constraints, as will be detailed in later sections; whereas the “other” block is there to represent all the other possible orbits.

All orbits are assumed to be Keplerian orbits. As such the orbit can be described as a plane located in 3D space. Therefore six elements will define the position of the satellite - the classical orbital elements. The elements are: the semimajor axis (a), the eccentricity (e), the inclination (i), the right ascension of the ascending node (Ω), the argument of perigee (ω) and finally the true anomaly (ν).

LEO ranges from 200 to 2000 kilometers with the lower limit arising due to air drag and the upper limit due to the van Allen radiation belts. MEO ranges from 2000 to 35700 kilometers, where the upper limit is the geosynchronous orbit altitude. GEO are orbit that are synchronous to the rotational period of the Earth, a special case of geosynchronous orbits is the Geostationary Orbit (GSO) which has an eccentricity and inclination of zero. HEO are all orbit above GEO, where a Highly Elliptical Orbit (HEllO) is a special case of HEO with a very large eccentricity.

4.5 Optical Emitting Payload

4.5.1 Introduction

Satellite altimetry missions use active remote sensing techniques. For that reason the quality of the system is dependent on the emitted electromagnetic radiation and the analysis of the returned signal.

To be able to select any optical emitting device, the important parameters for optimizing the altimetry results should be revised. Several problems occur if emitting radiation is chosen as the remote sensing technique.

- i First of all, general electromagnetic radiation will show isotropic behavior. This results in an effective energy loss, since most of the radiation is not pointed towards the desired position. Hence, a divergence limited source would be preferable.
- ii As mentioned before, the wavelength is an important parameter since it will influence the photons actually reaching Earth. Since the Earth's atmosphere is transparent for wavelengths in the visible spectrum, it would be better to have an electromagnetic radiation source with a wavelength in this interval. Next to that, a regular radiation source (like the Sun) emits radiation consisting of a whole spectrum of wavelengths. The less the number of discrete wavelengths (preferable in the visible spectrum), the higher the quality of the analysis can be.
- iii The total work done on the photons to reach the Earth's surface, scatter and return to the receiver, is generally very large. To cope with this large work, the energy of the pulses should be high.

4.5.2 Laser Types

There are actually many types of lasers. The main types are considered below:

1. Gas. A variety of lasers is based on gases as gain media.
2. Semiconductor lasers, also known as diode lasers, are lasers based on semiconductor gain media.
3. Solid-State lasers are lasers based on solid-state gain media such as crystals or glasses doped with rare Earth or transition metal ions. . [Paschotta(2008)]

Refer to the baseline report for more details about laser emitter.

4.6 Optical Receiving Payload

4.6.1 Introduction

A large fraction of the photons emitted by the laser are not suitable for detection since they are redirected by the atmosphere, spread due to surface scattering or they are simply absorbed by either of them. The decrease in photon quantity is really severe considering these factors. Since the number of photons actually reaching the perimeter of the Optical Receiving Device (ORD) is usually only in the order of one to ten, the ORD has to be able to detect and analyze individual small energy packets, preferably single photons.

4.6.2 Types of Optical Receiving Devices

A number of technologies, primarily based on quantum dynamics, and devices are already in production or in development.

- i Charge-Coupled Device (CCD).
- ii Photomultiplier Tubes (Avalanche Processes).
- iii Quantum Dots.
- iv Quantum Computers.

Refer to the baseline report for more details about the design options.

4.6.3 Important Parameters for Optical Receiving Devices

Obviously, the mass and the average power usage are important aspects for choosing the desired ORD in any satellite (constellation) mission.

Considering the fact that you want to detect as much photons as possible, another important characteristic is the Optical Field of View (OFOV). The OFOV (also field of vision) is the (angular or linear) extent to which the ORD is able to observe photons at any given moment. As mentioned earlier, the problem of noise increases if the OFOV becomes too large. However, since the OFOV is in the order of 0.001 radians, it can be stated that a higher values increases the amount of detectable photons.

The last aspect to consider when determining the ORD, is the detector quantum efficiency. It is defined as the efficiency that an incoming photon induces an exciton. It is an accurate measurement of the device's electrical sensitivity to light. Figure A.13 on page 122 gives the final design option tree of the laser receiver.

Chapter 5

N^2 Chart

The N^2 chart shows the interfaces between the different functions of the system. The chart can be found in figure 5.1 on page 27. The functions are in the dark grey boxes, while the interactions are shown by the dotted boxes and move clockwise. The system is split up in the emitter satellite, a receiver satellite and the ground segment, denoted by the large bold boxes. Outside of these boxes, the outside world, is composed of e.g. the Sun and customers. The starred interactions depend on the level of communication centralisation.

The basic workings of the system is that the laser sends down a laser pulse, which is reflected by the Earth and received by receivers in the receiver satellites and the main satellite. Combined with the time from the navigation subsystem the photon counts are stored in the data storage. The communication subsystem sends down the data to be received by the ground station. Before a laser pulse can be sent or received the satellites need to be pointed by the Attitude Control Subsystem and the pointing mechanism. The current attitude is determined by the Attitude Determination Subsystem (ADS) and it outputs to the attitude and pointing errors to the Attitude Control Subsystem (ACS) and pointing mechanism. The EPS subsystem provides power to all other subsystems. Mission control sends the data packages to researchers, who can create the digital terrain model. Researchers can ask for certain data sets, which mission control can make into commands for the satellites.

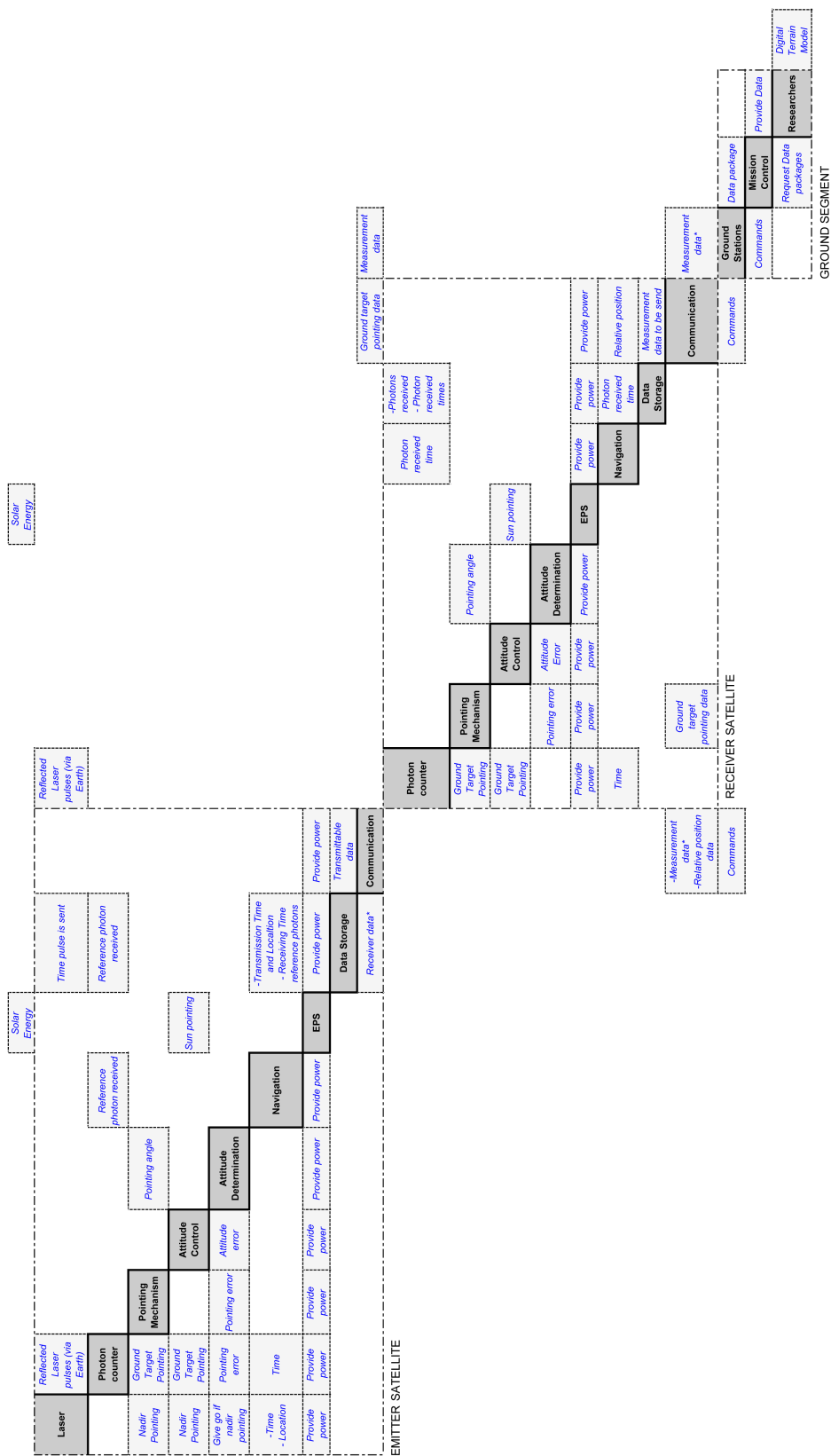


Figure 5.1: N^2 chart of the Laser Swarm mission

Chapter 6

Tradeoff

6.1 Attitude and Orbit Determination and Control Subsystem

The Attitude and Orbit Determination and Control Subsystem (AODCS) is used for determining and controlling the attitude and orbit of the satellites. In this section first the ADCS design option tree is pruned in section 6.1.1. The subsystem can be split up into four smaller parts; attitude determination (discussed in section 6.1.2), attitude control (section 6.1.3), orbit determination (section 6.1.4) and orbit control (section 6.1.5).

6.1.1 Pruning the Attitude Determination and Control Subsystem design option tree

The gravity-gradient stabilisation and passive magnetic options are eliminated because they provide insufficient accuracy and do not allow pointing to an any target other than the mass or magnetic centre of the Earth. The spin stabilisation option is pruned because the satellite needs to be able to make measurements continuously. Double gimbal CMGs are also not a viable option, because they are too complex and heavy compared to other systems. For the attitude determination the initial measurements and magnetometers options are eliminated because of their deteriorating accuracy over time.

The pruned design option tree can be found in figure 6.1.1 on page 29.

6.1.2 Attitude Determination Subsystem

The ADS consists for a collection of sensors to determine the roll, pitch and yaw angles and rates of the satellites. The design options left after the pruning in section 6.1.1 are GPS, Sun sensors, Star trackers and horizon sensors.

GPS uses one receiver and multiple antennas. By measuring the relative positions of the different antennas the attitude of the satellite can be calculated. Most modern LEO satellites are already carrying a GPS receiver, but a long baseline between antennas is needed for a high accuracy.

Sun sensors use the angle towards the Sun for making their attitude measurements. The technology behind Sun sensors has been around for a long time and several micro Sun sensors are available on the market. The Field Of View (FOV) of a typical Sun sensor is about 120° .

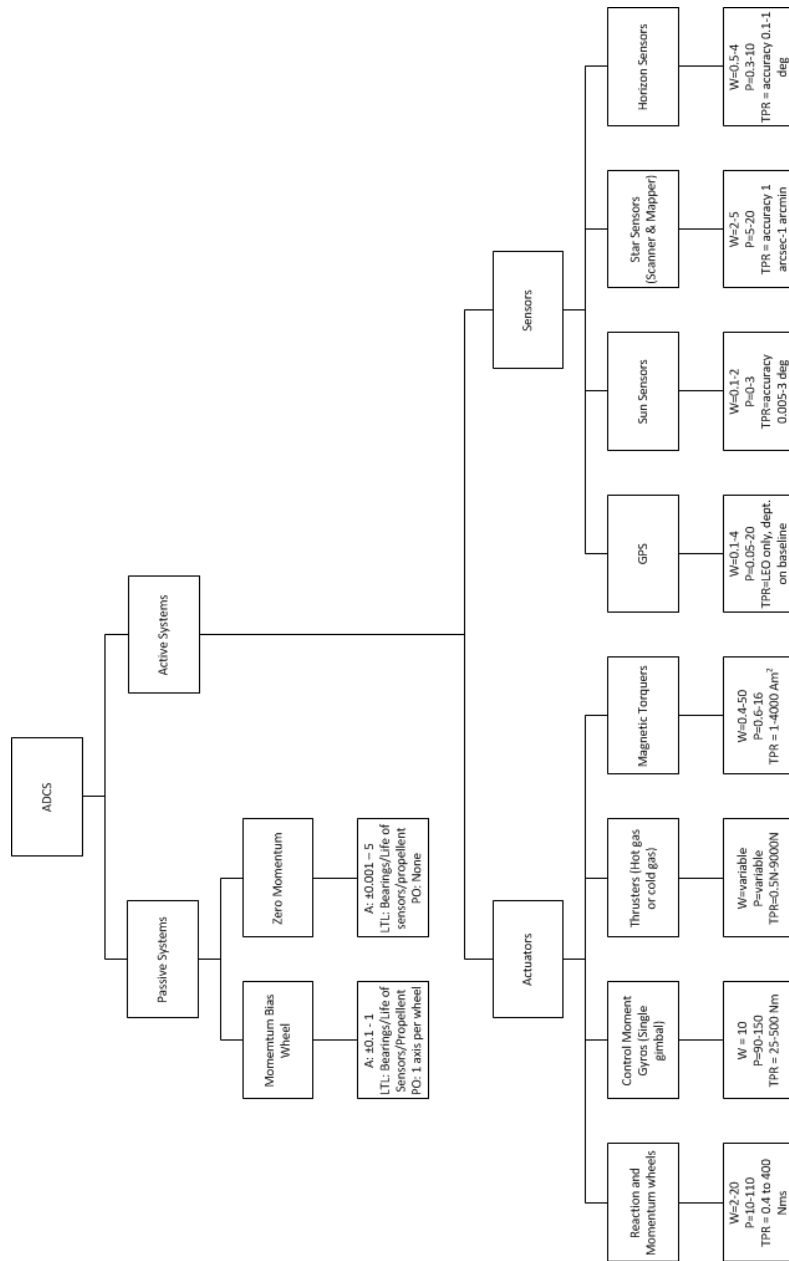


Figure 6.1: Pruned design option tree for the ADCS

Star trackers look at a portion of the sky and use familiar stars to determine the attitude of the satellites. This system can work autonomously, but the optics required are usually quite bulky.

Horizon sensors use the limb of the Earth, i.e. the transition of the solid Earth to cold space, to determine the attitude of the satellite. The system only works on the roll and pitch axes.

Another option is to use a complete Commercial Of The Shelf (COTS) ADCS system like the one from Maryland Aerospace Inc. [mar(2010)]. Their IMI-100 ADACS contains everything needed for complete ADCS with an accuracy of 1° . For attitude determination it uses 3 magnetometers, by adding additional sensors e.g. a ring laser gyro and a miniaturised star sensor the accuracy can reach 1-3 arcsec [imi(2010)].

6.1.2.1 Trade method

The trade-off is made by comparing three concepts for attitude determination. The first concept uses the Maryland Aerospace IMI-100, the second concept uses Sun sensors by day and a star tracker by night, the third concept uses GPS for attitude determination (see figure 6.2 on page 30). Scores are awarded to the performance on a number of criteria. The best weighed overall score wins the trade-off.

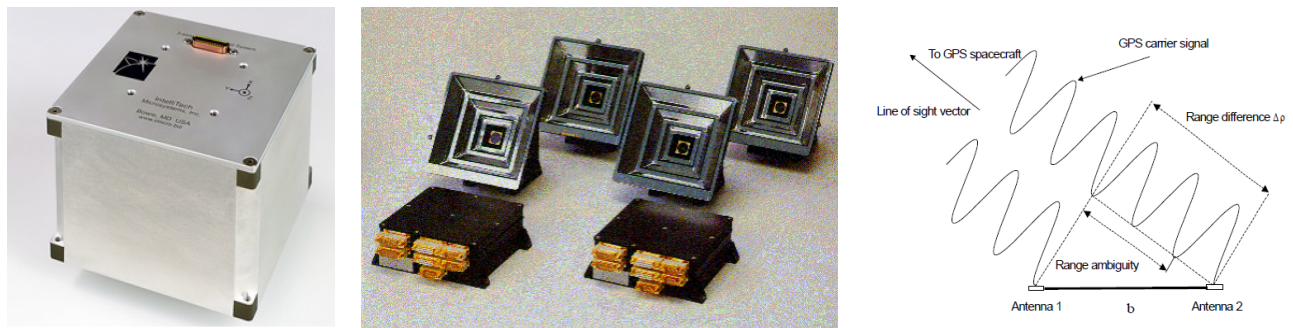


Figure 6.2: The three concepts for the design of the ADS. From left to right: Concept 1 uses the IMI-100 system from Maryland Inc. [imi(2010)], concept 2 uses Sun sensors and star trackers [Chu(2009b)], concept 3 uses GPS for attitude determination [Chu(2009b)]

6.1.2.2 Trade criteria

The concepts for ADS are traded in terms of attitude determination accuracy, purchasing price, power required, size and the amount of additional development required for implementing the concept.

6.1.2.3 Weight factors

The accuracy of the ADS is the main driver for the choice of the system so it is given a weight factor of 9. Because the volume and power for satellites are limited they are also important with a given weight factor of 7. Although the total cost of the system is relevant, if a better performance can be achieved at a higher cost that can be acceptable, wherefore it is given a weight factor 3. If a lot of work still is required to implement the system in the satellite the mission can be delayed, so development gets a weight factor of 5.

6.1.2.4 Trade-off

The results of the trade-off can be found in table 6.1 on page 31. The attitude determination accuracy of concept 1 and concept 3 are both around 1° for micro satellites, the performance of concept 2 is much better with an estimated accuracy of 0.01° .

In the Innovative Solutions In Space (ISIS)' webshop [cub(2010)] concept 1 costs about EUR 45000, the development costs of concept 2 are estimated to be about EUR 15000, a space qualified GPS receiver will cost about EUR 25000 [spa(2010)].

The first concept will use about 1.5 W on attitude determination, concept 2 uses a power of about 2 W, a GPS receiver takes about 1 W. The size of the IMI-100 is 100x100x79 mm, the Sun sensors can be as small as 30x30x14.5 mm [tno(2010)] and ISIS is currently developing a star sensor with a size of 50x50x100 mm, a space qualified GPS receiver is about 100x70x25 mm.

The IMI-100 system is completely developed and can just be build in, for a system with Sun sensors and a star tracker still some design needs to be done in for example locations on the satellite, for a GPS system the antenna positions need to be chosen for optimal accuracy.

Criteria	Weight Factor	Concept 1	Concept 2	Concept 3
Accuracy	9	4	8	4
Size	7	2	6	4
Power	7	6	5	7
Price	3	3	5	4
Development	5	8	4	5
Weighed total		141	184	150

Table 6.1: Trade-off graph for the attitude determination system. The weight factor signifies the importance of the criterion. Grades are given on a scale of 1 to 10, 1 being the worst, 10 the best

After the trade-off the best solution for the ADS is to use Sun sensors and a star tracker. Although this option requires most design work, it is able to give the best accuracy for the lowest price.

6.1.3 Attitude Control Subsystem

The satellites in the constellation all need to point accurately to the Earth, a passive ACS will therefore not be sufficient for the control of the attitude of the satellites. For active attitude control actuators are needed. After the pruning, four options remain for the attitude control. Reaction and momentum wheels, CMGs, Thrusters and Magnetic torquers.

Reaction wheels are basically torque rotors with a high-inertia wheel attached to it; they can provide single axis control to a spacecraft. Momentum wheels are reaction wheels with a nominal spin rate, adding gyroscopic stiffness to two axis of the spacecraft. Changing the spin rate gives control over the third axis. CMGs consist of a wheel with a constant rotation speed and one or two gimbals to rotate the wheel, determining the direction of the momentum. This way very accurate attitude manoeuvres can be made, but complex control algorithms are needed. Usually the weight and cost of CMGs are quite high. Thrusters expel mass to induce velocity or a momentum to the satellite. The velocity can be used for keeping the orbit and will be discussed in section 6.1.5. To be able to induce a momentum to a satellite multiple thrusters with an offset to the center of mass of the satellite. Thrusters are split up into hot gas types, which require a chemical reaction of the propellant, and cold gas types that rely on latent heat and phase change in the propellant. The power which can be generated by thrusters is high, but the fuel required will limit the lifetime of the

satellite. Magnetic torquers are magnetic coils or electromagnets generating dipole moments on the satellite. They can be used for both manoeuvring and desaturation of e.g. reaction wheels. Because they rely on the magnetic field of the Earth they are less useful in higher orbits.

The IMI-100 ADACS contains three miniature reaction wheels and three magnetic coils for desaturating the wheels. For a 2 kg, 2U cubesat it can provide a slew rate of $8.4^\circ/s$ [imi(2010)].

6.1.3.1 Trade method

In the trade-off three concepts for attitude control are compared to each other on a number of criteria. The first concept is using thrusters for attitude control, the second option is using reaction wheels with magneto torquers for desaturation, the third option is using Maryland Aerospace's IMI-100. The concept with the highest weighted score wins the trade-off. The options are shown in figure 6.3 on page 32.

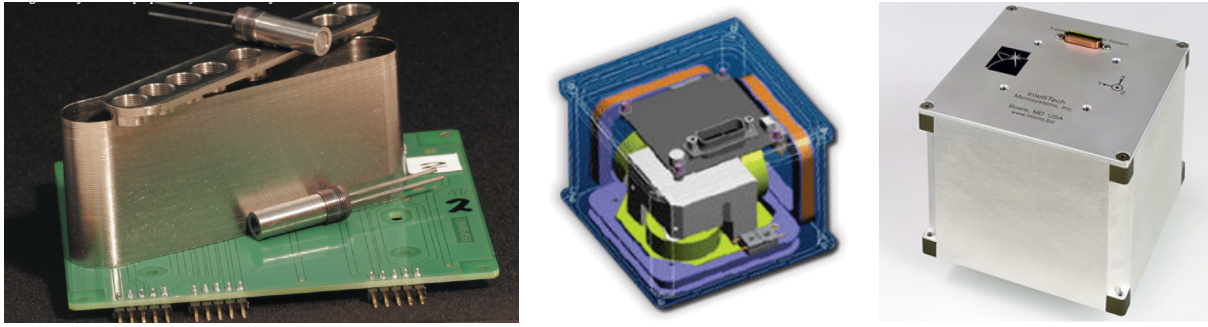


Figure 6.3: The three concepts for the design of the ADS. From left to right: Concept 1 uses thrusters [tno(2010)], concept 2 uses reaction wheels and magneto torquers [cub(2010)], concept 3 uses IMI-100 system from Maryland Inc. [imi(2010)].

6.1.3.2 Trade criteria

The concepts for ACS are traded in terms of the rate the concepts are able to adjust the attitude, attitude control accuracy, purchasing price, power required, size and the amount of additional development required for implementing the concept.

6.1.3.3 Weight factors

A high rate in which the satellite can be controlled is convenient, but not driving: weight factor 5. Since attitude control will be used for the pointing of the instrument the accuracy is very important, so it is given a weight factor of 8. Because the volume and power for satellites are limited they are also important with a given weight factor of 7. Although the total cost of the system is relevant, if a better performance can be achieved at a higher cost that can be acceptable, weight factor 3. If a lot of work still is required to implement the system in the satellite the mission can be delayed, development gets a weight factor of 5.

6.1.3.4 Trade-off

The results of the trade-off can be found in table 6.2 on page 33. Thrusters are able to make attitude adjustments with a high rate, both concept 2 and concept 3 use reaction wheels for attitude adjustments, so they will have comparable performance.

Attitude adjustments done by thrusters are really coarse, so they have a low accuracy. With a custom designed system the accuracy of concept 2 the performance will be better than a COTS system.

For the use of thrusters also other components are required like e.g. fuel tanks, fuel lines and pumps. Reaction wheels and magneto torquers all take up space in the satellite, but can be made relatively small. The IMI-100 system is encased in a separate box, so it will take more room.

To work the thruster system needs fuel, which has to be taken along for the entire mission. The reaction wheels in concept 2 and 3 require only power when the motors are running, as do the magneto torquers.

Combined with the fuel, tanks and other extra material the thruster system needs to bring it will be a very expensive option, especially for the small kind of satellites being considered for the mission. Not many micro propulsion systems are yet on the market. Developing the system with reaction wheels can be a much cheaper option. Buying the system as COTS will save working costs, but in the end will be a little more expensive than in house development.

Thruster systems for small satellites are rare, so a lot of development is still required. Some research has already been done on an active ACS for the student satellite Delfi-n3Xt [del(2010)], this research can be extended for the Laser Swarm mission. The IMI-100 system is ready and just has to be integrated.

Criteria	Weight Factor	Concept 1	Concept 2	Concept 3
Rate	5	8	6	6
Accuracy	8	4	8	7
Size	7	2	6	5
Power	7	3	6	6
Price	3	2	8	7
Development	5	4	6	8
Weighted total		133	232	224

Table 6.2: Trade-off graph for the attitude control system. The weight factor signifies the importance of the criterion. Grades are given on a scale of 1 to 10, 1 being the worst, 10 the best

After the trade-off the best solution for the ACS is to use reaction wheels and magneto torquers. Although the scores are close to concept 3, the more dedicated design improves on the performance of the COTS system.

6.1.4 Orbit Determination Subsystem

The determination of the orbit will be discussed in section 6.2.5.

6.1.5 Orbit Control Subsystem

The Orbit Control Subsystem (OCS) needs to counter the atmospheric drag forces with the ΔV calculated in section 6.5. The ΔV a propulsion system can produce is quantified by Tsiolkovsky's rocket equation:

$$\Delta V = gI_{sp} \ln \left(\frac{m_0}{m_0 - m_p} \right) \equiv gI_{sp} \ln \left(\frac{m_0}{m_f} \right) \equiv gI_{sp} \ln (R) \quad (6.1)$$

In this equation, g is the Earth's gravity constant, I_{sp} is the specific impulse of the engine, m_0 is the starting mass, m_p is the mass of the fuel used, $m_f = m_0 - m_p$ and the mass ratio R is $m_0 / (m_0 - m_p)$. From this the ratio of fuel to the total mass can be derived to be:

$$\frac{m_p}{m_0} = 1 - e^{-(\Delta V / I_{sp}g)} \quad (6.2)$$

Depending on the altitude of the satellite orbit a thruster for attitude keeping can be selected in a later stage of the design.

6.2 Communications

6.2.1 Trade off communication architecture

Three communication architectures were presented in the baseline review:

- Centralized architecture
- Decentralized architecture
- Extremely decentralized architecture

The advantages and disadvantages of each architecture will be discussed in the following paragraphs.

In a centralized architecture all communication flows through the emitter satellite, which means the receiver satellites do not require an independent link to the ground.

The main advantage is that this allows the receiver satellite to have a small and lightweight communications subsystem because there is only free space loss. Another advantage is that all scientific data can be partly processed in space and thus can be more efficiently compressed before being transmitted to Earth. Also because communication links exist between the satellites, they can be used for tracking.

The main disadvantage is that the receiver satellites completely depend on the emitter satellite, making the system not very robust. The communications subsystem of the emitter satellite is large since it has to handle all communications. In case too many receivers are required, multiple frequencies are required for intersatellite communication.

In a decentralized architecture each satellite has its own communication link to the ground, although communications between the satellites is also still possible.

The main advantage is that each receiver satellite can transmit its own scientific data in its own contact time with the ground station, reducing the data rate significantly. The communication links within the swarm can be used as a backup or to send commands from the emitter satellite to the receiver satellites. The links can also be used for tracking.

The main disadvantage is that all satellites require relatively large communication subsystems. In case too many receivers are required, multiple frequencies are required for ground-space communication and intersatellite communication.

In an extremely decentralized architecture each satellite has a communication link with the ground but no intersatellite links exist. The advantages and disadvantages are similar to those of a decentralized architecture, only the there is no backup for the ground-space communications and tracking which makes use of intersatellite links is also impossible.

The main advantage is that no frequency has to be acquired for intersatellite communication but the disadvantage is that if the swarm is not well synchronized, the receiver satellites will not be aimed correctly.

When comparing the architectures, the extremely decentralized architecture has a serious disadvantage, namely that it can get desynchronized resulting in useless scientific data, which is why the decentralized architecture will not be used.

This leaves only the decentralized and centralized architecture. Both have communication links between the satellites, but the decentralized architecture requires extra communication links while the centralized one does not. Since the difference between an intersatellite link for only command data and an intersatellite link for all data is small, whereas the difference in mass is very large, the centralized architecture was the architecture that was finally chosen.

6.2.2 Trade off D/L and U/L frequency

Since a large data stream is necessary between the emitter satellite and the ground, a frequency in the X-band will be used since it allows the largest data stream and is also most commonly used by Earth observation satellites at present [ice(2010)] [lan(2005)]. A frequency in the S-band will be used for housekeeping data.

6.2.3 Trade off crosslink frequency

After some research it became clear that only few satellites make use of frequencies in the V-band, only one mission made use of it: Milsat II [mil(2010)]. Since no figures about this system could be found, frequency in the V-band will not be considered. However other microwave frequencies can still be used, with X-band and S-band excluded since those with interfere with the other communication links. A frequency in the Ku-band will be used since a multiple systems already exist which make use of these frequency which can be used as a reference in sizing of the communications subsystem in the final report.

6.2.4 Trade off antenna configuration

The antenna for ground-space link could be a parabolic reflector or a phased array. The main advantage of a parabolic reflector is its low mass but has a high volume as a disadvantage while a phased array has a high mass but lower volume. Since the ballistic coefficient of the satellite is already low, the phased array was chosen.

As the antenna for the intersatellite link a simple horn antenna can be used: the frequency is below 4 GHz and a low gain is required because there is no atmospheric loss.

6.2.5 Trade off tracking method

The quality of the scientific data depends on how accurately the orbits of all satellites are known. This is why GPS is the preferred choice since it is the most precise method. It is however possible to combine GPS tracking and tracking based on the satellite crosslinks. Both methods are precise, but crosslink based method

give only a relative position to the other satellite. By placing a GPS only on the emitter satellite, its absolute position is known and consequently the absolute positions of the receiver satellites is known as well.

6.3 Trade-off for the Electrical Power System

This section is about the trade-off for the EPS. First the design option structure will be pruned with the obvious non-candidates eliminated so only the viable options remain for the trade-off. When this is done, the preparation of the trade-off can be done. First the method and rationale will be discussed. Afterwards the different criteria of the trade-off will be discussed. The important characteristics of the candidates are going to be determined and these will be the base on which the trade-off will be performed. In section 6.3.2.3 the importance of each criteria will be determined. The last section will give a summary of the entire trade-off with the corresponding results.

6.3.1 Pruning of the EPS design option structure

In the next section the design option tree for the EPS will be pruned. The design option trees for the power source, storage, distribution and regulation and control will be dealt with individually in sections 6.3.1.1, 6.3.1.2 and 6.3.1.3 respectively.

6.3.1.1 Power Source

Fuel cells have a high specific energy density but were not taken into account as a feasible power source because the amount of reactant they would have to bring for a long term mission is too large for microsatellites. Primary batteries were equally unfeasible because of their limited lifetime, which is in the order of minutes to months. Radio isotopes and nuclear fission reactors were discarded because of their high cost and low specific power, as were thermionic and thermoelectric conversion for static power sources. This leaves photovoltaics and concentrated solar radiation together with an engine in a thermodynamic power cycle.

The pruned design option tree for the powersource can be seen in figure 6.4

6.3.1.2 Power Storage

The only obvious candidate for power storage was secondary batteries because, as mentioned before, the lifetime of primary batteries is too short. Of the most common secondary batteries, sodium-sulfur batteries are not an option for us because their operating temperature at 350 degrees Celsius is too high.

The pruned design option tree for the power source can be seen in figure 6.5

6.3.1.3 Power Distribution, Regulation and Control

For the power distribution, regulation and control there were no obvious non-candidates. Because the power distribution, regulation and control depend on the type of power source, which depends on the payload power requirements, pruning will be done later on after these subsystems have been chosen — this is done in the tradeoff.

The design option tree for the powersource can be seen in figure 6.6

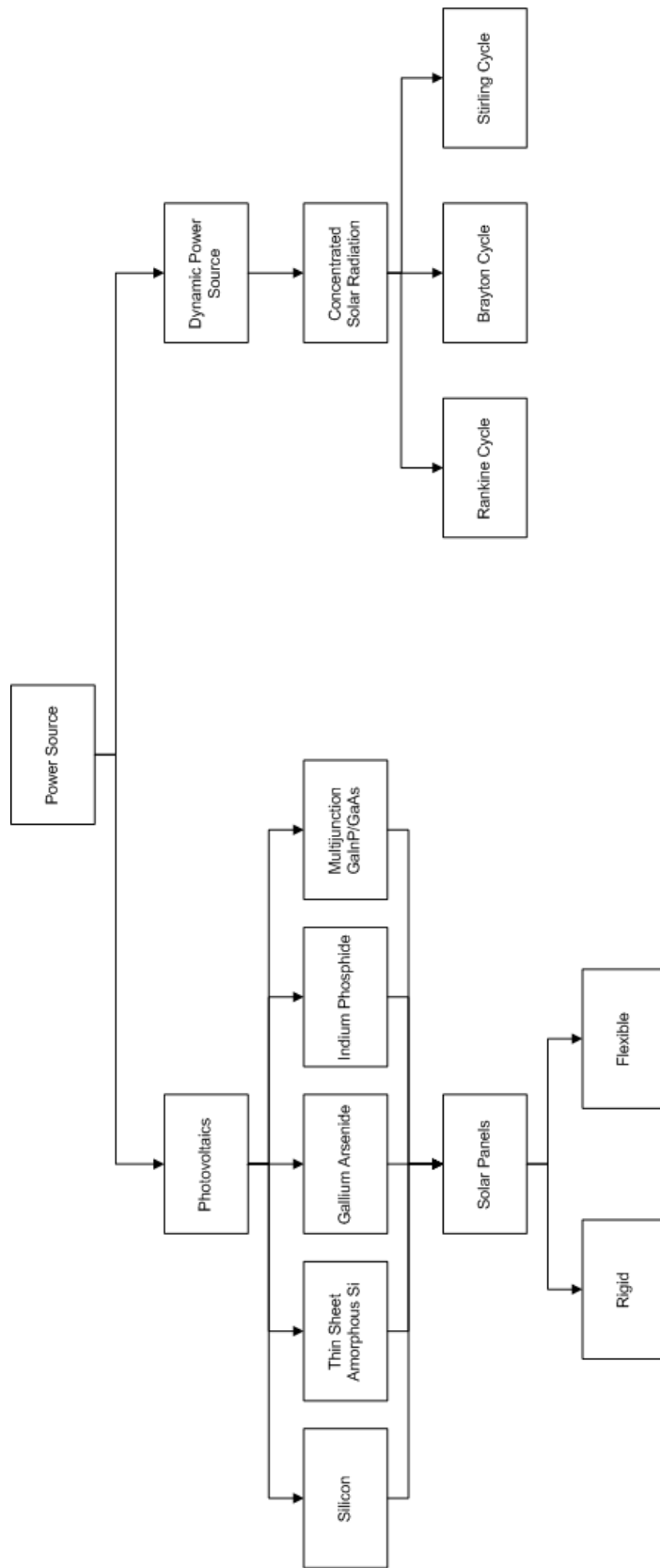


Figure 6.4: The pruned design option tree for the power source

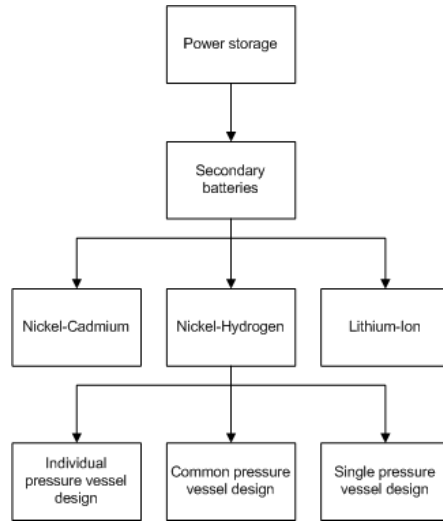


Figure 6.5: The pruned design option tree for the power storage

6.3.2 Trade method rationale and organization

In this section the question of how the trade-off is done will be answered. First some additional information of the two options for the trade-off are given and afterwards the method and organization itself will be discussed. After the pruning of the design option structure the only candidates left were photovoltaics and concentrated solar radiation together with an engine in a thermodynamic power cycle. After some further research the option of using concentrated solar radiation was also discarded. Almost no information was found about that kind of powersource for use in space. Therefore it was decided to abandon this kind of power source because without any data or information it will not be possible to determine if that option is feasible. So that leaves only photovoltaics. Solar cells come in a lot of different types. The most common are crystalline solar cells, multijunction cells and thin film solar cells. Soon it was clear that crystalline would not be a good option. Multijunction cells have a higher efficiency while thin film cells have a lower mass and production cost. Because the efficiency, mass and production cost are the most important characteristics and crystalline solar cells do not excell in any of these areas (compared to multijunction and thin film cells), they will not be considered as an option for the power source.

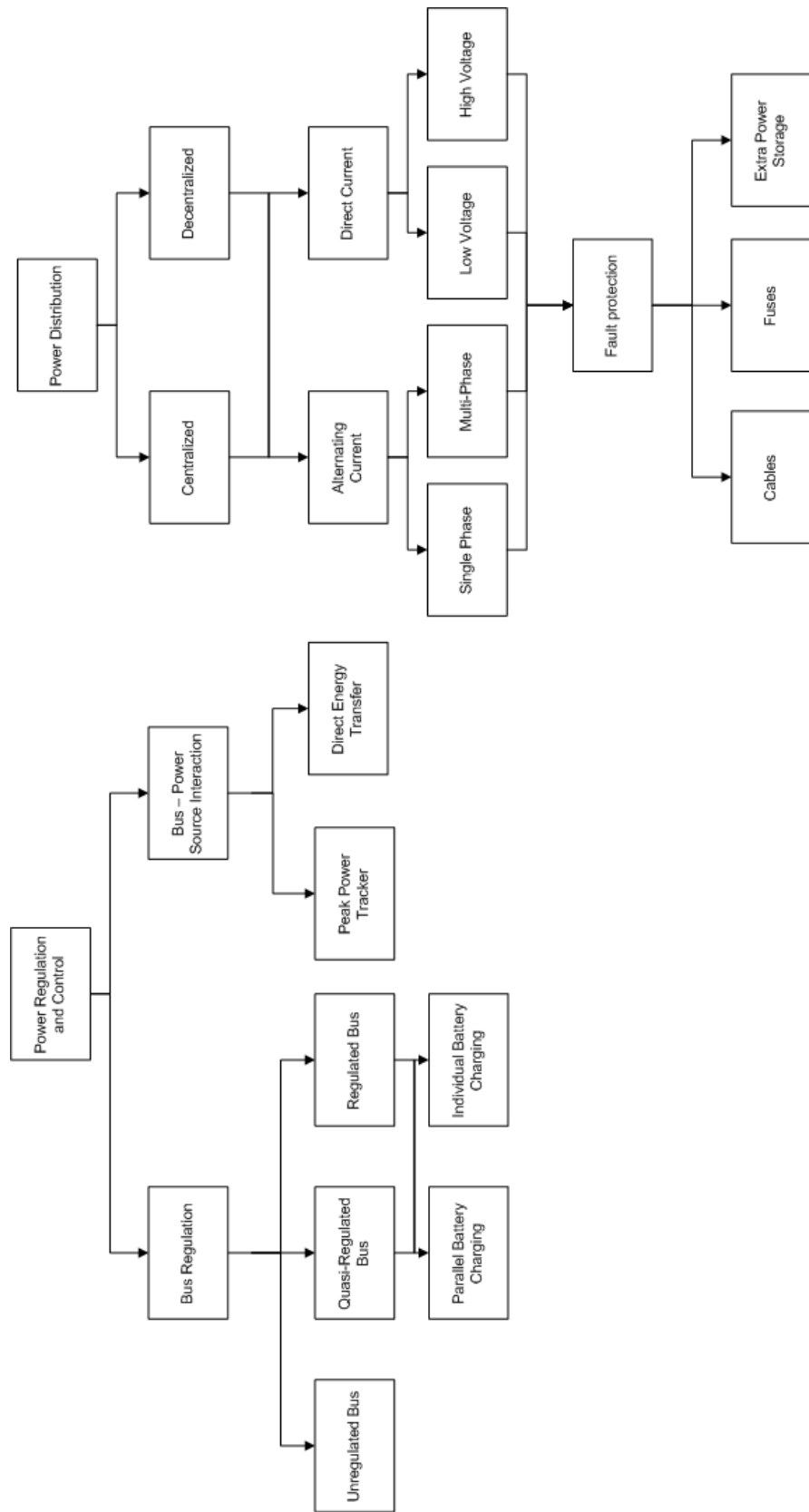


Figure 6.6: The design option tree for the power distribution and regulation and control

6.3.2.1 Multijunction solar cells

A solar cell converts solar energy to electrical energy. When a photon hits the surface of a solar cell it is either reflected or transmitted. If it is transmitted the energy it contains will excite an electron from the valence band to the conduction band. In the conduction band they have a higher energy than in the valence band, which allows them to move around. This happens in a so called pn-junction. Single crystalline solar cells have only one pn-junction whereas multijunction ones have more than one. Each pn-junction has a certain bandgap, depending on the material of the junction. The bandgap is the difference between the valence band and the conduction band.

This means that if a certain material has a bandgap of one electronvolt, one electronvolt of power needs to be given to an electron for it to be able to go from the valence band to the conduction band. From this it follows that one pn-junction will be able to use only part of the solar spectrum. Multijunction cells use several pn-junctions connected in series so that a larger part of the solar spectrum can be used.

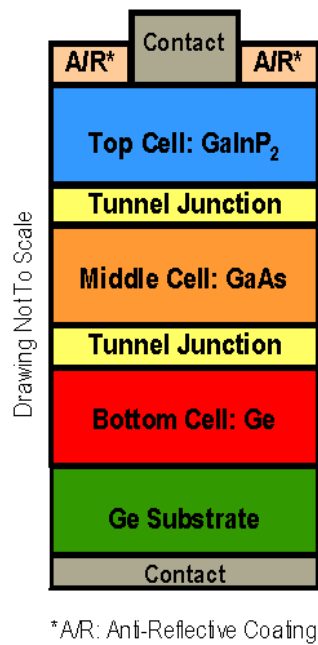
Figure 6.7 gives a schematic representation of a triple-junction solar cell [SPECTROLAB()]. The metallic contacts in aluminium are low resistivity electrodes that transfer the current from the solar panel to the power grid. They are present on the two sides of the structure but mainly on the backwards face so that the shadowing on the lit surface is reduced.

The anti-reflective coatings are primarily used to increase the transmission of the photons and correspondingly decrease the reflectance at the wavelengths that will be used.

Tunnel junctions provide a low electrical resistance and optically low-loss connection between two subcells. Without them, the p-doped region of the top cell would be directly connected with the n-doped region of the middle cell. Hence, a pn junction with opposite direction to the others would appear between the top cell and the middle cell. Consequently, the photovoltage will be lower. Tunnel junctions decrease this negative effect.

In figure 6.7, the three materials for the pn-junctions that were used are Gallium-Indium-Diphosphor, Gallium-Arsenide and Germanium. These three pn-junctions cover a larger part of the solar spectrum than single junction solar cells, making them more efficient.

Figure 6.8 [N.V.Yastrebova(2007)] shows the range of wavelengths that each junction of a triple-junction cell absorbs. From this picture it is clear that multiple pn-junctions cover a far larger part of the solar spectrum than one single pn-junction.



*A/R: Anti-Reflective Coating

Figure 6.7: Schematic representation of a triple-junction solar cell

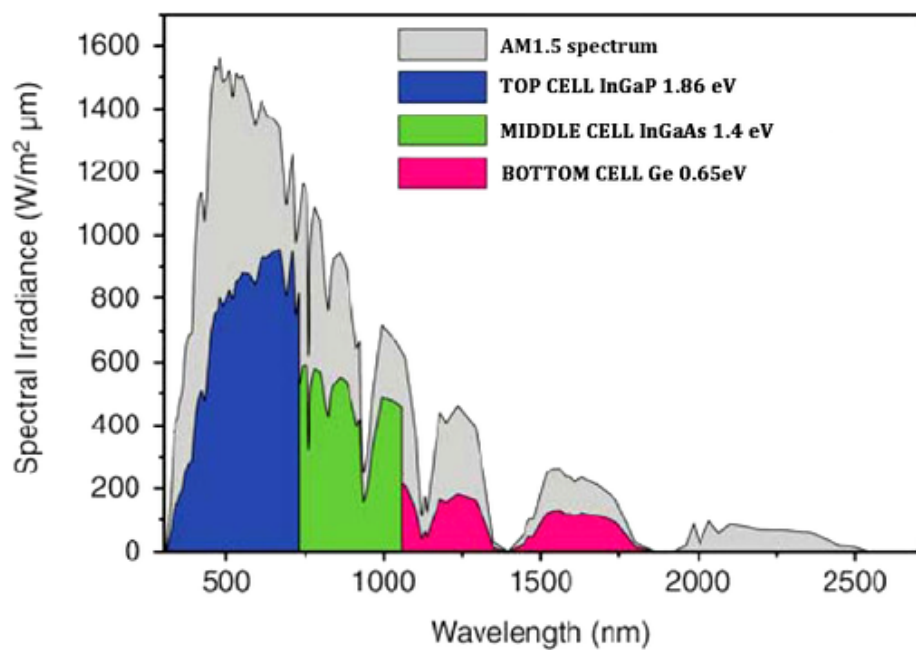


Figure 6.8: Spectral irradiance of a triple-junction solar cell in function of the wavelength

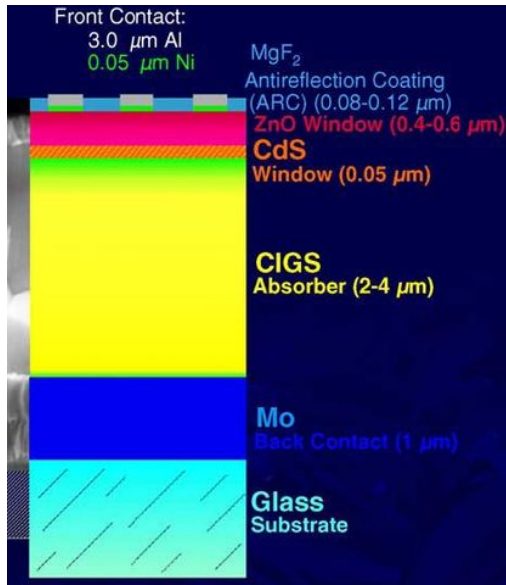


Figure 6.9: Schematic layout of a thinfilm CIGS solar cell

6.3.2.2 Thin film solar cells

Thin film solar cells are created by depositing one or more thin layers of photovoltaic material on a substrate. The thickness range of such a layer is wide and varies from a few nanometers to tens of micrometers. An example of a thin film solar cell shown in figure 6.9. Here the Copper Indium Gallium Selenide (CIGS) cell is shown. Glass is commonly used as a substrate. A molybdenum layer is deposited which serves as the back contact and to reflect most unabsorbed light back into the absorber. The absorberlayer is a p-type layer. The most efficient absorber is a so called CIGS absorber. It is a direct bandgap semiconductor with the highest absorption coefficient of all solar cells. Copper Indium Gallium Selenide are the materials of the four thin layers of which it consists. A thin n-type buffer layer is added on top of the absorber. The buffer is overlaid with a thin, intrinsic Zinc-Oxide layer which is capped by a thicker, Aluminum doped Zinc-Oxide layer. Despite increasing the series resistance, the Zinc-Oxide layer is beneficial to cell performance. The Aluminum doped Zinc-Oxide serves as a transparent conducting oxide to collect and move electrons out of the cell while absorbing as little light as possible [Dhere()].

6.3.2.3 Trade off method and rationale

Now that the two candidates are known, the preparation of the trade-off can begin. Thin film CIGS cells and triple-junction cells will be compared with each other with respect to certain criteria (i.e. cost, mass,...). For every criterium each candidate will receive points on a scale from one to ten, with ten being the highest. Each criterium will get a weight factor, depending on how important it is. To determine which solar cell type is the best, their points for each criterium will be multiplied with that criterium's weight factor. All these results will be added and the candidate with the highest total of points will be the best candidate for the mission. The first thing to do is to determine which criteria will be used. Efficiency, mass and cost are the three most important characteristics for the solar cells. They are also the ones that can deviate the most between different types of solar cells. Furthermore also the packing factor, degradation, solar cell height and resistance to vibrational noise during launch are trade-off criteria.

The three most important characteristics, mass, cost and efficiency, are all given a weight factor of ten. The degradation of the cells is also an important criterium. A large degradation factor will increase the solar array area dramatically, especially for missions lasting a couple of years. Therefore its weight factor will be eight. The height of the cells influences the space each satellite needs when being launched. It could mean the difference of having an extra satellite per launcher, so it also is important. It received a 7 for its weight factor.

When considering a solar panel, not the whole panel is filled with solar cells. Part of it is taken up by wiring, the metal contacts of the cells, the loss in area because of the shape of the cells, ... All these factors are bundled in the packing factor. The higher the packing factor, the less solar array area is needed. Its weight is 7.

During take-off, the launcher and its payload experience large vibrational loads. The solar panels of the satellites need to be able to resist these loads. If they are affected too much by it some cells might be damaged, resulting in less power generation. The weight factor in this case is five. This is on the low side, because these vibrational loads will not be really destructive.

6.3.3 Trade-off summary

In this section the summary of the trade-off process and the results will be discussed. For all the trade-off criteria, except for the resistance to vibrational loads, the marks each option receives are based on hard numbers. The candidate with the best characteristics will receive a ten and the other candidates marks are a fraction of that ten, based on the actual data. For example, if option 1 has a cost of 100 euros per watt, and option 2 costs 250 euros per watt, example 1 will receive a 10 for the criteria cost and example 2 will receive a four.

Table 6.3 lists the marks both candidates received and also their totals. From this it is obvious that the thin film CIGS is the better candidate for our mission.

The chosen thin film CIGS solar cells were developed by Dutch Space. They are some of the best available and have been proven in flight with the Delfi-C3 satellite. For the triple-junction cells those developed by AzurSpace were chosen. They are also one of the most efficient multijunction cells currently on the market and have been proven in flight. The data gathered for use of the exact numbers was taken from those two sources.

The efficiency of the CIGS cells is about 12% and that of the triple-junction cells is 28%. This gives scores of ten and four respectively. The mass of the cells are 240g/m² and 850g/m², resulting in a ten and a three for the thin film CIGS and the multijunction respectively. Degradation is low for both options, but the thin film CIGS has almost no open current and open voltage degradation, giving it a ten and the multijunction a nine. Average values of the packing factor found in the literature were used for the trade-off.

	Weight Factor	Candidates	
		Thin film CIGS	Triple-junction
Efficiency	10	4	10
Mass	10	10	3
Cost	10	10	4
Degradation	8	10	9
Packing Factor	7	8	8.5
Resistance to vibrational loads	5	8	6
Cell Height	7	10	2
Total		486	345.5

Table 6.3: Trade-off table for the power source

The found values were 80% and 85%, resulting in grades of eight and eight and a half. The height of the thin film CIGS cells is about $20\mu m$ giving it a ten. The triple-junction cells have a thickness of about $150\mu m$, giving it a two. The grading of the resistance to vibrational loads was not done by comparing values because there are none available. It is known that stiffer panels have less resistance to vibrational loads than flexible panels, giving the thin film CIGS an advantage. This results in an eight for that type of cells and a six for the multijunction cells.

The data in the paragraph above was taken from [ESA-DutchSpace(2007)], [Delfi-C3(2010)], [DutchSpace(2007)], [SPECTROLAB()], [cub(2010)] and [solar energy GmbH(2010)].

For the power storage in the form of secondary batteries no real trade-off was needed. Nickel-Hydrogen batteries have been used extensively over the past years, but recently Lithium-Ion batteries have been tested for space application. Their specific energy can be up to three times as high as Nickel-Hydrogen batteries. It has been proven that, when kept within a certain temperature range, they have the same performance in space as on Earth [Shelley Brown(2008)]. This is why Lithium-Ion batteries are chosen for power storage.

6.4 Orbit Analysis

This section is about the trade-off for the orbit characteristics. First the orbit design options are compared with the killer requirements. After that the section is split into two major pieces, one containing special orbits and the altitude of the orbit, and another one that considers the swarm in greater detail.

6.4.1 Eliminating the obvious losers

The orbits of the satellites are determined by the characteristics of the emitter and receivers. Because the payload uses a low power laser this means that the orbits will have to be LEO in order for the receivers to receive enough, or any, photons. The resulting design option tree can be found in figure 6.4.1, on page 52. Further pruning is not possible without a detailed analysis of the remaining options, which is done in the following section.

6.4.2 Analysis of the remaining options

In subsection 6.4.1 the design option tree was pruned by comparing the orbit altitudes with the altitude requirement that follows from the payload. As a result the MEO, GEO and HEO were eliminated. The remaining options will now be analyzed.

No trade-off table will be made for this section. Instead the four special types of orbits seen in figure 6.4.1 will be compared with the mission requirements and eliminated separately. The four orbit types are polar orbit, sun synchronous orbit, repeating ground track orbit and frozen orbit. After that another section will investigate preliminary parameter values for the final design option.

6.4.2.1 Polar orbit

An orbit is a polar orbit if the orbit inclination is exactly 90 degrees. However, it is not uncommon for an orbit to be classified as a polar orbit if the inclination is close to 90 degrees. For the case of the laser swarm it is assumed that an orbit is a polar orbit if the inclination is between 80 and 100 degrees.

The laser swarm should be able to observe any region on Earth, including the poles. As such the final orbit design option has to be a polar orbit.

6.4.2.2 Sun Synchronous orbit

A sun synchronous orbit is an orbit that uses the fact the Earth is not a perfect sphere, thus allowing a satellite to orbit the planet in such a way that the plane of the orbit rotates around the Earth's polar axis exactly once a year. Thus fixing the satellite's orbital plane with respect to the sun vector.

While providing useful conditions, it is not required for the swarm to use this kind of orbit unless certain power or lighting requirements have to be met, as the simulation has shown this to be unnecessary the final orbit design will not be sun synchronous.

6.4.2.3 Repeating ground track orbit

Repeating ground track orbits, or in short repeat orbits, are orbits that repeat after a predefined amount of time after the satellite has traveled an integral amount of revolutions. This type of orbit is useful as it allows one to revisit the same area, thus making it possible to view an area at different times. Which may provide useful information on variables that change over time. To determine if it is an option for the laser swarm, a calculation is made to check whether the constellation can actually see the entire Earth in five years.

The Earth circumference is 40.000 [km], now assuming a footprint of 100 [m] this means that it will take $40.000.000 / (2 * 100) = 200.000$ revolutions to see all of this 40.000 [km]. Note that the factor 2 arises from the Earth being a sphere, thus the satellite sees the equator twice during a single revolution. Assuming a very low orbit of 300 [km] with a period of 90 [minutes]([Wertz(2006)]) the time taken for these 200.000 revolutions is $200.000 * 90 = 1.800.000$ [minutes]. This is equal to approximately 34 years.

From the previous calculation it is clear that a repeat orbit is undesirable as it would mean even less of the Earth surface is covered in the 5 year lifetime. Also the type of sensor used, a SPAD array, can oversample an area when viewing it.

6.4.2.4 Frozen orbit

A frozen orbit is an orbit for which the time rate of change of the inclination, eccentricity and argument of perigee are equal or close to zero. These conditions are favorable as they reduce the amount of stationkeeping, thus reducing the need for attitude control. This in turn means less fuel which makes the structure lighter, etc. This setup is very advantageous to the laser swarm as the formation has to remain the same, and because many satellites have to be launched even a small weight reduction will have significant effect on the total weight. For these reasons the frozen orbit is also a design choice.

6.4.3 Preliminary Orbit Parameters

The resulting design choice for the laser swarm is a frozen polar orbit. In this section some of preliminary values for the six orbital elements will be determined, using the constraints given by 6.3.

$$\frac{d\omega}{dt} = 0, \quad \frac{di}{dt} = 0, \quad \frac{de}{dt} = 0, \quad 80 \text{ [deg]} \leq i \leq 100 \text{ [deg]} \quad (6.3)$$

The equations used to make an orbit a frozen orbit are given by 6.4 for the time derivative of the eccentricity, 6.5 for the time rate of change of the eccentricity and finally 6.6 for the time rate of change of the argument of perigee. Note that 6.7 is a continuation of 6.6. The terms n and p in these equations represent the mean motion and semiparameter respectively, and are given by equations 6.8 and 6.9.

$$\dot{e} = \frac{3}{2} \frac{J_3 r_{eq}^3}{p^3} (1 - e^2) n \sin i \cdot \cos \omega \left(\frac{5}{4} \sin^2 i - 1 \right) = 0 \quad (6.4)$$

$$\frac{di}{dt} = \frac{3}{2} \frac{J_3 n}{(1 - e^2)^3} \left(\frac{R_e}{a} \right)^3 e \cos i \cdot \cos \omega \left(\frac{5}{4} \sin^2 i - 1 \right) = 0 \quad (6.5)$$

$$\dot{\omega} = \frac{3 J_2 n}{(1 - e^2)^2} \left(\frac{R_e}{a} \right)^2 \left(1 - \frac{5}{4} \sin^2 i \right) F \quad (6.6)$$

$$F = 1 + \frac{J_3}{2J_2(1-e^2)} \left(\frac{R_e}{a}\right) \left(\frac{\sin^2 i - e^2 \cos^2 i}{\sin i}\right) \frac{\sin \omega}{e} \quad (6.7)$$

$$n = \sqrt{\frac{\mu}{a^3}} \quad (6.8)$$

$$p = a(1 - e^2) \quad (6.9)$$

Before investigating these equations the eccentricity is set equal to zero, the reason for this is that the mirrors or lenses on the satellites do not have to refocus and it allows for easier data handling. The result is that equation 6.5 is automatically satisfied for any inclination, eccentricity, argument of perigee and semimajor axis. So the orbit is frozen w.r.t. the inclination.

Another effect caused by setting the eccentricity to zero is that the argument of perigee can not be distinguished from another point in the orbit. While it would still indicate the perigee, it is meaningless because the orbit is circular. As such the argument of perigee assumed to be able to take any value and so is set equal to 90 degrees, resulting in $d\omega/dt$ to become equal to zero for any inclination and altitude.

Figures 6.4.3 shows the only remaining condition for a frozen orbit for several values of inclination. From this figure and equation 6.6 it can be seen that $d\omega/dt$ is equal to zero if the inclination is equal to 63.43 [deg]. However the constraints (6.3) indicate this is not a possibility. Figure 6.4.3 shows that $d\omega/dt$ is maximal at 90 degrees inclination, however the difference between $i=80$ [deg] and $i=90$ [deg] is only 0.5 [deg/day]. As a result the extra 0.5 [deg/day] is considered an acceptable loss compared to the increased coverage provided by the increased inclination. However an inclination of 90 [deg] creates problems with collision avoidance for the swarm, so instead an inclination of 85 [deg] is chosen. This allows for an almost complete coverage and a small decrease in the value of $d\omega/dt$, as seen in figure 6.4.3. Note that an inclination of 85 [deg] is chosen instead of an inclination of 95 [deg] is that 85 [deg] inclination means the orbit is prograde, which reduces the required ΔV . Equation 6.6 indicates that the rate of change for the argument of perigee is the same.

Summarizing the results so far yields that the inclination is equal to 85 [deg], the eccentricity is equal to 0 [-], and the argument of perigee is equal to 90 [deg].

6.5 Orbit Altitude

During the design of the orbit, very careful attention has to be given to the choice of the mission altitude for the entire formation. This parameter is vital for the lifetime requirement.

Initially it was apparent that the choice of the emitting payload would give a hard altitude constraint, however as described in section 6.7.4, with the use of complex optical instruments it was possible to open a wider range of altitudes for selection. The governing properties of the orbit for altitude selection have now become the orbit perturbations.

This section details the considerations in regards to these properties. A separate radiation exposure analysis is also done. Finally a suitable altitude is chosen based on this analysis.

6.5.1 Earth Oblateness

The perturbation sensed by the satellite due to Earth's oblateness effect only influences the rate of precession of the orbit which is given in the following equation:

$$\dot{\Omega}_{J_2} = -1.5nJ_2(R_E/a)^2(\cos i)(1-e^2)^{-2} \quad (6.10)$$

The rate of precession is a function of the semi-major axis, however $\dot{\Omega}_{J_2}$ does not affect altitude directly.

6.5.2 Perturbations due to other Celestial bodies

The gravitational forced of other celestial bodies like the Sun and the moon cause periodic variations in all orbital elements, however in LEO these perturbations are very minor (and above all are constant for formations) relative to atmospheric drag, thus will not be considered in this report.

6.5.3 Solar Radiation Pressure

All orbiting bodies are affected by solar radiation pressure. The acceleration due to this phenomenon can potentially affect stationkeeping of the swarm if all satellites have different cross-sectional areas normal to the sun. This perturbation is not directly related to orbit altitude, however it is an important step in orbit analysis. In figure 6.12 on page 53, the relationship between the acceleration and the normal area to the sun for different satellite masses is shown. Similarly, a graph relating the mass to the acceleration for different cross-sectional areas is shown in figure 6.13 on page 53.

These figures present design boundary overviews and a general feeling of behavior due to solar radiation pressure is shown. The inverse relationship is obvious. In order to minimize this perturbation it is required to have high mass while retaining the smallest possible area normal to the sun.

What is important to note is that if the ratio of area to mass could be maintained constant between the emitting and the receiving satellites, then they would experience the same perturbation, which is a favorable condition. Acceleration with respect to this area/mass ratio can be seen in figure 6.14 on page 54.

	Total Mass	Max. Area
Emitter	119	2.5
Receiver	10.7	0.2

Table 6.4: Mass and area estimates

Based on preliminary mass and area estimates shown in table 6.4 on page 48, it is estimated that the both the emitter and the receiver platforms will experience a deceleration in the order between 10^{-9} and 10^{-10} . While these values might not seem significant at first, especially relative to atmospheric drag (see section 6.5.4), they will become relevant for stationkeeping as explained earlier.

6.5.4 Atmospheric Drag

Atmospheric drag is by far the most relevant perturbation for LEO satellites. It directly relates to mass as it influences the amount of fuel required to maintain the orbit, whereas the mass influences the rate at which the orbit decays. Altitude selection relies heavily on estimation and analysis of drag data as for longer mission times, higher altitudes are preferred, while optical instruments prefer lower altitudes for increased accuracy.

The drag that the satellite experiences due to atmospheric density is described by the following formula:

$$D = -\frac{1}{2}C_D \rho V^2 A \quad (6.11)$$

It follows that orbital parameter changes (semi-major axis, period and velocity respectively) per orbit are calculated using the following equations (assuming negligible eccentricity):

$$\Delta a = -2\pi \left(C_D \frac{A}{m} \right) \rho a^2 \quad (6.12)$$

$$\Delta P = -6\pi \left(C_D \frac{A}{m} \right) \rho \frac{a^2}{V} \quad (6.13)$$

$$\Delta V = \pi \left(C_D \frac{A}{m} \right) \rho a V \quad (6.14)$$

The fundamental problem with accurately predicting effects due to atmospheric drag is twofold: firstly it is very hard to predict the satellite's ballistic coefficient:

$$\frac{m}{AC_D} \quad (6.15)$$

Even with a well known mass to area ratio, the coefficient of drag can be highly variable, highly dependent on the shape of the satellite and its orientation with respect to the velocity vector. Throughout the following analysis a C_D of 4 has been used as a worst-case scenario. This value is representative of a flat plate traveling with its normal vector pointing in the direction of velocity. In reality this drag coefficient changes. The cross-sectional area normal to the velocity vector can also vary for the swarm satellites if the whole platform is reoriented for instrument pointing. The whole ballistic coefficient typically ranges from about 25 kgm^{-2} to 100 kgm^{-2} . The satellites being considered, at this early stage in the design process, have a much lower coefficient - in the range of 10 kgm^{-2} .

The second reason drag calculations are so unreliable, is because air density at any altitude is highly variable. Raising air density is primarily connected with solar activity. As solar activity increases every 11 years (see figure 6.15 for recorded and predicted solar activity), the atmosphere heats up. Contrary to conventional gas laws that would dictate a fall in density as the gas expands, the atmosphere simply rises, increasing density at higher altitudes.

The density difference during maxima and minima for different altitudes is shown in figure 6.16. Depending on the altitude, the density could vary for up to a whole order of magnitude between the minimum and maximum.

Orbit decay periods for the emitter and receiver satellites are shown in figures 6.17 and 6.18 respectively. The Orbit decay is calculated using equations 6.12 - 6.14. Orbit maintenance is not taken into account. The time range considered is a 5 year mission lifetime. The basis for the receiving satellite sizing was taken to be around 0.2 m^2 (based on preliminary sizing). The mass of the said satellite was the same as in table 6.4 on page 48. The emitter satellite is sized to be about 2.5 m^2 frontal area (including solar panels and communications arrays). The mass is again taken from table 6.4.

From the analysis of the orbit decay it is strikingly obvious how important the solar activity is during mission lifetime. Even at an altitude of 500 km neither satellite would be able to maintain its orbit for more than a 100 days. From this analysis it is clear that substantial orbit maintenance is required as the satellites will most probably not have refocusing equipment for the optical instruments. A more comprehensive idea of the orbit maintenance can be gathered from total ΔV estimations shown in figures 6.19 and 6.20 (pages 58 and 59) and tabulated in table 6.5 on page 50. This is the total velocity change required to keep the satellites in a certain circular orbit. The calculations are based on equation 6.14.

Altitude	SOLAR MIN			TIME AVERAGE			SOLAR MAX		
	300	400	500	300	400	500	300	400	500
EMITTER	3240.95	285.39	34.50	7716.55	1060.48	187.88	15670.53	2943.61	691.58
RECEIVER	2883.54	253.92	30.70	6865.56	943.53	167.16	13942.38	2618.99	615.32

Table 6.5: Required ΔV for various orbit altitudes for a 5 year mission. In m/s .

It can be clearly seen that ΔV budget is almost five times larger at low altitude at solar maximum when compared to the solar minimum. Overall the values for ΔV at high altitudes, at solar minimum and time average look very favorable.

Three important conclusions can be drawn from the preceding analysis:

- In order to avoid fast orbit degradation, and in turn greater mass due to propellant necessary to maintain orbit, the satellites should be placed as high as it is allowable by optical instruments. Based on drag analysis it is recommended to inject at 500 ± 25 km.
- The launch timeframe should be designed in such a way that the mission halftime falls under the solar minimum to reduce drag. This will also allow for a reduction in mass.
- The area/mass ratio for the emitter and receiver satellites should be designed as equivalent as possible. This will allow for slower constellation decay and for generally better stationkeeping.

Simulations of photon returns at different altitudes can be found in the Simulation chapter.

6.5.5 Exposure to Particle Radiation

In space, satellites are exposed to streams of highly energetic charged particles coming from the sun. Radiation from these particles can cause severe damage to satellite subsystems, including the payload. The main particle radiation source encountered by the swarm in the LEO comes from the Van Allen Belts. These are regions around the Earth where charged particles (protons, electrons and ions) are trapped inside the magnetic field of the planet.

The total radiation dose consists of three components: proton dose, electron dose and the so-called Bremsstrahlung X-Ray dose produced by the interaction between the electrons and the shielding material of the satellite. In LEO, energetic protons in the inner radiation belt contribute most to the total radiation dose. This total is also strongly linked to the orbital altitude and below 1000 km will increase at approximately by the 5th power of the altitude. Furthermore, just like with atmospheric drag, the solar activity plays a major role, thus all cases will be examined.

The number of particles trapped in the Van Allen belts in the vicinity of the orbit under question can be modeled using The Space Environment Information System (SPENVIS) that can be located at the following address: <http://www.spenvis.oma.be/>. SPENVIS contains a large array of NASA and ESA (as well as other) tools and models for complex orbit analysis. For the purposes of this evaluation two models are used: AP-8 and AE-8. The first model predicts proton flux with energy levels above 100 MeV. The latter estimates the flux of electrons with energy of 0.5 MeV or above.

Figure 6.21 on page 60 illustrates the trapped proton flux for solar minimum and maximum as a function of distance from Earth Center. It is evident that in LEO, the proton flux stays relatively static w.r.t. solar activity. For the considered altitudes of 300 to 500 km (1.047 to 1.078 Earth radii) the satellites would encounter relatively the same order of magnitude of proton radiation. It is also evident that any higher

PARAMETER	VALUE
Apogee [km]	500
Perigee [km]	500
Inclination [deg]	85.00
R.A.A.N. [deg]	0.00
Argument of Perigee [deg]	90.00
True Anomaly [deg]	0.00
Period [hrs]	1.57
Revolutions per day	15.18
Maximum eclipse [min]	35.75
Semi-major axis [km]	6871
Eccentricity [-]	0.00
Mean motion [rad/day]	95.78
Integration step [deg]	0.50
Node spacing [deg]	23.72
Circular velocity [km/s]	7.613
Angular velocity [deg/min]	3.805
ΔV required to deorbit [m/s]	-129.8

Table 6.6: Parameters of the base orbit for the emitter satellite.

altitude would mean a substantial increase in bombardment and hence reduction in the reliability of the subsystems.

Figure 6.22 on page 61 illustrates the trapped electron flux for solar minimum and maximum as a function of distance from Earth Center. It is evident from this figure that lower altitudes would considerably reduce the radiation flux (up to one order of magnitude).

Based on this data, the following conclusion emerges: while altitudes of around 500 km remain relatively safe, a lower orbit will result in a lower particle radiation flux, increasing reliability. Altitudes above 500 km become more and more dangerous for the mission.

6.5.6 Final Orbit Parameters

From the above sections it is possible to compile a list of orbit parameters for the base emitter orbit. All other orbits will be designed relative to this one. Figures 6.23 and 6.24 display the look of the orbit in 3D and a representative ground track, respectively. The images were generated using the AGI Satellite Tool Kit (STK).

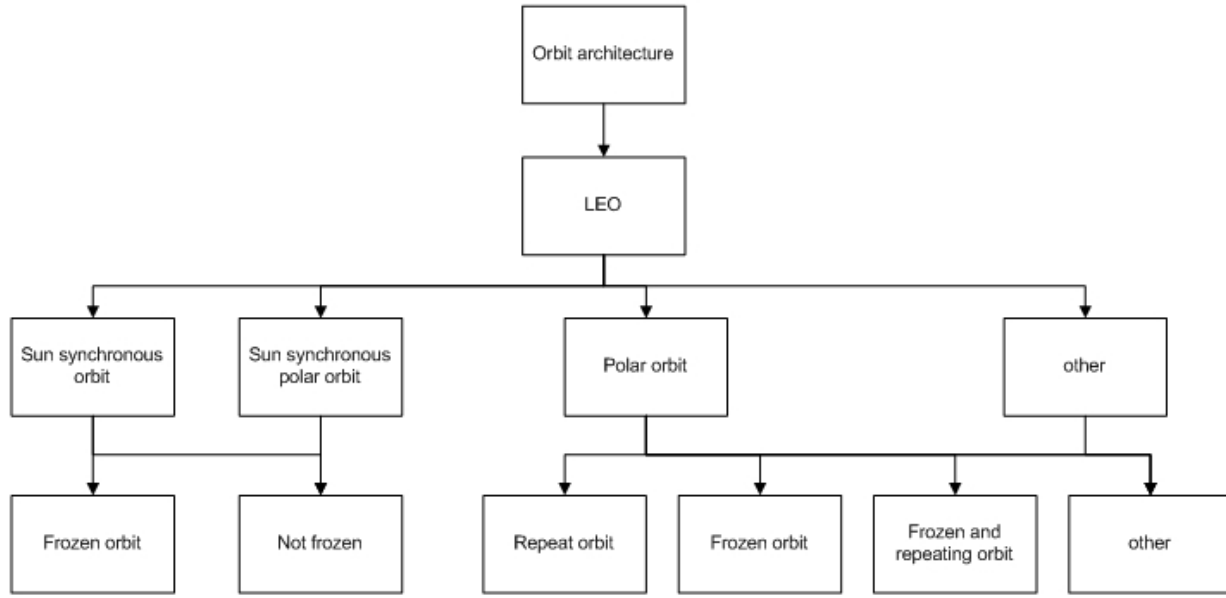
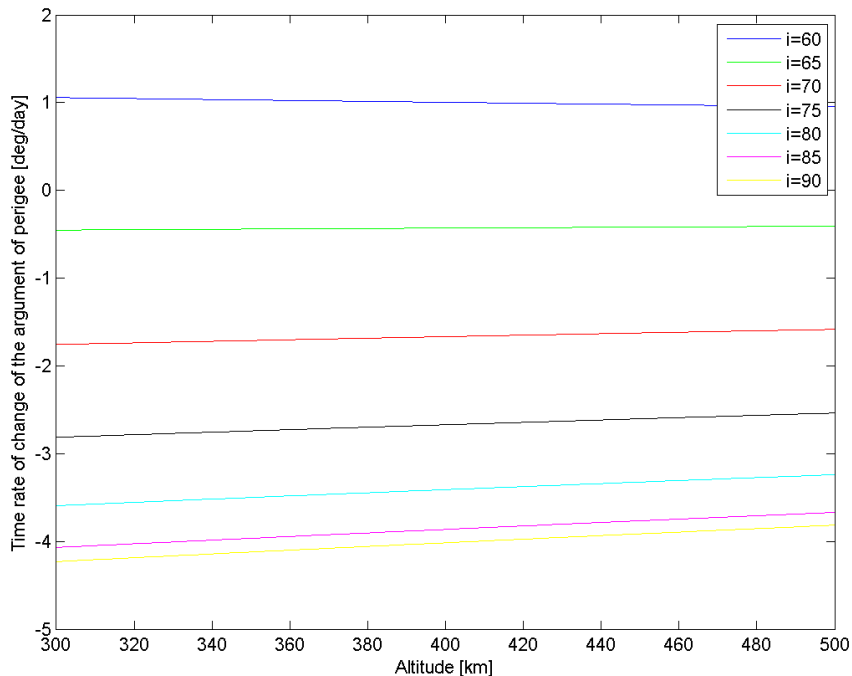


Figure 6.10: Pruned design option tree for the orbit characteristics

Figure 6.11: $d\omega/dt$ for a range of altitudes and several different inclinations.

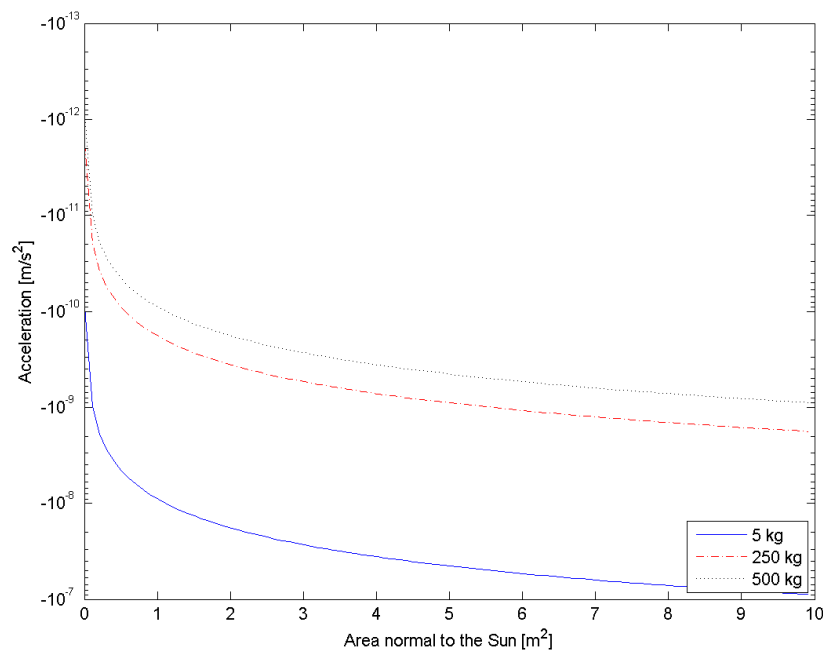


Figure 6.12: Acceleration due to solar radiation pressure vs. area normal to the sun, for different satellite masses.

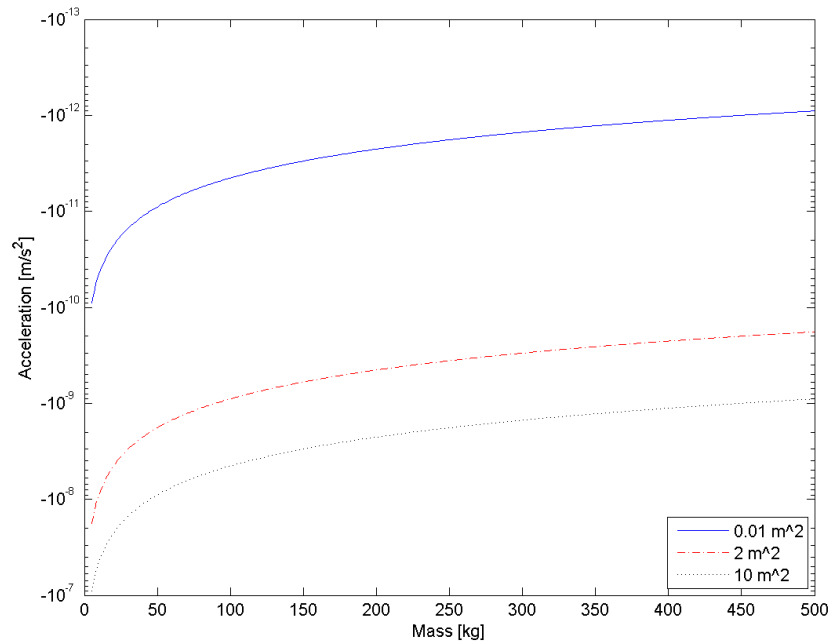


Figure 6.13: Acceleration due to solar radiation pressure vs. mass, for different areas.

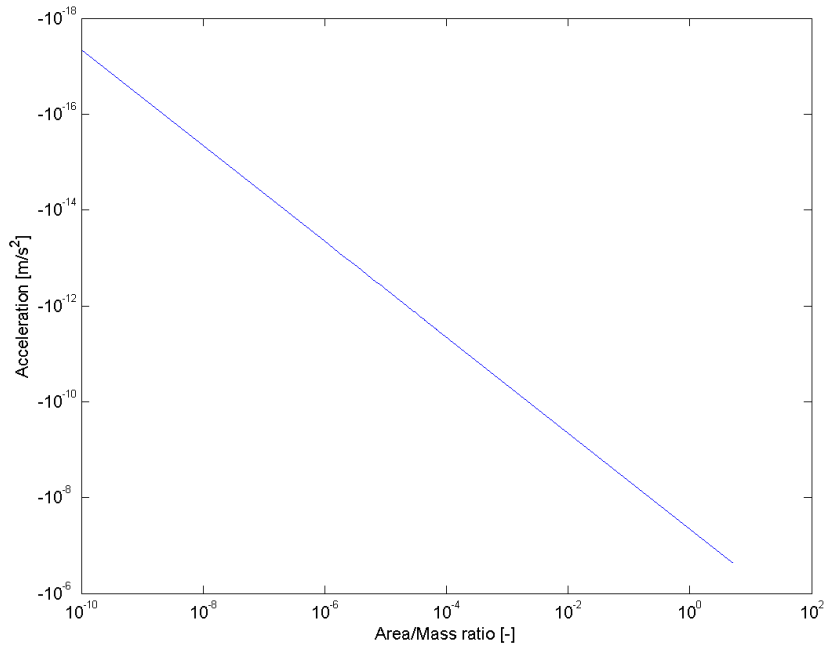


Figure 6.14: Acceleration due to solar radiation pressure vs. Area/Mass ratio.

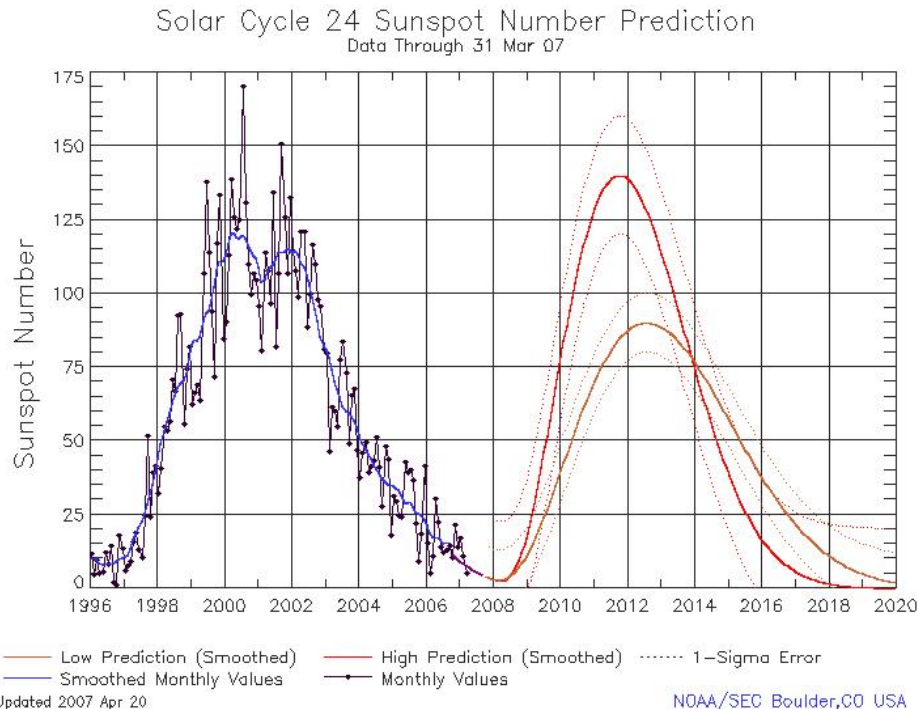


Figure 6.15: The solar cycle, clearly showing the solar maxima at 11 year intervals. Data after 2007 is projected. *Source: NASA*

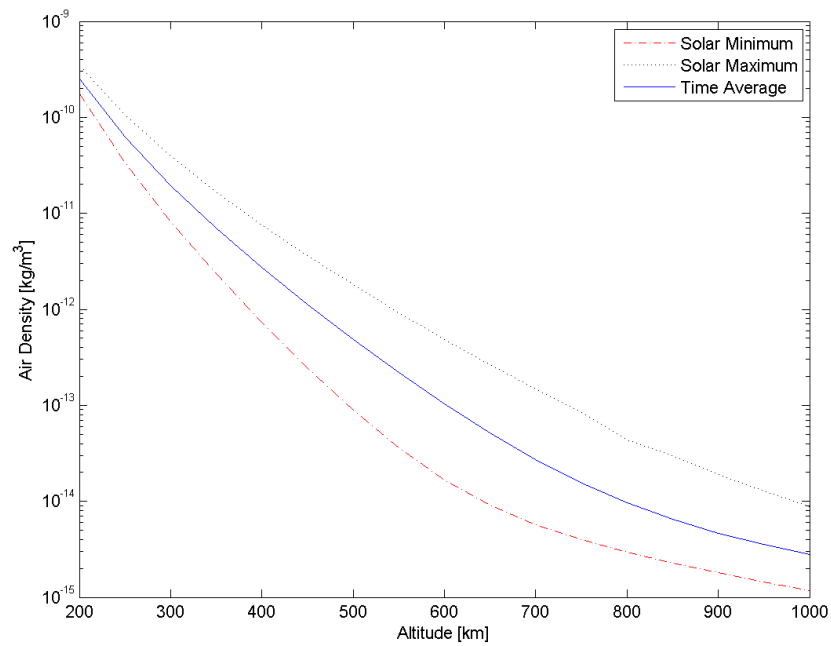


Figure 6.16: Air density vs. orbit altitude for different solar cycle stages.

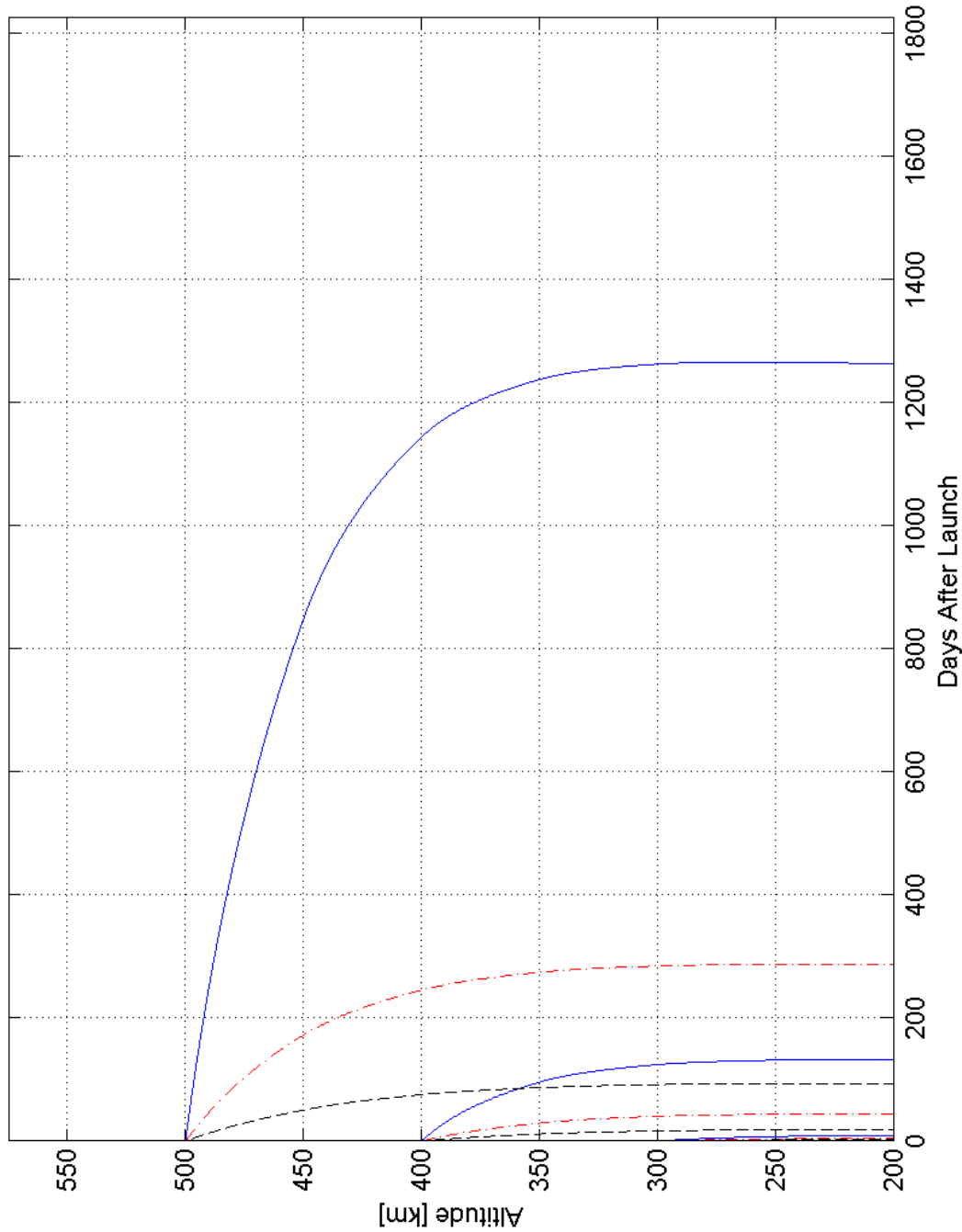


Figure 6.17: Orbit decay for a satellite with $C_D = 4$, $A = 2.5 \text{ m}^2$ and $m = 119 \text{ kg}$. Estimates for initial orbital altitudes of 300, 400 and 500 km at solar maximum (---), solar minimum (—) and time average (---).

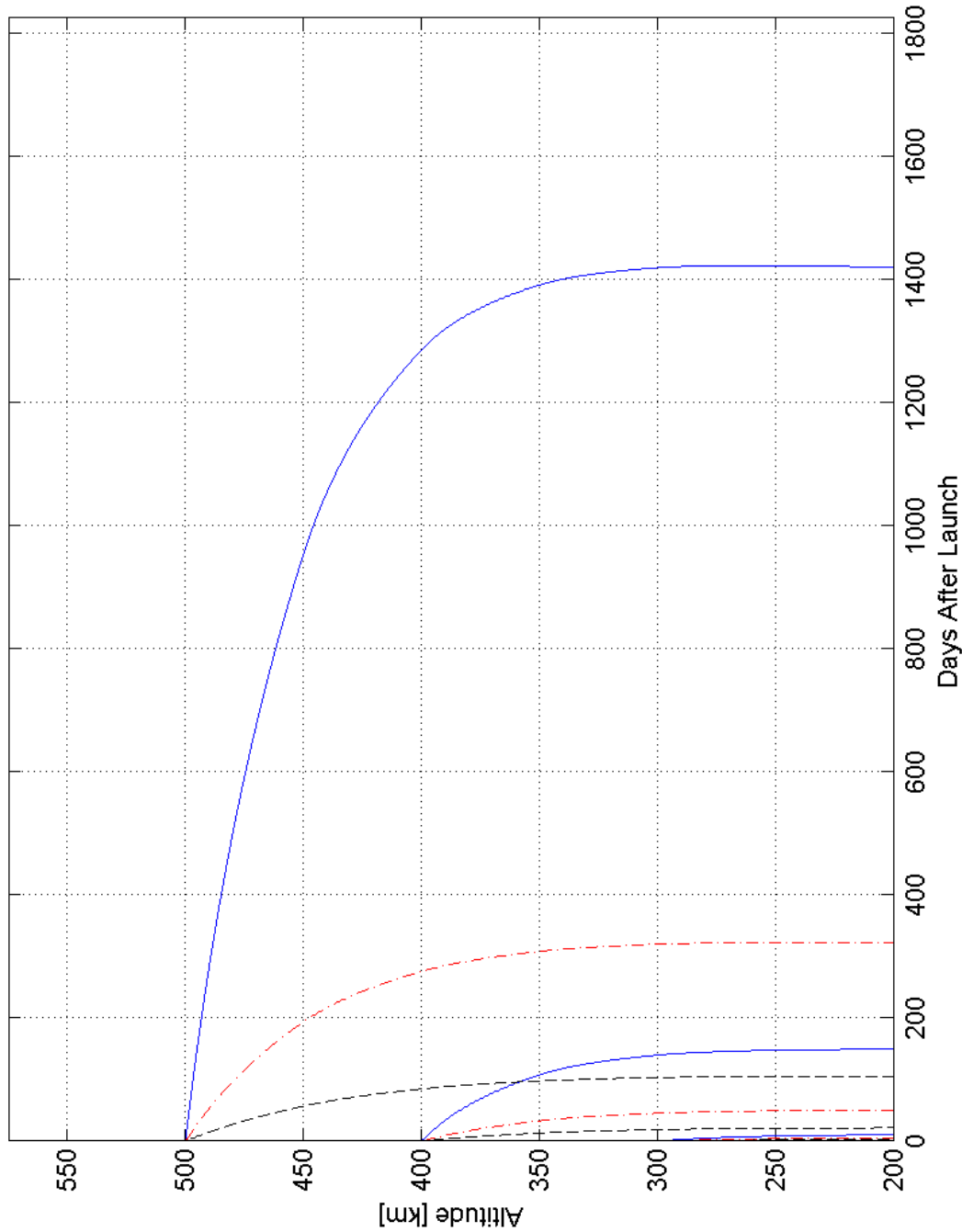


Figure 6.18: Orbit decay for a satellite with $C_D = 4$, $A = 0.2 \text{ m}^2$ and $m = 10.7 \text{ kg}$. Estimates for initial orbital altitudes of 300, 400 and 500 km at solar maximum (- -), solar minimum (-) and time average (---).

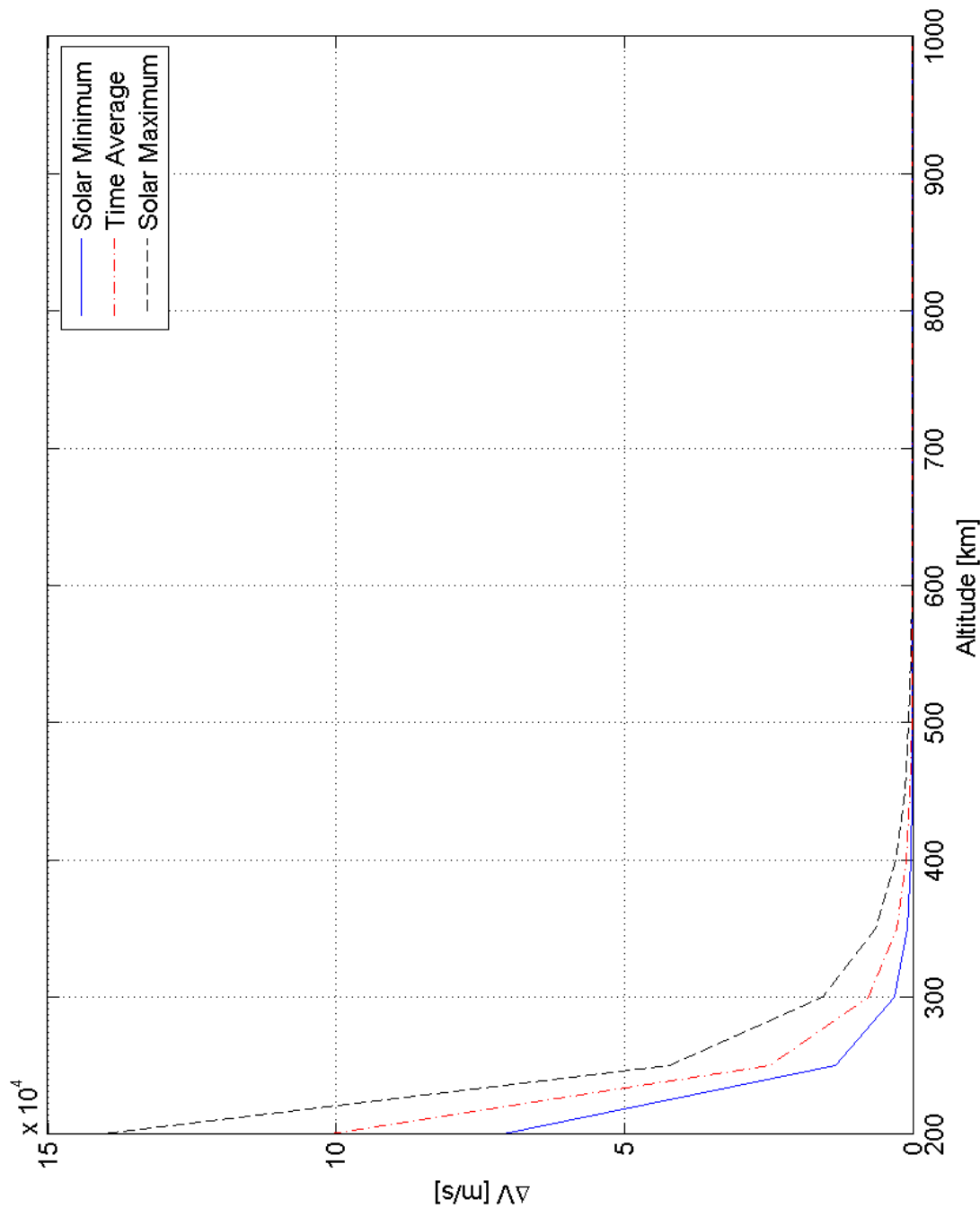


Figure 6.19: Total ΔV for a satellite with $C_D = 4$, $A = 2.5 \text{ m}^2$ and $m = 119 \text{ kg}$. Estimates for a range of orbit altitudes and different solar cycle stages.

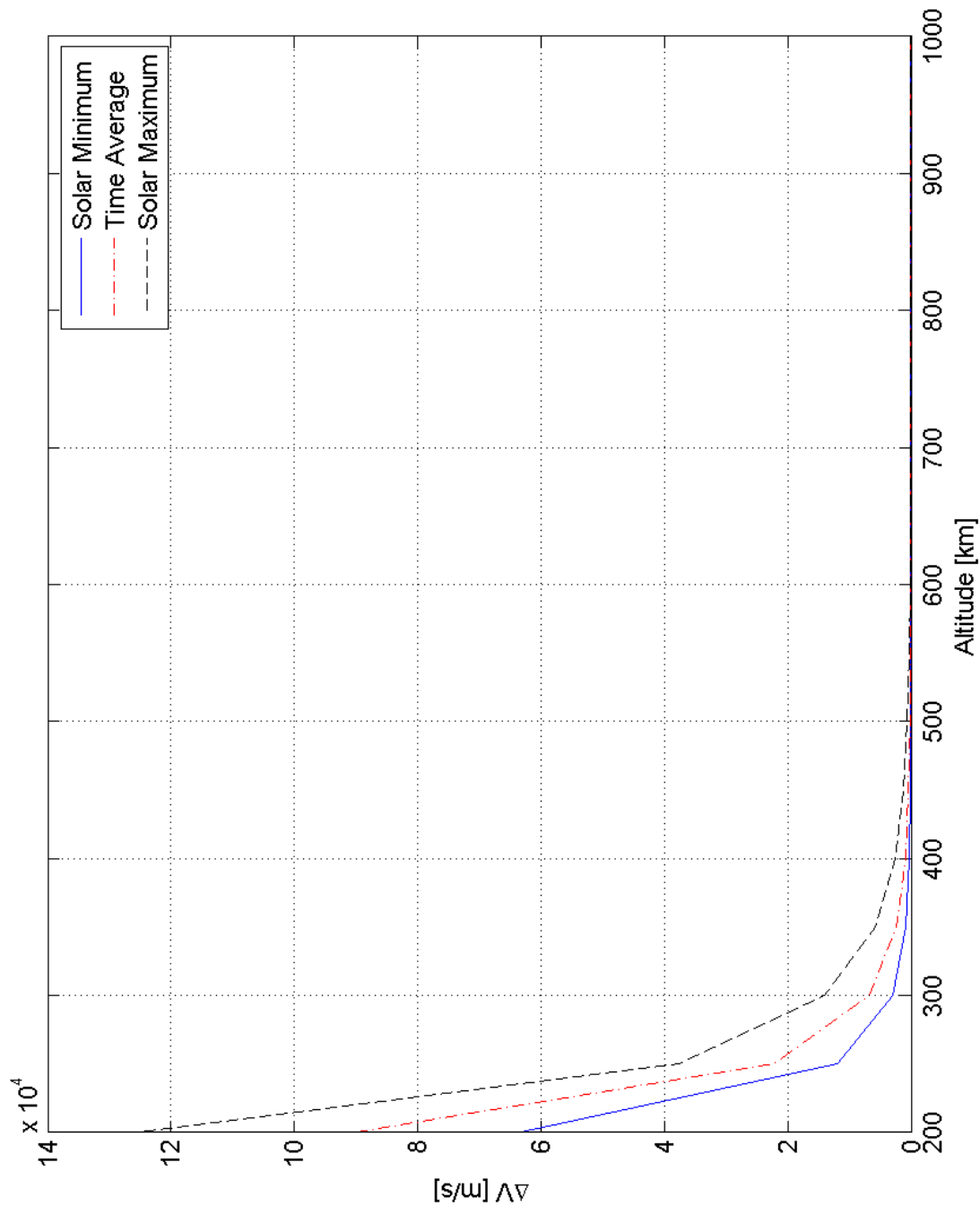


Figure 6.20: Total ΔV for a satellite with $C_D = 4$, $A = 0.2 m^2$ and $m = 10.7$ kg. Estimates for a range of orbit altitudes and different solar cycle stages.

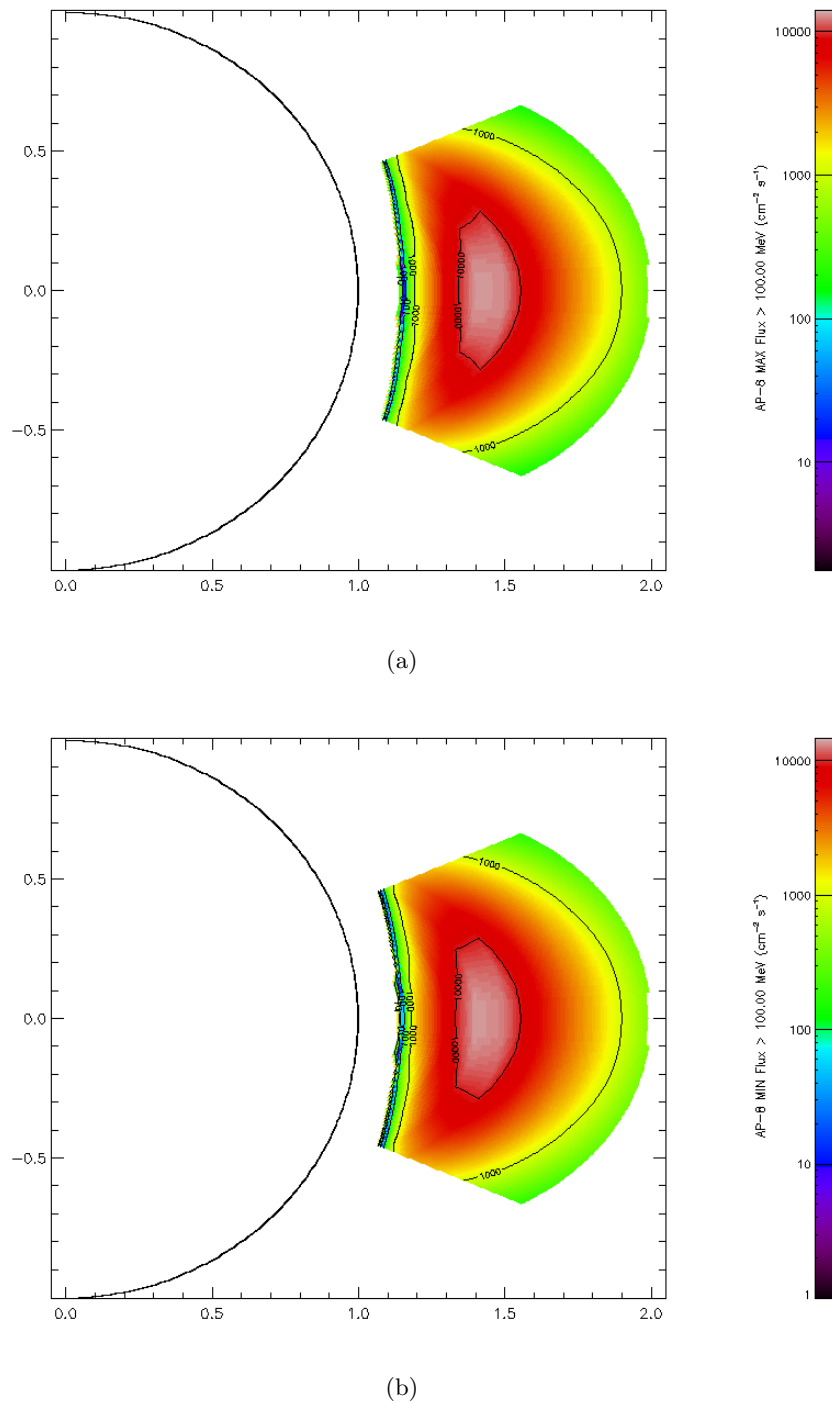


Figure 6.21: AP-8 Proton Flux Model (energy > 100 MeV) at solar maximum (a) and solar minimum (b) as a function of distance in mean Earth radii.

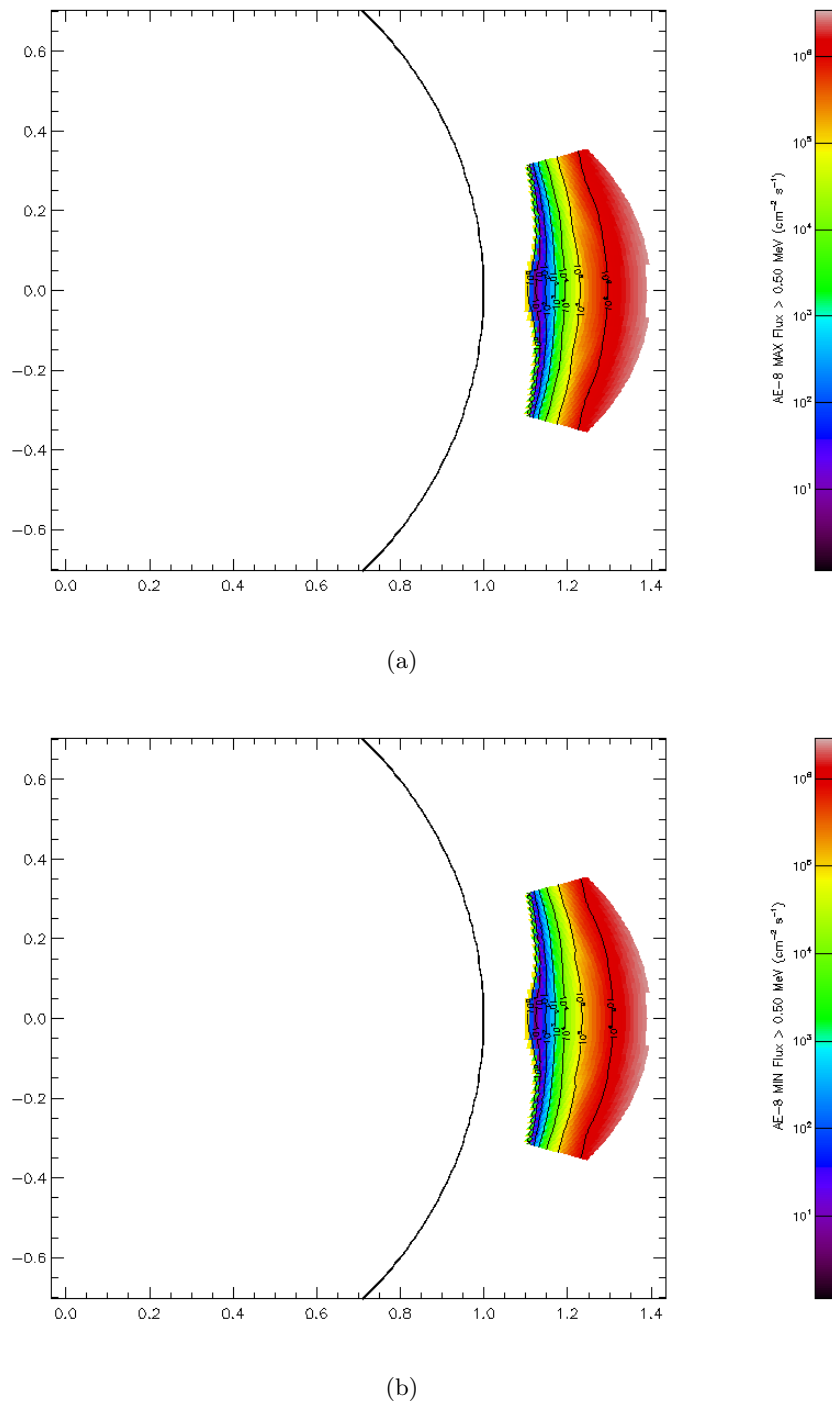


Figure 6.22: AE-8 Electron Flux Model (energy > 0.5 MeV) at solar maximum (a) and solar minimum (b) as a function of distance in mean Earth radii.

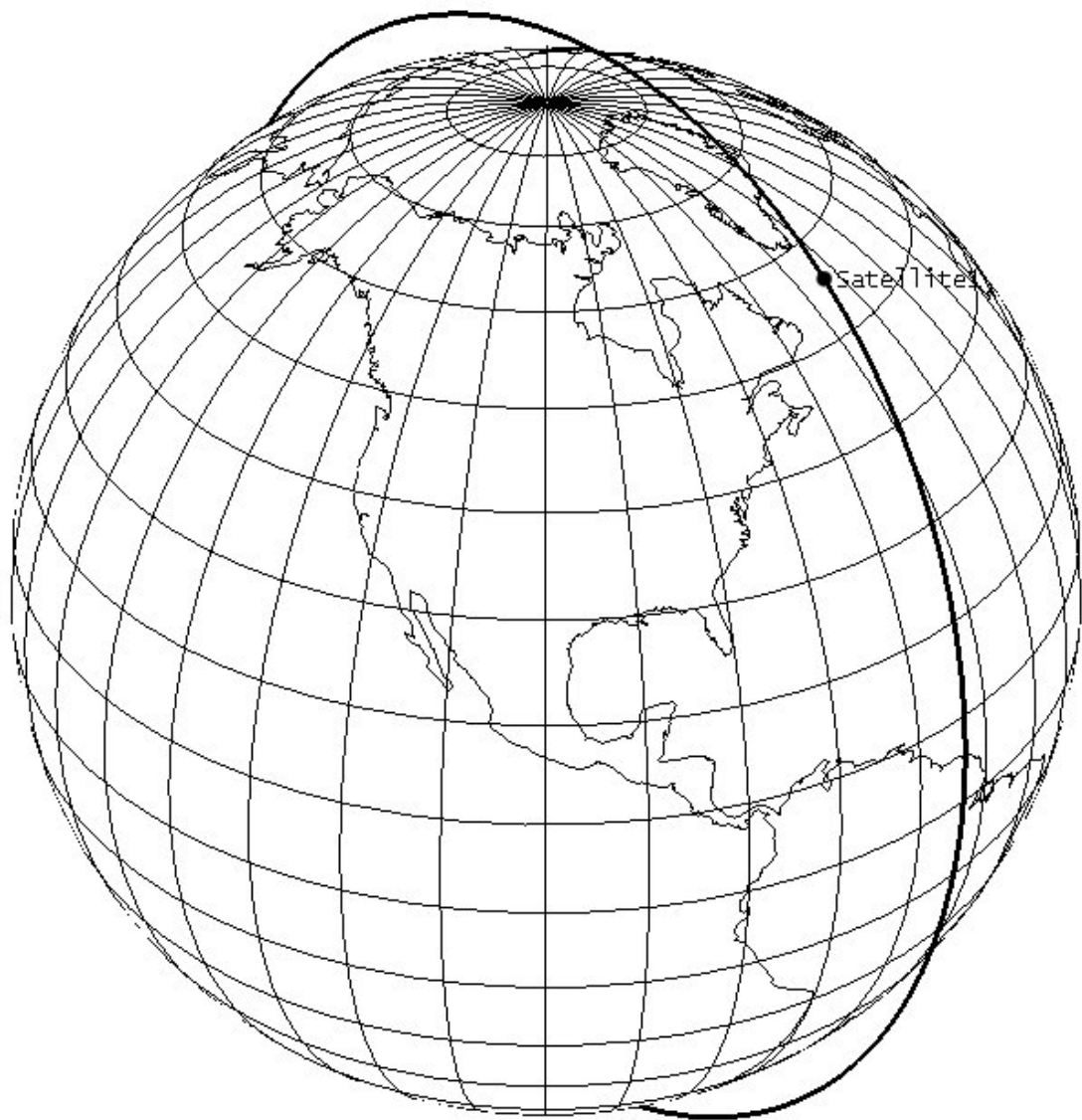


Figure 6.23: 3D view of the base orbit.

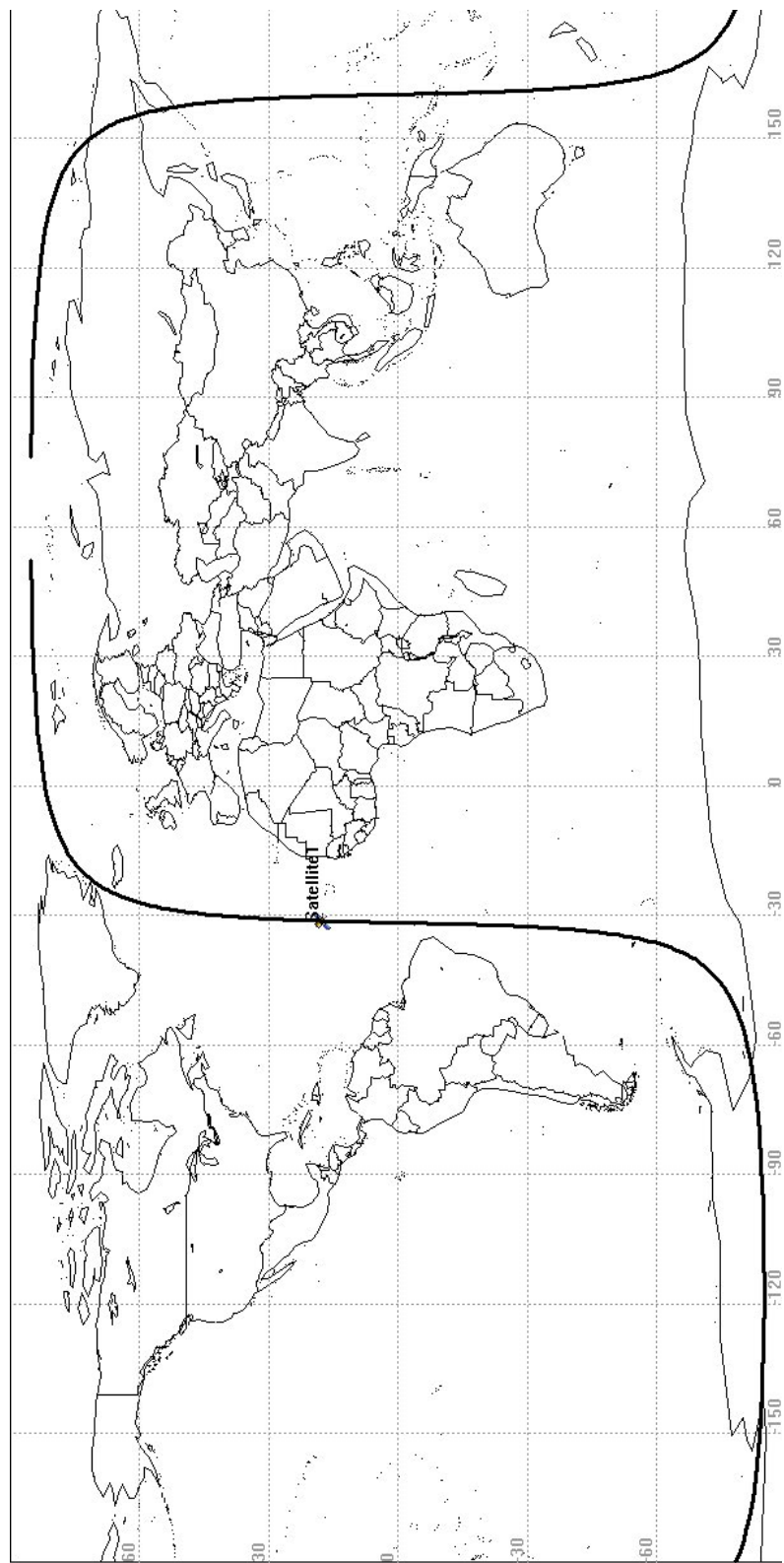


Figure 6.24: Ground track of the base orbit.

6.6 Satellite Formation Design

One of the most important aspects of this project is the fact that multiple satellites have to work in unison to achieve a common objective. This concept is called a constellation. In the case of Laser Swarm, it is necessary to design a formation as the platforms will need to be in close proximity to each other.

A historical overview of satellite constellations presented on page 672 in [et al.(2001)] has yielded the fact that constellations are very mission specific and vary greatly. What is apparent though, is that altitudes of constellations are very high (1000 km and higher). This is mainly done in order to make stationkeeping easier as the main orbital perturbation, atmospheric drag, is less prominent.

In this section, the design of the swarm formation is looked at. Orbital characteristics are discussed in section 6.6.1, while sections 6.6.2 and 6.6.3 are concerned with stationkeeping and collision avoidance respectively.

6.6.1 Orbital Parameters

The relative motion of satellites flying in formation can be separated in 3 parts: large-scale relative motion due to satellites not being in the same orbit, small-scale motion due to individual perturbation effects and also the relative motion of one satellite as seen from the other.

The important thing to note is that for the design of the Laser Swarm, only a co-altitude constellation is considered. This will significantly simplify stationkeeping (all satellites have the same orbital period) as well as make instrument pointing much easier. Also two types of formation designs will be examined: along-track motion and cross-track motion. Along-track motion involves satellites following each other on the same orbit, while cross-track motion involves intersecting orbital planes at either same or varying orbit inclinations.

The large-scale relative motion of two satellites in different orbits is governed by only two key variables: the relative inclination, i_R and relative phase, ϕ_R . The relative inclination is the angle at which the two orbit planes intersect. The relative phase is the angular separation of the satellites at the time they intersect each other's orbit plane. This happens four times per orbit. The two angles are shown in figure 6.25 on page 65.

Two cases of cross-track motion exist:

1. Inclination of each orbital plane is the same ($i_1 = i_2 = i$) while the ascension nodes have a certain angular separation. This is the most common constellation type.
2. Inclinations vary with each orbital plane. In this case all satellites can also have the same node of ascension, however this might not necessarily be the case.

Out of the two cases, the most convenient one for the purpose of formation flying is method number 1. Since orbit precession is a function of only the inclination, it is smart to keep it the same for all satellites. This method is demonstrated in figure 6.26 on page 65.

In figure 6.26 the ΔN is the angular separation between the ascending nodes on the equator. For this case the following equations can be used:

$$\cos i_R = \cos^2 i + \sin^2 i \cos \Delta N \quad (6.16)$$

$$\phi_R = (T_2 - T_1)n + \Delta\phi \quad (6.17)$$

where

$$\Delta\phi = 180 - 2\phi \quad (6.18)$$

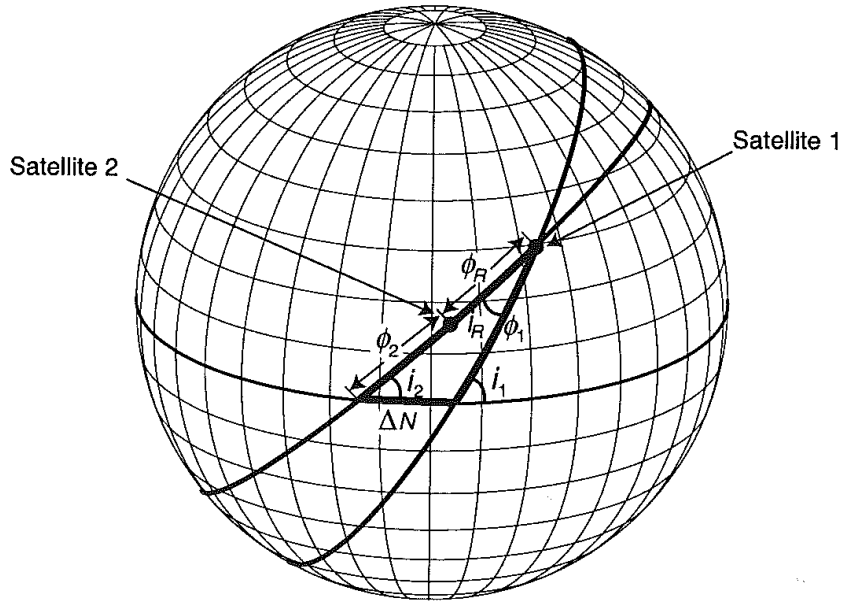


Figure 6.25: The relative motion of co-altitude satellites in circular orbits. Relative inclination and relative phase are shown. *Source: [et al.(2001)]*

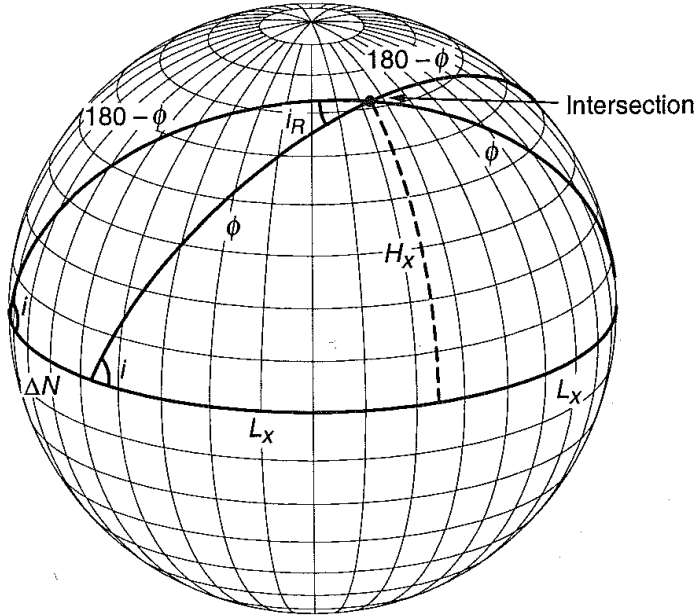


Figure 6.26: Intersection of two orbits with the same inclination. *Source: [et al.(2001)]*

$$\tan\phi = \frac{\tan(90 - \Delta N/2)}{\cos i} \quad (6.19)$$

Furthermore the relations for minimum and maximum angular separation of the two satellites are given:

$$\sin\left(\frac{\lambda_{min}}{2}\right) = \sin\left(\frac{\phi_R}{2}\right)\cos\left(\frac{i_R}{2}\right) \quad (6.20)$$

$$\cos\left(\frac{\lambda_{max}}{2}\right) = \cos\left(\frac{\phi_R}{2}\right)\cos\left(\frac{i_R}{2}\right) \quad (6.21)$$

The angular separation is a very important factor. To be able to determine the BRDF of the surface under observation, the separation should be as large as possible, as the BRDF is an angular property. However, for the purposes of ADCS and inter-satellite communications, the separation should be kept small. Figure 6.27 demonstrates the geometry of separation of the satellites.

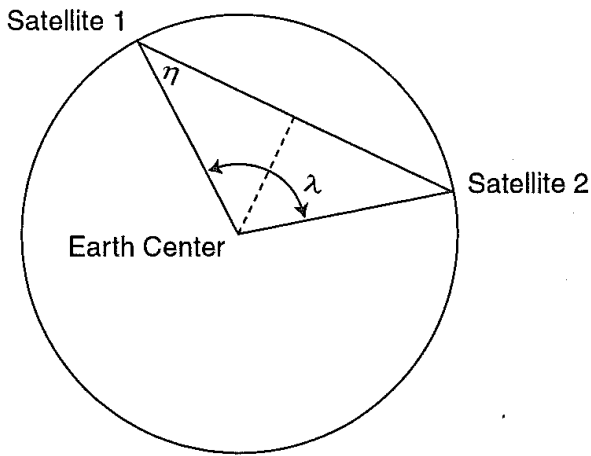


Figure 6.27: Geometry of angular separation. *Source: [et al.(2001)]*

All of the above equations are in terms of degrees. Based on these relations it is possible to calculate the relationships between the equatorial angular separation and relative inclination, relative phase and the minimum and maximum angular separation.

It is obvious from figures 6.28 and 6.29 that the relative inclination and the maximum angular separation are almost equivalent to the equatorial separation.

From the point of view of instrument pointing, the receiver should be at such separation from the emitter that the return signal is in the range of 1 to 30 degrees with respect to emitter nadir (for the outermost receiver satellite). This geometry is demonstrated in figure 6.30. This translates to a maximum angular separation of 2.18 degrees in both across-track and along-track directions. For along-track satellites that is simply a phase difference on the same orbit. For cross-track, the ΔN can be calculated to be 2.18 degrees as well. Resulting relative phase is 0.19 degrees. This is also then the minimum angular separation for the cross-track satellites.

The exact formation spread will be examined closer when the detail design will be performed, however it is assumed at this point that 2 satellites will be placed along-track (one fore and one aft of the receiver)

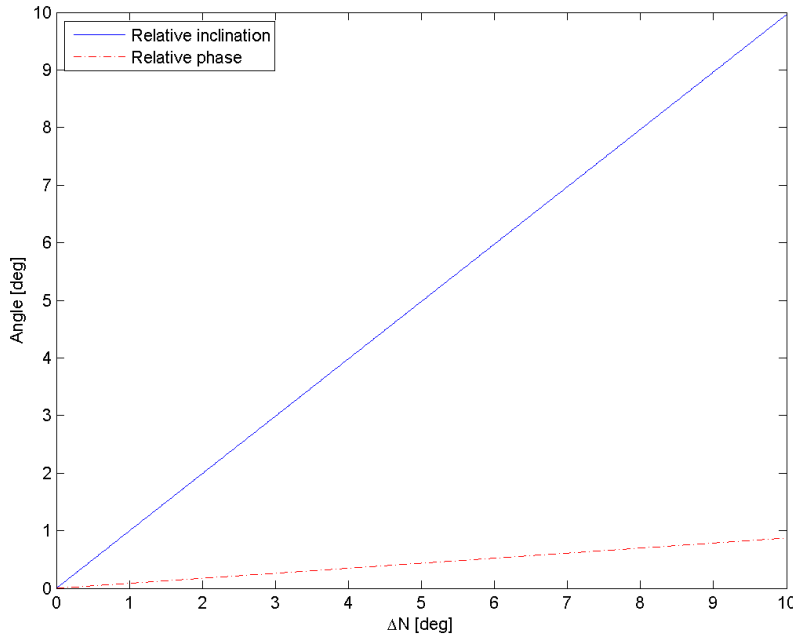


Figure 6.28: i_R and ϕ_R vs. equatorial angular separation. Orbit inclination of 85° .

and two satellites with across-track separation of 2.18 degrees. Depending on the results of the simulation concerning data processing, further satellites might be integrated into the swarm.

The relative analemma of two satellites in a 500 km orbit with a relative inclination of 2.18 degrees is shown in table 6.7.

i_R [deg]	ross-track motion [deg]	cross-track motion [km]
2.18	± 2.18	± 262

Table 6.7: Height and width of the relative motion analemma for two co-altitude satellites in a 500 km orbit with an inclination of 85 degrees.

Small scale relative motion of the satellites will be looked at in more detail at later stages of the design.

6.6.2 Stationkeeping

Stationkeeping is the process of keeping the satellite within a well defined box relative to another satellite. The main reason for stationkeeping is overall maintenance of the constellation, and in the case of the Laser Swarm formation, for more accurate receiver pointing. When the receiver positions are well known and defined, maintaining concise data streams will be easier. Furthermore, precise stationkeeping reduces the chances of collisions and more precise inter-satellite communications.

Two main things that affect the relative positions of satellites:

- Orbit perturbations such as atmospheric drag and Earth's oblateness effects, affect each satellite differ-

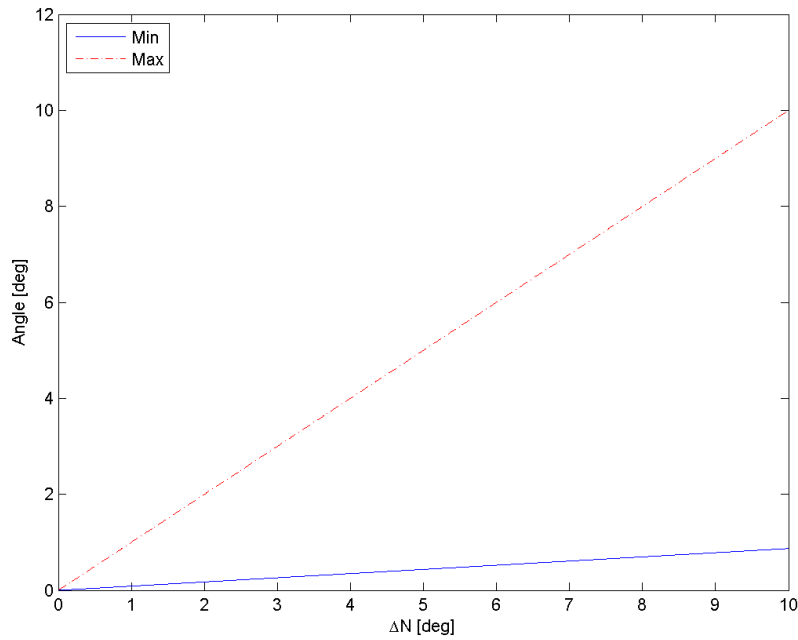


Figure 6.29: Minimum and maximum angular separation vs. equatorial angular separation. Orbit inclination of 85° .

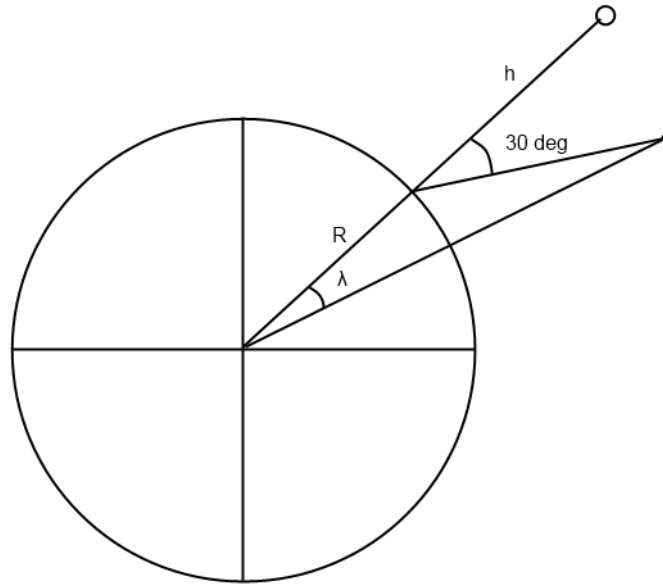


Figure 6.30: Orbit separation geometry.

Perturbation	Impact	Handling
Atmospheric Drag	Secular decay ranging from 1-100 m/day	Altitude maintenance
Oblateness	Secular node rotation of 0.5 deg/day	Inclination maintenance
	Secular phase rotation of 14 deg/day	Altitude maintenance
	Changes in shape of orbit up to 5 km variation between adjacent satellites	Uncompensated
Solar/Lunar	Secular drift in inclination and node of up to 3.5×10^{-5} deg/day	Inclination maintenance
	Low amplitude oscillations in inclination and node	Uncompensated
Solar Radiation Pressure	Small	Typically uncompensated

Table 6.8: Recommended methods of handling the principle perturbations in LEO. Source: [et al.(2001)]

ently. One was of countering the complications concerned with drag were already discussed in section 6.5.4. It was noted that by keeping the ballistic coefficients of both the receiver and the emitter satellites as close together as possible, the orbit degradation due to drag will be similar for all satellites (since the formations are tight, it can be assumed that the air density experienced by all satellites is the same). This fact would entail that the same ΔV impulse would be required for all platforms. Earth's oblateness effect constitutes the J_2 factor and causes the orbital precession. Over many orbits, the formation would drift apart if this effect was not managed. Since the rate of precession is a function of the semi-major axis, eccentricity and inclination, it is vital that these orbital parameters are kept constant for all satellites (as already noted in the previous section).

- Subtle variations in initial conditions can start a chain of events that will slowly drift the formation apart. Small variations in initial altitudes would mean small differences in orbital periods, and variations in inclination would give different rates of precession and would also increase risk of collision.

There are also three ways of dealing with perturbations for all satellites:

1. Do nothing - do not compensate and let the formation float apart gradually. This option is not viable in the context of the mission lifetime. Orbits will completely decay before mission end.
2. Control the perturbing disturbances to be the same for all satellites. In this case the satellites maintain the same relative position but cease to have Keplerian orbits. This option is also not viable as the payloads rely on precise orbits for pointing, and there is also no possibility to refocus the instruments.
3. Negate the perturbing forces. All orbital characteristics are kept to the initial conditions by constant maintenance. Such perturbations as drag have to be constantly maintained in order to prevent the orbits from decaying. This is the only viable option in the context of the mission

Table 6.8 on page 69 summarizes ways to handle perturbation stationkeeping. The concept can be implemented in two ways: relative and absolute stationkeeping. In the relative stationkeeping concept, the

satellites are maintained in the same relative position to each other. In essence the situation may arise when the whole formation may be allowed to decay together. In contrast, absolute stationkeeping, maintains and controls each orbit separately. It has several advantages over the relative concept:

- In practice, it has shown to use up less ΔV .
- It is simple to command.
- Each satellite maintains itself in the pattern.
- Orbit position is precisely known without large data traffic.
- Can be fully autonomous.
- Easy monitoring from ground.
- Will not require instrument refocusing.

However it will require more constant attention. Absolute stationkeeping will be the right choice for the considered formation, as it will allow for greater accuracy of observation.

6.6.3 Collision Avoidance

Collision avoidance is an integral part of formation design, yet this analysis cannot be properly performed without the detail design of the constellation. However some design approximations can be already made to estimate the risks.

In the context of this formation, collision avoidance is important for two reasons: potential loss of two vehicles in a collision, one of them possibly being the emitter, and creation of a debris field which can jeopardize the safety of the rest of the platforms. A debris field evolution can be seen in figure 6.31 on page 71.

Some preliminary formation collision estimates are shown in table 6.9 on page 72. Based on this information it is obvious that the danger of a collision between satellites rises exponentially as more platforms (and orbital planes) are introduced into the system.

In order to successfully implement a safety-conscious formation design the following rules will have to be followed:

1. Maximize spacing between platforms on orbit crossing.
2. Remove satellites at end of life.
3. Keep tracking the motion of "dead" satellites.
4. Remove launcher upper stages from the orbits.
5. Design replacement injections with collision avoidance in mind.
6. Capture any ejected components.
7. Avoid self-detonation.

Following these rules will lead to a safer formation and eventually to an extended mission lifetime.

Another topic is collision avoidance of objects that are outside the considered formation, however this discussion is out of the scope of this document and will be examined in further reports.

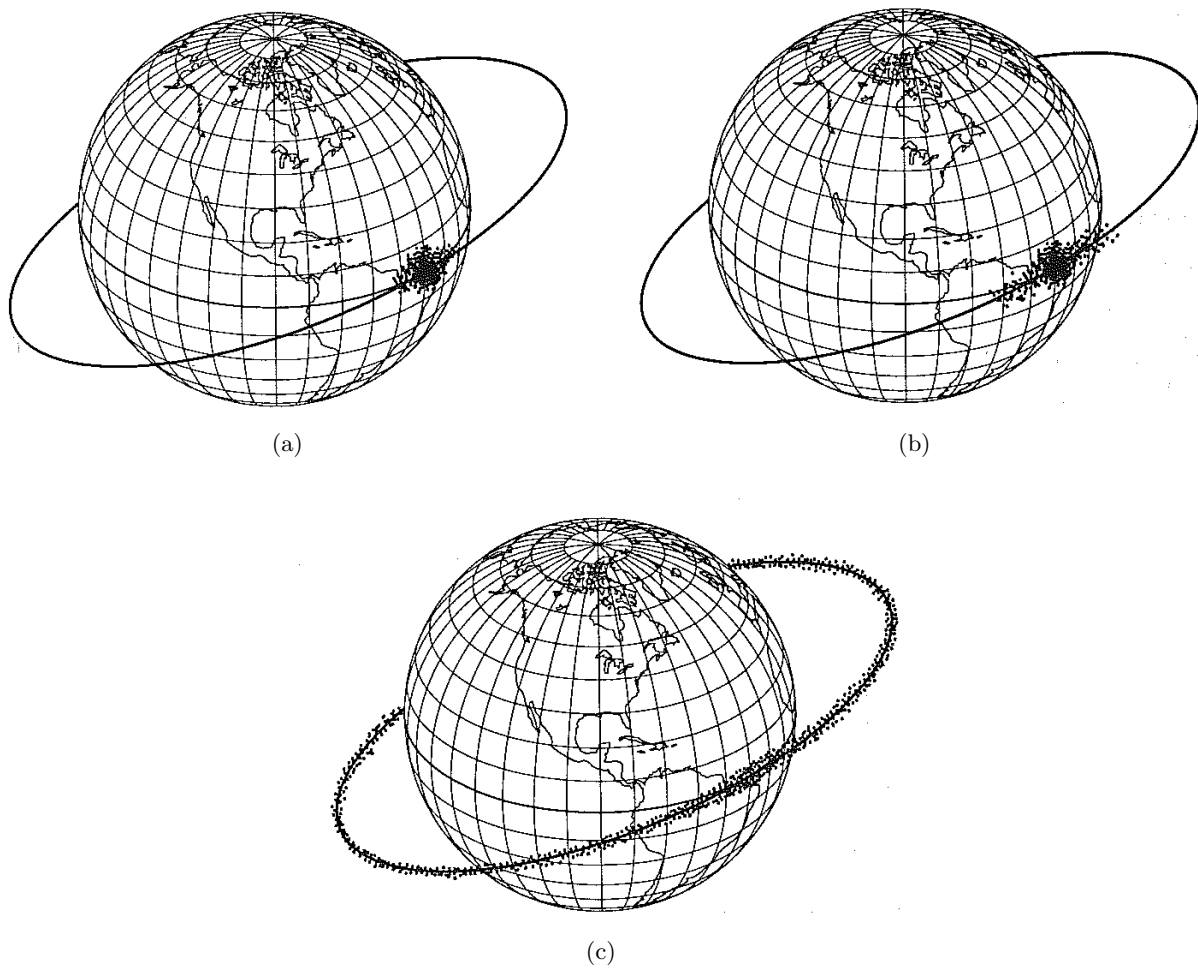


Figure 6.31: Debris field evolution, (a) immediately after impact, (b) spreading out after some time and eventually settling into the orbit (c) and decaying. *Source: [et al. (2001)]*

Parameters	5 Satellite Formation in 3 Planes	9 Satellite Formation in 5 Planes
No. of satellites	5	9
No. of orbit planes	3	5
Vertical dispersion [km]	1	1
In-track dispersion [km]	276	276
Potential impact area [km ²]	276	276
Collision opp. per orbit	20	72
Orbit period [min]	94.62	94.62
Collision opp. per year	1.1×10^5	4.0×10^5
Collision opp. in 5 years	5.6×10^5	2.0×10^6
Collision prob. per opp.	1.0×10^{-6}	1.0×10^{-6}
Mean number of collisions per year	0.11	0.4

Table 6.9: Inter-satellite collision estimations for a formation of 5 and 9 satellites. Probability values based on extrapolation of values given in [et al.(2001)].

6.7 Optical Sensing

6.7.1 Introduction

Laser profiling (or *laser altimetry*) is the simplest application of the LiDAR technique. The main principle is pretty straightforward; electromagnetic radiation (visible or near-infrared radiation) is emitted towards the Earth's surface by a laser and the reflected radiation is detected some time later. By measuring the time delay and knowing the speed of propagation, the range (distance) from the instrument to the surface can be determined. Detailed topographic maps of very high accuracy are produced by airborne or satellite laser altimeter terrain mapping. The unique capabilities of this technique yield more comprehensive and precise topographic information than traditional methods. Airborne laser altimeter data can be used to accurately measure the topography of the ground, even where overlying vegetation is quite dense. The data can also be used to determine the height and density of the overlying vegetation, and to characterize the location, shape, and height of buildings and other man-made structures.

The capacity of any instrument to be able to detect and emit electromagnetic radiation for laser altimetry mission depends on optical characteristics, like (wavelength dependent) atmospheric absorption, surface reflectance (ground and oceans) and scattering. These optical phenomenon should be taken into account when multi-angular laser altimetry results are wanted. Considering these characteristics, the right instruments can be chosen.

6.7.2 Atmospheric and Oceanic Effect

6.7.2.1 Atmospheric Transmission

For optical signal propagation in the atmosphere, the physical processes dictating the choice of wavelength are summarized in figure 6.32 on page 74, which illustrates the effects of the strong absorption by atmospheric gases act to limit transmission to distinct wavelength regions, or *spectral bands*.

Within these bands, the atmosphere is relatively transparent and imaging sensor systems can operate efficiently. For wavelengths longer than about one micro-meter, the dominant absorption is related to excitation of molecular vibrations in water vapor and carbon dioxide. When examined in detail, these processes three distinct transmission windows: the near or shortwave infrared bands (NIR $\lambda \sim 0.7$ to 1.1 [μm] and SWIR $\lambda \sim 1.1$ to 2.5 [μm]), the midwave IR band (MWIR $\lambda \sim 3.3$ to 5.0 [μm]), and the long-wave IR band (LWIR $\lambda \sim 8$ to 14 [μm]). Figure 6.33 on page 74 shows the absorption and scattering of direct light in the earth's atmosphere.

At the other extreme, for wavelengths much shorter than visible, the same processes responsible for generating airglow limit transmission through the atmosphere. In fact, for wavelengths shorter than 0.26 [μm] [Ultra Violet (UV)], these processes are so strong that no solar radiation reaches the ground and the earth's surface is in perpetual darkness (solar-blind). However, this UV light does propagate for short distances, all owing sensors designed to respond exclusively in this spectral region to detect many man-made emissions. For example, even when pointed directly at the sun, under conditions where a visible or Infra Red (IR) system would be completely overwhelmed by the sun's emission, these sensors can detect a UV flash emitted by flames, firearms, or missile plumes. Solar-blind sensors are also of interest because they operate in a region of the spectrum important for detecting certain characteristic fluorescence associated with biological agents (e.g., anthrax) when illuminated by sources operating at even shorter wavelengths.

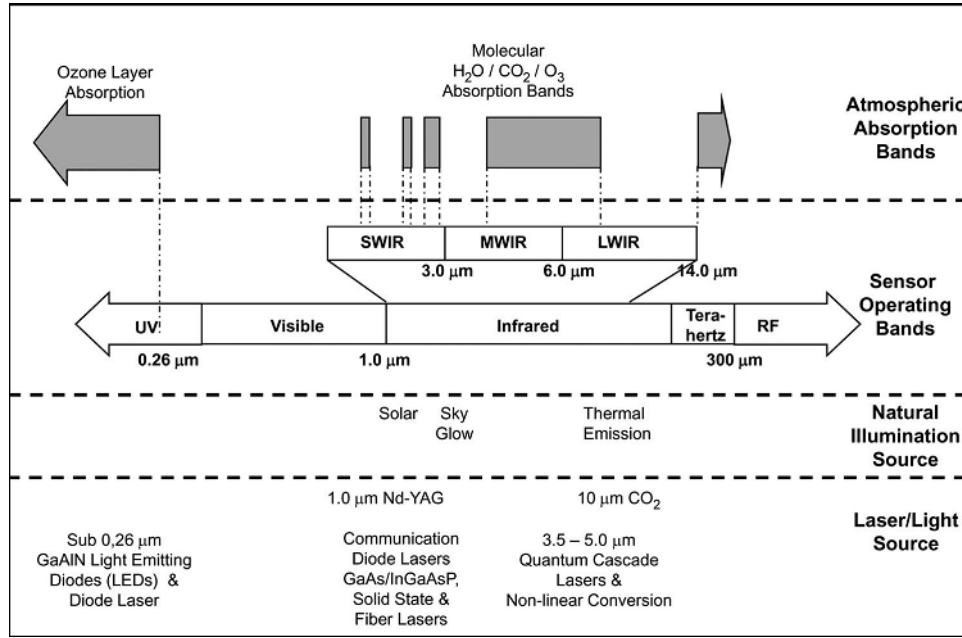


Figure 6.32: A schematic summary illustrating how absorption by various constituents in the atmosphere influences the propagation of light and divides the spectrum into distinct bands.

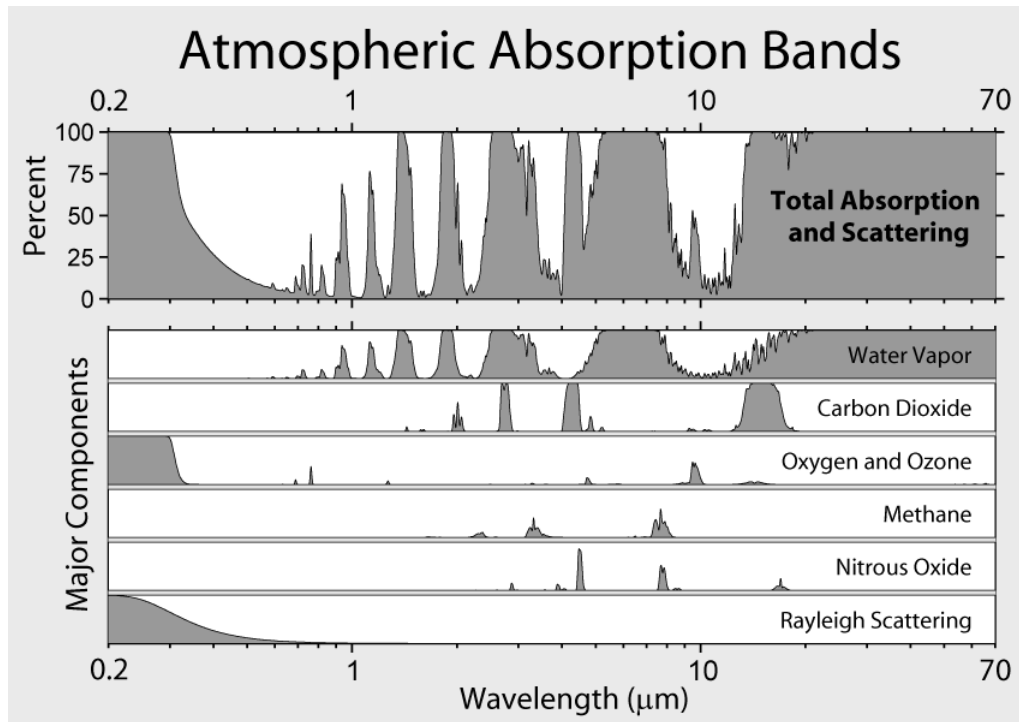


Figure 6.33: Atmospheric Absorption Bands

6.7.2.2 Ocean scattering

To be able to make any oceanographic elevation model, the incident photons should be scattered by the oceans. This is a particularly important factor for the entire mission, since the coverage of oceans (water in general) is particularly abundant on Earth. The downside of water is the presence of large fractions of absorption in the visible wavelength. This is shown in figure 6.34 on page 75. In this picture it can be seen that relatively low wavelengths (or high frequencies) in the visible spectrum (referred to as 'blue') has the highest penetration depth. However, wavelengths in the order of 350 - 450nm have the highest fraction of reflectance on the ocean surface [Robert P. Bukata(1995)]. In comparison, the absorption depth of higher wavelengths, like 'red' (600nm-750nm), has a low value, but almost all radiation with this frequency is absorbed.

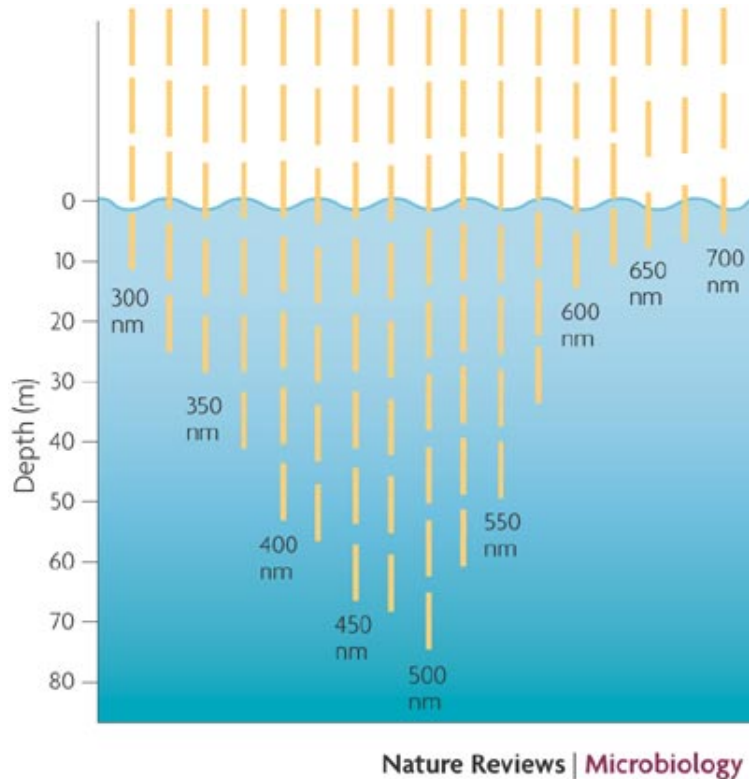


Figure 6.34: Light penetration ocean depth with different wavelength

6.7.3 Optical Receiver Device

The main objective of the ORD is to detect the individual energy quanta. A large fraction of the photons emitted by the laser are not that easy for detection since they are redirected by the atmosphere, spread due to surface scattering or they are simply absorbed partly by either of them. The decrease in photon quantity is really severe considering these factors and that is why a photon detector with comparable high quantum efficiency is required. Since the number of photons actually reaching the perimeter of the ORD is usually only in the order of one to ten, the ORD has to be able to detect and analyze individual small energy packets, preferably single photons. In this section, a general introduction about photon detection is drawn first, after which the laser wavelength estimation is performed to narrow down the potential wavelength range. After that, the design option tree is pruned according to the wavelength requirement and technology availability. Finally the trade-off is performed, which is split up into trade method, trade criteria and weight factor,

followed by trade-off summary. The design selection for the optical receiver device is done at the end of the section.

6.7.3.1 General Introduction to Photon Detection

Photon detection typically occurs in a two-step process: the absorbed photon creates a measurable change in the detector's electrical properties, and the changes are registered in an external read-out integrated circuit (ROIC). In general, the detector material responds either *directly* to the incident photon by generating a free charge, with this charge then being responsible for producing the change in electrical properties, or *indirectly*, with the absorbed optical power generating a temperature rise in the detector material, which is responsible for producing the change in electrical properties. In either case, this photon-induced analog signal is registered and amplified in the ROIC digitization for further signal processing.

Additional factors include the detector material *sensitivity* and the detector *device speed of response*. Sensitivity is a measure of how few photons are required to raise the detector output above any background noise level present in the absence of incident light. Response speed is a measure of how faithfully the detector's electrical output responds to changes in the intensity of the input light signal.

- Solid-State Photon Detection Solid-State imaging is based on the physical principle of converting light (photons) into a measurable quantity (electrical voltage, electrical current). Photons falling onto and penetrating into a semiconductor substrate can transfer part of their energy to the substrate by generating electron-hole pairs. For an n-type semiconductor, if the energy content of the photons is high enough, electrons can be released from the valence band and swept into the conduction band, leaving behind a hole in the valence band. To generate an electron-hole pair, the energy of the photons has to be larger than the bandgap of the semiconductor substrate.[McGlone(2004)]

For reasons of cost and miniaturization, a solid state solution for single photon detection is highly desirable. Figure 6.35 on page 77 shows a classification that covers the current state-of-the-art on optical solid-state 3D image sensors.

- SPAD SPAD are solid-state semiconductor devices based on a p-n junction reversed biased at a voltage V_a higher than V_B .

At this bias, the electric field is so high (higher than 3105 V/cm) that a single charge carrier injected in the depletion layer can trigger a self-sustaining avalanche. The current rises swiftly (sub nanosecond rise-time) to a macroscopic steady level, in the milliamper range. If the primary carrier is photo-generated, the leading edge of the avalanche pulse marks (with picoseconds time jitter) the arrival time of the detected photon. The current continues until the avalanche is quenched by lowering the bias voltage V_D down to or below V_B : the lower electric field is not able any more to accelerate the carriers to impact-ionize with lattice atoms, therefore current ceases. In order to be able to detect another photon, the bias voltage must be raised again above breakdown.[S.Cova and F.Zappa(1996)]

6.7.3.2 Wavelength estimation

Laser wavelength is one of the most important parameters influencing the whole design of photon detection and laser emitter device. Different emitter wavelengths have different photon detection efficiency or probability to photon receiver. To choose which type of laser is feasible, it is best to start with which wavelength the receiver can detect.

According to the photon detection probability distribution diagram for SPAD and MPD in figure 6.37 and 6.38 on page 78 and 78, the general most sufficient wavelength range is between 400nm to 900nm.

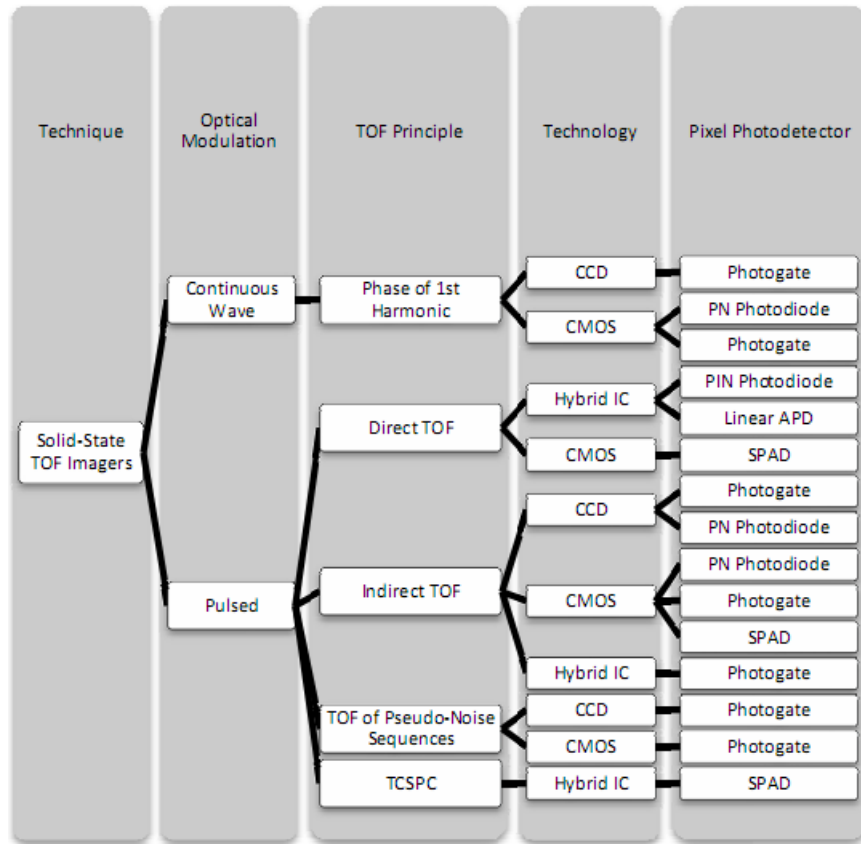


Figure 6.35: Classification of state-of-the-art optical TOF image sensors.

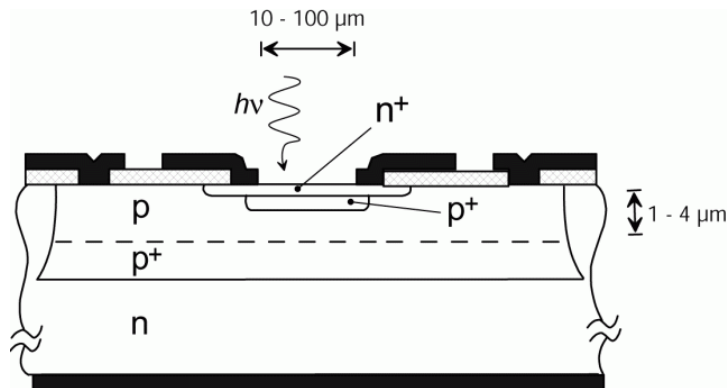


Figure 6.36: SPAD cross-section diagram.

There are not much qualified lasers that can be considered below the wavelength 400 [nm], and the photon detection probability is insufficient if the wavelength goes above 900 [nm]. In order to narrow the wavelength range, the atmospheric transmittance versus photon detection efficiency ratio is introduced, which means that larger ratio indicates larger chance the receiver can detect photon. The actual formula to calculate the ratio is $R = \text{transmittance}^2 \times \text{photon efficiency}$. The transmittance is squared because the light go through the atmosphere twice. Calculate all ratio between wavelength 400 to 900 [nm] by interval 25 [nm], and plot

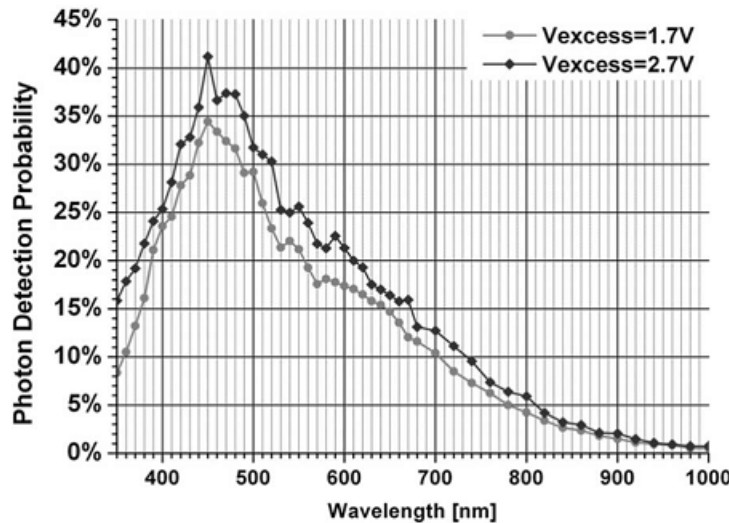


Figure 6.37: SPAD photon detection probability as a function of wavelength for two values of excess bias voltage

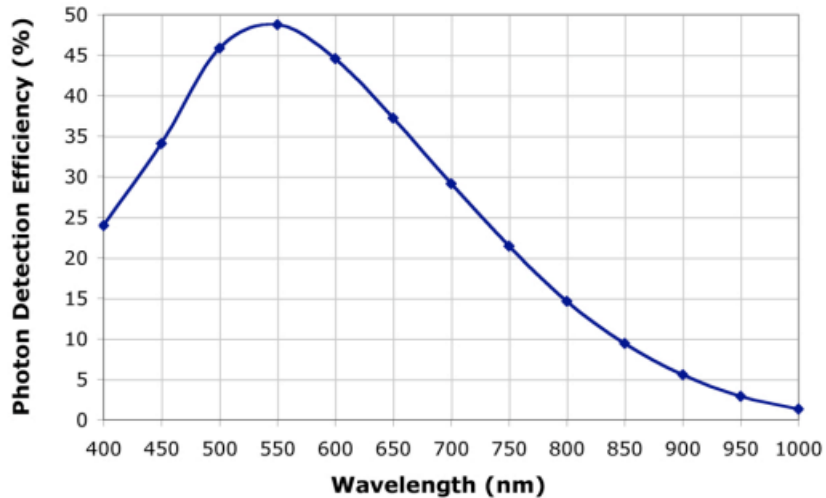


Figure 6.38: MPD photon detection probability as a function of wavelength

the ratios in figure 6.39 on page 79. From the graph, it is easy to narrow down the wavelength range to 425 - 500 [nm]. The following sections will give brief trade-offs between laser emitters and receivers.

6.7.3.3 Receiver Prune

In the design option tree, the GLAS branch is obviously dropped out, since we are trying to improve the whole concept. Meanwhile, the Micro Photon Device (MPD)'s single-photon detection modules branch has different quantum efficiency for different wavelength, which means MPD could be a good option for the blue laser detector with 35% efficiency. The SPAD chip could be a new approach since it has reasonable high quantum detect efficiency at laser wavelength 425nm to 500nm. Both MPD and SPAD are not optimal for

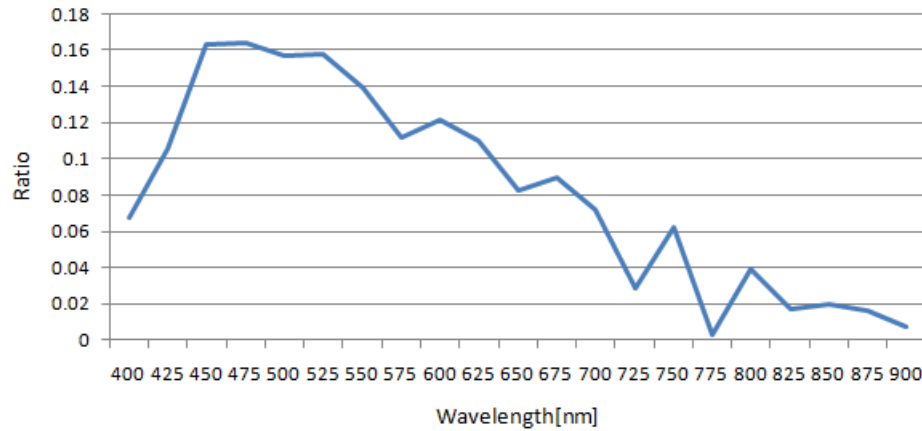


Figure 6.39: Ratio of atmospheric transmittance versus photon detection efficiency

NIR or IR laser detect with low quantum efficiency around 1%, So it means the mission mainly focus on single wavelength.

The pruned design option tree for the laser detector can be seen in figure 6.40 on page 90.

6.7.3.4 Trade Method

There are mainly four options after pruning and each has different strong points and weak points due to different configuration and structure.

The first option is Stereo Imaging Laser Altimeter (SILAT), which combines two optical cameras with a low-power photon-counting laser altimeter. It means that SILAT operates both pulse laser and photon detector, and it need to be configured as only a photon detector (more information is needed about the configuration). The main strong point is that SILAT should has relative higher reliability since it is designed suitable for space missions, like spectral imagery and satellite topographic study.

MPD's photon detection efficiency is obtained through the use of epitaxial silicon SPAD and patented Integrated Active Quenching Circuits (IAQC), which is specifically designed and optimized for photon counting. The main drawback is that it is difficult to achieve the precise ground resolution due to diffraction, and it also has large volume and power consumption.

The final option is use a 32×32 pixel array with in-pixel photon counting, which also use SPAD but in Complementary Metal Oxide Semiconductor (CMOS) technology [Cristiano Niclass and Charbon(2007)]. It has the highest quantum efficiency for blue laser(425nm to 500nm), but only 2% of the chip area can detect the quanta. In this case, micro lenses or faceted mirrors are used in order to collect most of the incoming quanta focus on such a small area. The solution draft design is shown in figure 6.41 on page 91. Both designs use the parabolic mirror placed at certain position to the small SPAD chip with a specified curvature, then the prism barrier is designed to filter other noise lights except wavelength about 425nm to 500nm blue light. After that, different receiver assemblies are designed.

The draft design diagram of assembly micro lenses is shown on figure 6.42 on page 91. The micro lenses are placed just above the SPAD chip to focus light source on the specific pixel 2% area. These lenses can increase the sensing area by factor of 5, which means 10% area can be used for detection. On the other hand, the micro lenses could be very heavy due to the high density of the lens material, and it could also has the

risk of falling off due to vibration during launching and boosting. Since the micro lenses is manufacturing in scale of micro meters, it could be an extra problem to achieve the precision.

Another way to increase the receiving efficiency is using the faceted mirror such as the figure 6.43 on page 92 shown. Instead of the heavy micro lenses, the multi-faceted elliptical mirror can be placed to achieve the focusing. In this way, the sensing area can be increase enormously from 2% to around 80%. Meanwhile, faceted mirror is manufacturing in scale of mini meters, so fabrication precision can be achieved.

6.7.3.5 Trade Criteria

In the last paragraph, the general trade off method is elaborated, but not in a quantitative way. It is more precise and clear to give some trade criteria to compare between options, which can be graded from 1-10 (worse to best) to indicate each criterion performance. Mass, power, volume are criteria considered as design of a constellation of micro- or nanosatellites. The criteria such as efficiency, reliability, resolution and FOV are defined whether the receiver can detect photon or not and the precision it could be done with. Last but not the least, cost, lifetime and availability need to be noticed generally in each subsystem.

6.7.3.6 Weight Factor

Weight factor is given differently to each criterion due to mission objective and instrument performance requirement. Lifetime is the top objective and the efficiency determines the photons can be detected or not, so both are given as maximum of 10. Power, mass, volume are important since micro or nanoreceivers are considered. Meanwhile resolution, reliability and FOV are also important to ensure the system can perform continuous accurate measurements. The mission objective is mainly about feasibility study, so cost and availability should not be the essential part.

6.7.3.7 Trade summary

The trade off table is shown in figure 6.10 on page 81. The SPAD plus micro lenses and faceted mirror designs have the much higher grades than SILAT or MPD. The SPAD with micro lenses has lowest grade for efficiency, which is mentioned in early chapters, because the lenses which is manufactured in scale of micro meters can only increase the efficiency by factor of 5. On the other hand, the faceted mirror can increase the fill field from 2% to 80%, that is why faceted mirror has much larger efficiency. The SPAD with faceted mirror design has the large advantages on power consumption($100\mu\text{W}$), mass(tens of grams) and volume($5 \times 5 \times 3[\text{mm}^3]$) comparing to either SILAT or MPD, that is much more realistic and practical if the swarm of receiver satellites are in scale of micro or even nano. The SPAD with faceted mirror turns to be the best option after all, and it should be further invested later on in detail design.

6.7.4 Optical Emitting Payload

LiDAR altimetry missions are dependent on electromagnetic or acoustic radiation transmission. In order to make a multi-angular DEM, a Light Amplification by Stimulated Emission of Radiation (laser) system is chosen. Since there are myriad types of lasers, it is crucial to understand the basics behind this technology.

Criteria	Weight Factor	MPD	SILAT	SPAD + microlenses	SPAD + mirrors
Power	7	6	6	9	9
Mass	8	5	5	9	8
Volume	8	4	3	8	8
Reliability	7	8	8	6	5
Efficiency	10	7	6	1	5
Cost	5	4	3	7	5
Availability	3	10	8	5	3
Lifetime	10	8	8	6	6
Resolution	8	7	7	10	10
FOV	6	6	6	9	9
Weighted total		462	433	495	504

Table 6.10: Receiver tradeoff table.

6.7.4.1 Optical Transition

[Chow(1999)] Solving the time-dependent Schrödinger equation for free electrons (represented as harmonic oscillators) shows the presence of certain energy gaps, i.e. the existence of quantized energy states, according to quantum mechanics. In a more mathematical view, the quantum particles in a particular system share the same eigenfunction, but have different eigenvalues. Among energy states, the state with the lowest energy is the most stable one. If they are *excited* by thermal energy, light or electron beams, the electrons absorb these energies and transit to a higher energy state. These transitions of the electrons from low energy states to high energy states are called *excitations*. Higher energy states, however, are unstable. As a result, the electrons in higher energy states transit to lower energy states in certain *lifetimes*. These transitions of the excited electrons from high energy states to low energy states are referred to as *relaxations*. In the recombination of negatively charged electron and positively charged holes (exciton pairs) there are radiative (emission of photons) and non-radiative (phonon emission through crystal lattice) recombinations.

6.7.4.2 Exciton Dynamics

Figure 6.44 on page 92 schematically shows the possible radiations and absorption. In the radiations, there are spontaneous emission and stimulated emission. Spontaneous emission is a radiative process in which an excited electron decays in a certain lifetime and a photon is emitted. In contrast, with stimulated emission, an incident photon induces a radiative transition of an excited electron. The emitted photon due to stimulated emission has the same wavelength, phase, \mathbf{k} -vector, polarization and direction. Therefore, the light generated is highly monochromatic, coherent and directional. As a result of the two photons generated from this process, the electromagnetic radiation is amplified. These quantum particles can on their turn start the same procedure on different electrons.

When a light is incident on a material, the stimulated emission and the absorption simultaneously take place. In thermal equilibrium, there are more electrons in a lower energy state than in a higher one, because the lower energy state is more stable. In order to obtain a net optical gain, the number of electrons in a higher energy state should exceed the number of electrons in a (relative) lower energy level. This condition is referred to as *population inversion*, because the electron population is inverted compared with that in thermal equilibrium.

6.7.4.3 Laser Geometry

The laser oscillator uses fractions of the spontaneous emission as the optical input and amplifies the fractions by the stimulated emission under population inversion. Once the optical gain exceeds the optical losses, laser oscillations take place. An oscillator has a gain and amplifies an input. To feed back light, *optical resonators* or *optical cavities*, which are composed of reflectors or mirrors, are adopted. Due to this configuration (which is used by pretty much all laser types), characteristics of lasers are affected by the optical gains and optical resonators.

6.7.4.4 Efficiency

Unfortunately, the induced power (pump power) cannot be perfectly transmitted to the electromagnetic radiation, i.e. the efficiency of the laser cavity and laser resonator are not equal to 100 percent. A number of mechanisms cause this decrease in efficiency:

1. Cavity Losses

Intercavity laser power losses are always presence, depending on the configuration. Next to the fact that the optical components will absorb some of the radiation (dependent on wavelength), some photon excitation will actually be lost (since the cavity only 'uses' a single direction of electromagnetic radiation). Hence, the energy pumped in the cavity cannot be used optimally.

2. Optic Misalignment

The radiated laser emission has a highly divergent-limited character. Considering the fact that the radiation is reflected through multiple optical components, small deviations and the low value of divergence can ultimately decrease the effective power.

3. Optical Transition

By theory, two-level energy systems can be used for lasing action. However, normal ('real') electron configurations show multiple-level characteristics. This principle is shown in figure 6.46 on page 93.

6.7.4.5 Pulsed vs Continuous Waves

Without any alterations of the electromagnetic radiation created by the stimulated emission within the laser cavity, the radiation, once in equilibrium, behaves like a continuous wave. The energy within this wave is equal to the pumper power minus the *round-trip inter cavity power losses*. However, the wave can also be pulsed. The pulse energy E_p is simply the total optical energy content of a pulse. For regular pulse trains, the pulse energy is often calculated by dividing the average power (measured e.g. with a powermeter) by the pulse repetition rate [Hz]. However, this is a valid procedure only if the energy emitted between the pulses is negligible. There are cases where, e.g., a mode-locked laser emits a pulse train together with a low-level background emission. Even if the background power level is far below the peak power, the background can significantly contribute to the average power.

The pulse energy together with the pulse duration is often used to estimate the peak power of pulses. Conversely, temporal integration of the optical power results in the pulse energy.

Typical pulse energies from Q-switched lasers range from microjoules to millijoules, and for large systems to multiple joules or even kilojoules. Mode-locked lasers achieve much lower pulse energies (picojoules, nanojoules or sometimes several microjoules) due to their high pulse repetition rates and sometimes due to limiting nonlinear effects in the laser resonator. Much higher energies of ultrashort pulses can be achieved by amplifying pulses at a lower repetition rate.

The pulsed configuration can be beneficial in laser altimetry missions, since individual pulses can be detected and analyzed. Hence, the footprint can be subdivided and the analyses of the incoming photons (energy packages) can result into a more detailed DEM.

6.7.4.6 Blue Laser Types

In the baseline report, a number of lasers was listed. Considering the fact that the receiver should be able to detect single photons, the actual OED characteristics are dependent on the receiver. Since the receiver efficiency is a function of wavelength, the appropriate wavelength should be transmitted. Since lasers show discrete wavelength characteristics, the type of laser should be determined from this criteria.

The analysis of the chosen wavelength is determined in chapter wavelength estimation.

The receiver characteristics show that the laser should have a wavelength in the interval of 425 - 500 [nm] (within visible spectrum designated as 'blue'). Hence, every laser with different wavelengths is not viable for this analysis.

Potential laser types for this altimetry mission:

Helium-Cadmium (He-Cd) laser

Wavelength: 441.6 [nm]

Gain medium type: Gas

Neodymium-doped Yttrium Aluminium (Nd-YAG) laser

Wavelength: 946 [nm] (473 [nm] with frequency doubling)

Gain medium type: Solid-State

Argon (Ar) laser

Wavelength: 454.6 [nm]

Gain medium type: Gas

laser diode systems

Wavelength interval 400 - 480 [nm] (tunable). The wavelength interval of this kind of laser is excellent, but they are difficult to produce for high output power and long (> one year) lifetimes. Since the determined lifetime in this mission exceeds this laser lifetime, this laser is not part of the trade-off.

6.7.4.7 Trade-off Criteria

Table 6.11 on page 84 shows the trade-off for the different lasers. The most important criteria and the ones that clearly need some explanation, are discussed in more detail in this section for the different gain media.

Wavelength ratio. The emitted wavelength is an important factor for the possibility of photon detection as function of atmospheric absorption and receiver efficiency. Considering the wavelength dependency of these last two terms, the laser types have a different wavelength ratio (see: chapter receiver).

Cost. Gas lasers in general are relatively cheap, because of the high Technology Readiness Level (TRL) and the relatively simple optical subsystems within the laser cavity. The cost of the optical emitting payload is considered to have a low weight factor. The typical cost estimation for a gas laser equals \$20,000 and \$30,000, whereas the solid-state laser can cost almost double (\$45,000 - \$50,000). However, since the total cost of the mission is in the order of 200 M\$, this difference is negligible.

Minimum Pump Power. [Paschotta(2008)]The threshold pump power of a laser is the value of the pump power at which the laser threshold is just reached, usually assuming steady-state conditions. At this point, the small-signal gain equals the losses of the laser resonator. For an optically pumped laser, the

Criteria	Weight Factor	Nd-YAG	Ar	He-Cd
Wavelength Ratio	9	9	7	5
Technical Readiness Level	6	8	8	10
Cost	5	5	9	10
Minimum Pump Power	8	6	7	7
Repetition Rate Manipulation	7	10	2	2
Volume	7	10	4	3
Mass	7	10	4	3
Chemical Stability	4	8	6	4
Thermal Control	4	8	6	5
Efficiency	8	7	1	7
Weighted total		532	338	359

Table 6.11: Emitter tradeoff table.

definition of threshold pump power may be based either on the incident or absorbed pump power. A low threshold power requires low resonator losses and a high gain efficiency.

Calculation for the laser types:

$$p_{p.th} = \frac{I_{rt}}{\eta_p \tau_2 \sigma_{em}}$$

P: Threshold power [W], I: Round-trip intercavity power loss [W], η : Pump efficiency, τ : Upper laser level lifetime, σ : Stimulated emission cross section

Helium-Cadmium Pumping efficiency: 0.82

Upper laser level lifetime [s]: $7.1 \cdot 10^{-7}$

Round trip power losses [$10^{-28}W$]: 2.357

Stimulated emission cross section [m^2]: $9.0 \cdot 10^{-18}$

Minimum Pump Power [mW]: 45

Nd-YAG Pumping efficiency: 0.92

Upper laser level lifetime [s]: $2.30 \cdot 10^{-6}$

Round trip power losses [$10^{-28}W$]: 5.01

Stimulated emission cross section [m^2]: $2.8 \cdot 10^{-23}$

Minimum Pump Power [mW]: 75

Argon Pumping efficiency: 0.82

Upper laser level lifetime [s]: $1.0 \cdot 10^{-8}$

Round trip power losses [$10^{-28}W$]: 2.787

Stimulated emission cross section [m^2]: $2.6 \cdot 10^{-16}$

Minimum Pump Power [mW]: 50

Repetition Rate Manipulation. To be able to create short pulses, the electromagnetic radiation present due to stimulated emission should be altered. This can be done with multiple mechanisms, like Q-switching, mode-locking or mechanical interference. However, only two of these (Q-switching and mechanical interference) can be used with gas lasers, giving rise to only moderately short pulses. Mode-locking, which is possible for solid-state lasers, allows the user to create shorter pulses and next to that, if active mode-locking is considered, the pulses can actually have a temporal deviation.

Volume and mass. The mass and volume are particularly dependent on the laser cavity length, which

equals 0.1 - 0.15 [m] for the solid state-laser and 0.25 - 1.5 [m] for a particular gas laser. However, the solid-state laser usually exhibits more optical components, increasing the weight.

Chemical Stability (lifetime). The use of gas as gain medium can alter and decrease the optical properties of the mirrors. The quality of the internal laser components can be decreased and hence, the lifetime is lower.

Thermal Control. Operational temperatures for the gas laser are in the order of 573 [K] (Argon and He-Cd temperature interval as well), whereas the operational temperature for the solid-state laser is 300 [K] with a relatively larger operational temperature interval compared to the gas laser configuration.

Efficiency. The Argon laser has very poor power efficiency, hence the transfer from the pump energy to the actual electromagnetic radiation is low, giving rise to (very low efficiency). The efficiencies (as described as above) are pretty equal for the other two options, around 40

6.7.4.8 Trade-off Summary

From the trade-off it is obvious which laser should be chosen in this mission. Especially the active pulse manipulation, the chemical stability (directly related to the lifetime) and the mass/ volume characteristics are really good for the Nd-YAG laser. The main drawback of the Argon laser is the poor power efficiency, resulting in pump powers in the order of kilowatt's. The main disadvantage of the gas laser in general is the poor performance of pulse manipulation. However, these types of lasers are generally cheaper.

6.7.5 Laser Thermal Control

[Paschotta(2008)]The functioning of the optical payload is dependent on a specific temperature interval, so in order to be able to meet the top level requirements, thermal control considerations for the emitter and receiver should be taken into account.

6.7.5.1 Thermal Physics

Two important mechanisms of thermal conductivity are (free) electron translation (crystal momentum) and phonon states. A phonon (state) is a quantum of acoustic energy, analogous to the quantum of electromagnetic radiation, the photon. Thermal excitations in a crystal or in an elastic medium can be described as a population of phonons. Basically, phonons represent a mode of vibration occurring in a rigid crystal lattice. Since, on one side, individual electrons in a crystal lattice are bound in terms of quantized energy levels and on the other side they are interconnected to neighboring particles by electric force (attraction or repulsion) as a function of distance, in most solids the energy given to lattice vibrations is the dominant contribution to the heat capacity, i.e. induced thermal energy is converted to a change in rate of crystal momentum or phonon state, which can be represented by a difference in internal energy. In this light, the terms 'thermal energy' and 'internal energy' represent the same quantity.

From an electron point of view, a change in temperature (or any change in state variable) represents the quest for a new thermal equilibrium situation. Since electrons are fermions, their orbit population is described by the temperature-dependent Fermi-Dirac distribution. Fermions show the tendency to occupy the lowest energy levels and since they are limited due to Pauli's exclusion principle, which states no identical fermion with equal intrinsic spin can occupy the same energetic orbit, not every electron can be in the ground state. Increasing the internal energy will therefore represent thermal excitation.

6.7.5.2 Theoretical Thermal Limits For Lasers

- Gain Medium Thermal Overloading Thermal overloading can be divided to the temperature interval at which electron excitation is impossible and the interval at which permanent crystal lattice deformation occurs.

Short term temperature increase ($T > 323.15[K]$)

To begin with the first phenomenon, in order to excite any electron, the conduction band should not be completely filled in thermal equilibrium. Any excitation, so also stimulated excitation, would be impossible and hence no lasing action would occur. In the real world, a small part of the electrons will give rise to stimulated emission since not all electrons would occupy the highest energy bands, considering the temperature to increase. However, population inversion would not be present. If the temperature is decreased afterwards, the gain material would be able to provide lasing action, making it an short-term problem with no permanent significance.

Long term temperature increase ($T > 323.15[K]$)

However, if the induced (thermal) energy is increased even further, the crystal lattice can eventually alter in time. This crystal lattice deformation not only implies the gain material, but all optical subparts, causing possible lasing failure. Recrystallization of the material can occur if the upper limit of the temperature interval is reached, giving birth to long-term (partial) failure. Another longterm effect is thermal fatigue for parts within the laser.

- Thermal Lensing

Long term temperature increase ($T > 303.15[K]$)

Particularly in high-power lasers, the appearance of a temperature-gradient in the gain medium often causes a significant 'thermal lens'. The gain medium has higher internal energy on the beam axis, typically causing some transverse gradient of the refractive index according to the temperature-dependent Sellmeier equation.

Thermal lensing occurs due to the combined effect of the thermal expansion and thermally induced refractive index change. The magnitude of the thermal lensing scales proportional to the power absorbed by the gain medium and the thermo-optic coefficient of the material, and inversely proportional to the thermal conductivity of the material.

The Sellmeiser equation could be used for the change in refractive index for all other optical subparts in the laser, like the lenses, and is dependent on the optics material. Since the refractive index will change due to the change in temperature, this has to be taken into account. Temperature gradients can alter the lasing action severely.

External induced thermal energy can therefor cause the formation of a thermal lens, causing the beam quality to alter. Especially beam divergence tends to decrease by the formation of a thermal lens, i.e. the change in refractive index change per unit temperature (dn/dT) should be kept within limits. The absence of thermal control can even lead to non-localized thermal lensing, since temperature-gradients can be localized away from the principal axes.

- Multi-Phonon Transitions

Long term temperature increase ($T > 353.15[K]$)

The upper-state lifetime (the lifetime of the population of the upper laser level) can be strongly reduced by decay processes which involve the simultaneous emission of multiple phonons. Multiple phonons are typically required for such transitions because the energy of a single phonon is not sufficient to match the difference in level energies. The rate of multi-phonon transitions decreases with the increasing number of phonons required. Temperature-gradients can influence the phonon transition and hence influence the the upper-state lifetime, decreasing the beam quality.

- Dielectric Transmission

Long term temperature increase ($T > 313.15[K]$)

Optically absorbing layers (dielectric transmission decrease) can form on the exit face of the fully

reflective mirror and on the doubling crystal, resulting in a decay of output power. The absorbed optical energy creates thermal gradients with which affects phase matching and hence lowering the beam quality.

- Limit in Electron Movement

Long term temperature decrease ($T < 273.15[K]$)

If the internal energy decreases to much, the exciton dynamics would alter, i.e. electrons will not be able to be excited to higher energy levels. This temperature dependent tendency is caused by the Boltzmann distribution, giving rise to an increase of potential energy at the lowest energy level.

6.7.5.3 Thermal Control

As seen in the previous paragraphs, the temperature interval for proper lasing action roughly equals $273.15 < T [K] < 313.15$. Since the thermal environment is extremely harsh (extremely cold background temperature, intense solar radiation, sudden loss of temperature in shadow and the presence of vacuum), thermal control considerations should be taken into account. Since active thermal control considerably adds weight, complexity and power to the system, passive thermal control should be considered, like coatings and constant conductance heat pipes.

6.8 Receiver Pointing

For the pointing of the receiver instrument three options are considered. The first concept is pointing the entire satellite towards the Earth using an active ACS. Using this system will also influence the behaviour of the solar cells, since the solar cells will move as well along with the satellite. The second concept is using two stepper motors for moving the instrument only. This concept will allow the instrument to move independently from the satellite, but will add more mass and moving parts to the satellite. Concept number three is a hybrid system. The rotation along the yaw-axis of the satellite is done by rotation the satellite, while the rotation along the other two axis is done using a single stepper motor. This way the satellite and the instrument can move semi-independent from each other and look at both the ground target and the Sun. Schematics of the different options are shown in figure 6.8 on page 94.

6.8.1 Trade Method

The trade-off is done by comparing the three concepts on a number of criteria. Each criterion is given a weight factor to show how important the criterion is compared to the others.

6.8.2 Trade Criteria

The trade-off criteria used are pointing accuracy, pointing rate, added weight, reliability, power, influence on other subsystems and the system complexity.

6.8.3 Weight Factors

Because the instrument can not work if the satellite is not pointed towards the ground target the pointing accuracy and pointing rate are given a weight factor of 5. The complexity, reliability and influence on other subsystems are less important comparably since the swarm is used for redundancy in making measurements

and other subsystems can be adapted to meet their requirements, a weight factor of 3 is given. The weight and power use of the system is given a factor of 2, because it is important for the satellite as a whole, but not the main driver for the mission.

6.8.4 Trade-off

Table 6.12 on page 88 shows the numerical values assigned to the different criteria. Pointing with only stepper motors can be done the most precise, the combination with a reaction wheel for the yaw-axis the precision around that axis will be lower, using only the ACS the accuracy will be the lowest. Stepper motors are able to respond really quickly, the reaction wheel option takes a lot longer to respond, since it has to move the entire satellite, not just a part. The pointing speed for the hybrid system will be somewhere in between, but will be better than average given the change in ground elevation will be larger than the change in relative position of the emitter. When the entire satellite is turned almost no extra mass need to be added, since attitude control is needed in the satellite anyway. With two actuators the two extra masses are added to the structure. In the hybrid concept only one additional actuator has to be taken. Since no additional parts are added to the system at concept one, the reliability of the concept will be just as high as the entire ADCS. Using only actuators adds two moving parts to the satellite and moving parts always add risk to spacecraft. Although the hybrid system only adds one moving part, it is still less reliable than none. Although concept one uses the existing ACS still a little more power is needed to make the manoeuvres for pointing towards the ground target. Stepper motors use power and two use more than one. Turning the entire satellite will mostly effect the other subsystems, e.g. the solar panels need to be pointed towards the Sun and the atmospheric drag will change throughout the orbit putting an extra load on the Attitude and Orbit Control Subsystem (AOCS). The second concept will add much mass to the satellite, not only for the motors, but also for the support structure. This will lead to more launch mass and more fuel needed to keep the satellite in orbit. The third concept will also add mass, but less than the second concept. In the latter two cases the solar panels still can be pointed towards the Sun, if required. The ACS will need to be made more precise for the concept to work, also the control algorithms will need to be very advanced. A lot more structure has to be added to the satellite in option two to make the satellite move in both directions. For concept three also some extra structure need to be added, but far less than with concept two. Also extra communication with the ADCS is required.

Criteria	Weight Factor	Concept 1	Concept 2	Concept 3
Pointing accuracy	10	2	8	6
Pointing rate	10	2	8	6
Added weight	4	8	2	5
Reliability	6	8	3	7
Power	4	7	2	4
Influence	6	2	3	7
Complexity	6	8	2	6
Weighted total		208	221	228

Table 6.12: Trade-off graph for the pointing mechanism. The weight factor signifies the importance of the criterion. Grades are given on a scale of 1 to 10, 1 being the worst, 10 the best

Concept number one is the clear loser in this trade-off. Concepts two and three are much closer together. Concept two scores high at the pointing accuracy and rate, but rather low scores for the rest, while concept three scores average overall. Concept number three is chosen, because there are no extreme scores on the criteria found.

6.9 Final Preliminary Design

After all trade-offs are done a final preliminary design can be compiled.

The system will contain:

- A Neodymium-doped yttrium aluminium garnet (Nd:YAG) laser for the emitter satellite
- SPAD receivers with dedicated mirrors for receiver satellites
- A pointing mechanism using a stepper motor and a reaction wheel
- Sun sensors and a star tracker for attitude determination
- Reaction wheels and magneto torquers for attitude control
- Thin film Copper Indium Gallium Selenide (CIGS) solar cells
- A X-band downlink with a phased array
- A S-band uplink
- A Ku-band cross-link with a horn antenna
- A GPS receiver for tracking
- A centralised communication structure

The satellites will have a circular orbit ($\text{eccentricity} = 0$), with an inclination of 85° and an altitude of 500km. The right ascending node will vary for the different satellites.

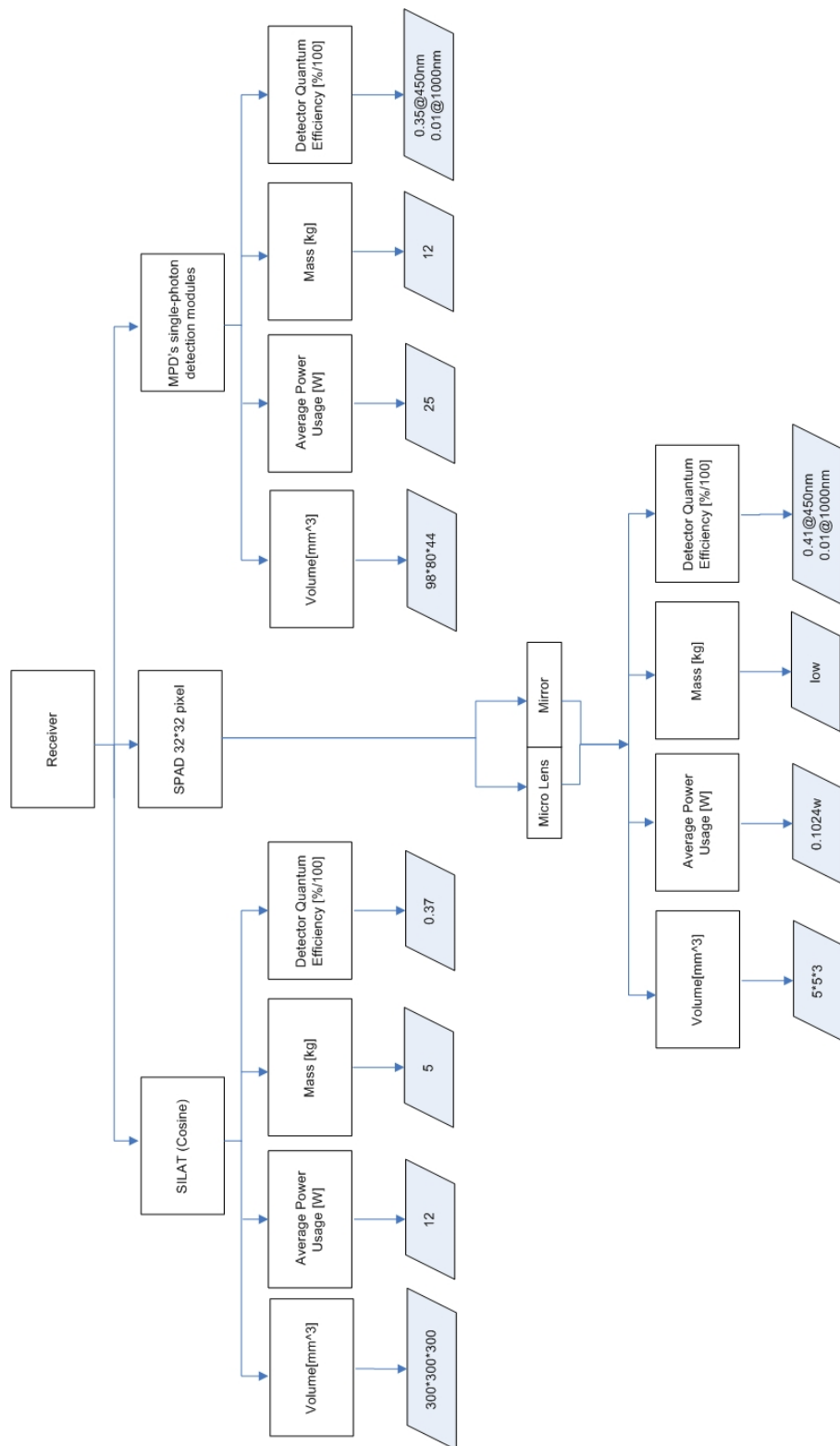


Figure 6.40: The pruned design option tree for the Laser receivers

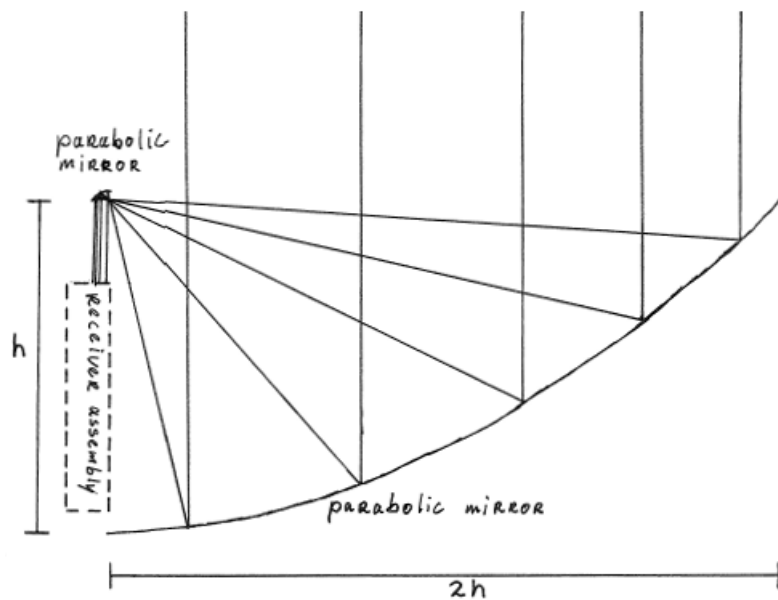


Figure 6.41: The diagram of the parabolic mirror

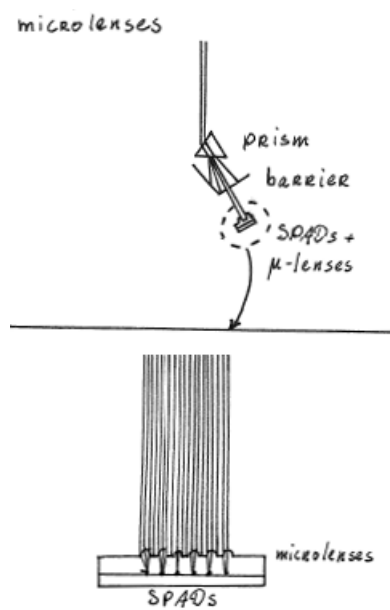


Figure 6.42: The diagram receiver assembly micro lenses

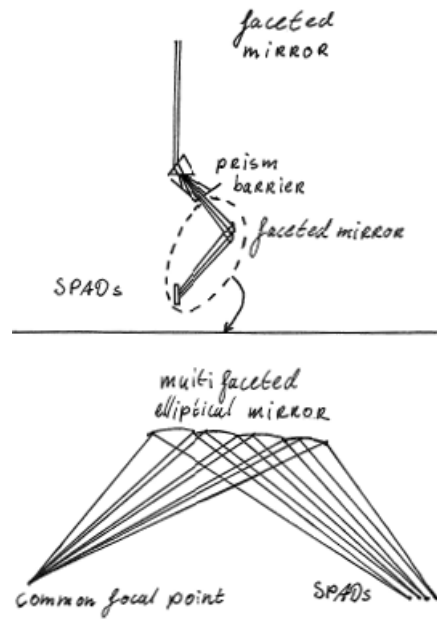


Figure 6.43: The diagram receiver assembly faceted mirror

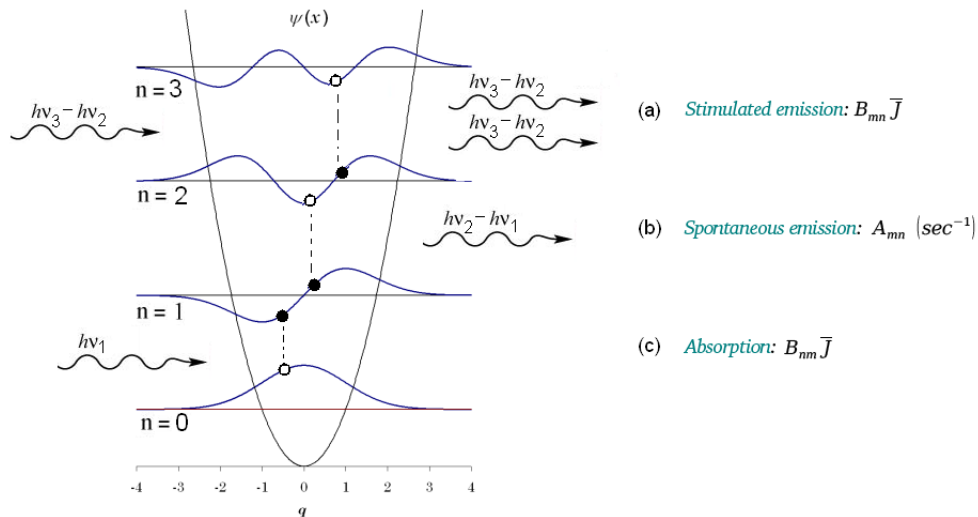


Figure 6.44: Left: individual energy quantum energy levels occupied with individual wave equation. Optical transitions given in random electron orbit; emission and absorption could take place at any energy level. Right: Einstein coefficients for optical transmission. 'J' represents the photon density in \mathbf{k} -space. Spontaneous emission is independent on photon density.

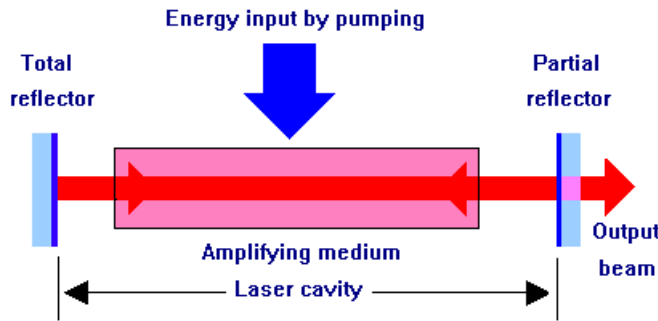


Figure 6.45: General layout of a laser. laser cavity with fully reflecting mirror (left) and partially reflected mirror (right). Under the stimulation of population inversion lasing action occurs due to optical reflection.

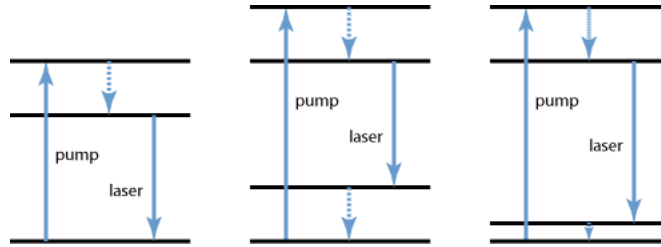


Figure 6.46: Three possible laser level system. Left: Three-level system. Middle and right: Four-level system with equal pump power level. The difference is the bandgap between energy level one and two. Hence, the efficiency of the four-level system in the middle is higher, since the effective lasing action energy quantity is higher with equal pump power

$$n_e^2(\lambda, T) = A + \frac{B + b(T)}{\lambda^2 - [C + c(T)]^2} + \frac{E}{\lambda^2 - F^2} + D\lambda^2$$

Figure 6.47: Refractive index as function of radial position, where the Sellmeier coefficients A, B, C, D, E, and F are constants dependent on gain material, c and b are temperature dependent, T is the temperature in degrees centigrade, and λ is the wavelength in micrometers.

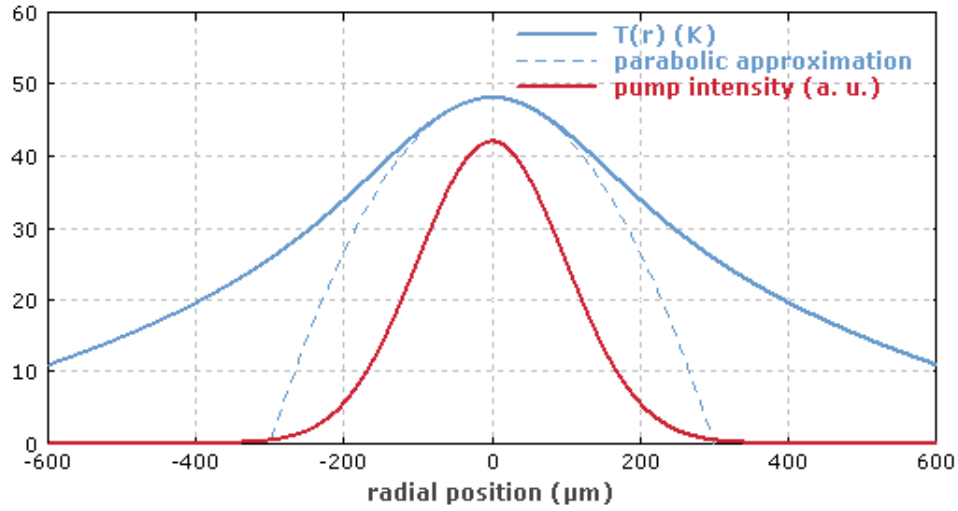


Figure 6.48: Transverse pump intensity distribution (red) and thermal profile (blue). The temperature profile is approximately parabolic only near the center of the crystal.

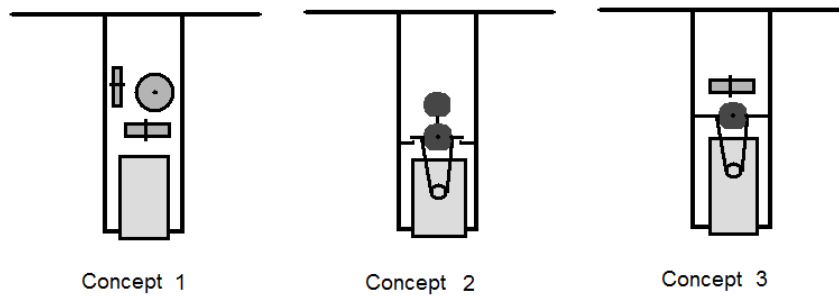


Figure 6.49: Design options for the pointing mechanism. The first option uses only the ACS, the second option only mechanical actuators, the third option is a combination of both using the ACS for the yaw-axis and a mechanical actuator for the other axis. The light grey box represents the instrument, one shade darker are reaction wheels and the dark boxes are actuators.

Chapter 7

Operations and Logistics

In order for the laser swarm to be successful it has to operate efficiently and effectively, so that the obtained surface model and other data can be sold on the market. This chapter will consider some of these operations and their required logistics. Note that only operations after successful orbit injection and deployment, and before the End-of-Life (EOL) are considered. A graphical representation of the hierarchy of the options considered here can be found in figure 7 on page 96.

Navigation and orbital control is an important operation for the laser swarm mission. All satellites have to be aware of where there are relative to each other, and the position of the formation as a whole has to be known as well. Although most of this system can be automated it is important there are people on the ground who check for any anomalies and give corrections whenever necessary.

Mission control entails the real time control of the satellites. Most of the mission can be automated given the predictable nature of the mission. The amount of people for mission control can therefore be limited. The only active inputs by humans should be inputs that correct some sort of anomaly. This being dependent on other operations like navigation and orbital control and various supporting operations.

The measurements will be performed completely autonomous, with human inputs only being used to correct an error in the automation or to change the routine. The measuring operation includes the both the emitter and the receivers, for a greater detail of the functions that have to be performed the function flow diagram from [?] may be consulted.

Payload support is comprised of one or more people who monitor the condition and performance of the payload of the emitter, and a separate group of people who monitor the receivers. In case of an anomaly they determine the severity and change the satellite or payload operations if necessary.

Spacecraft operations is similar to payload support, except that the person or people who work on this operation monitor the rest of the satellite.

Computer and communications support has a staff of several people who monitor the computers and the automated systems, and one or two persons who monitor the communications between satellites and satellites to the ground. Their main job is to make sure the system remains operational if an anomaly occurs.

Data services entails everything that happens with all data both on ground and aboard the satellites. The data can be anything from measurement data to navigational data. This operation support all the other ones. While largely automated some human interaction is needed to ensure the data is decoded, debugged, archived and generally handled properly. Minimal human interaction will be required to reduce the mission costs.

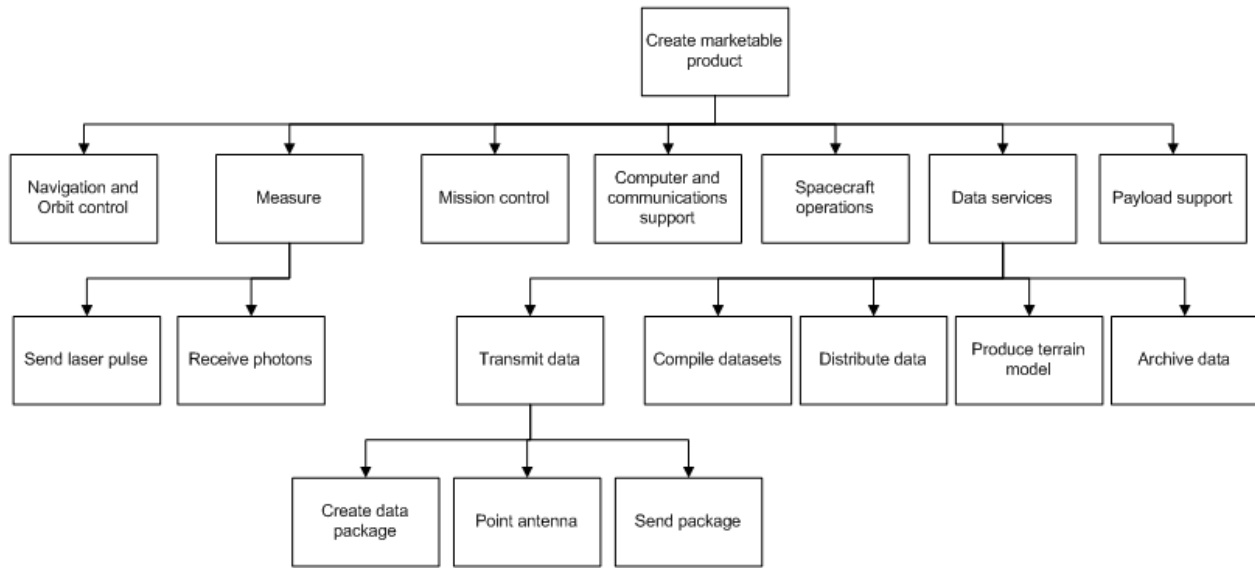


Figure 7.1: Hierarchy of the operations for the laser swarm mission.

Data transmission involves the sending of data between satellites and from the satellites to a ground station. It is a fully automated process as the orbits of the swarm have been simulated before the launch.

Chapter 8

Stability & Control

This chapter contains the requirements for stability and a short general introduction to the control of the satellites. Conditions for stability are derived in section 8.1, the control of the satellite is discussed in section 8.2.

8.1 Stability

A satellite is considered in a nadir pointing, circular orbit around the Earth. When small rotations are assumed, the equations of motion can be linearised. The linearised combined dynamic and kinematic equations are:

$$J_{11}\ddot{\theta}_1 - n(J_{11} - J_{22} + J_{33})\dot{\theta}_3 + 4n^2(J_{22} - J_{33})\theta_1 = 0 \quad (8.1)$$

$$J_{22}\ddot{\theta}_2 + 3n^2(J_{11} - J_{33})\theta_2 = 0 \quad (8.2)$$

$$J_{33}\ddot{\theta}_3 + n(J_{11} - J_{22} + J_{33})\dot{\theta}_1 + n^2(J_{22} - J_{11})\theta_3 = 0 \quad (8.3)$$

where J_{nn} is the inertia tensor, θ_n are the rotation axis (roll, pitch and yaw) and n is the orbital rate defined as

$$n = \sqrt{\frac{\mu}{|R_c|^3}} \quad (8.4)$$

where μ is the Earth's gravitational constant and R_c the radius of the orbit of the satellite center of mass. As can be seen in equation 8.2 the rotation around the pitch axis is independent of the rotation rates about the other two axis. By taking the Laplace transform of this equation the characteristic equation is found to be

$$s^2 + \frac{3n^2(J_{11} - J_{33})}{J_{22}} = 0 \quad (8.5)$$

Stability requires that the characteristic roots are purely imaginary. This is only true if

$$J_{11} > J_{33} \quad (8.6)$$

For simplification of equations 8.1 and 8.3 the parameters $k_1 = (J_{22} - J_{33})/J_{11}$ and $k_3 = (J_{22} - J_{11})/J_{33}$ are defined. The linearised equations of motion for roll and yaw then become

$$\ddot{\theta}_1 + (k_1 - 1)n\dot{\theta}_3 + 4n^2k_1\theta_1 = 0 \quad (8.7)$$

$$\ddot{\theta}_3 + (1 - k_3)n\dot{\theta}_1 + n^2k_1\theta_1 = 0 \quad (8.8)$$

Laplace transforming equations 8.7 and 8.8 gives

$$\begin{bmatrix} s^2 + 4n^2k_1 & (k_1 - 1)ns \\ (1 - k_3)ns & s^2 + n^2k_3 \end{bmatrix} \begin{bmatrix} \theta_1 \\ \theta_3 \end{bmatrix} = \begin{bmatrix} 0 \\ 0 \end{bmatrix} \quad (8.9)$$

To find the non-trivial solution the determinant of the matrix in 8.9 needs to be zero.

$$s^4 + (1 + 3k_1 + k_1k_3)n^2s^2 + 4k_1k_3n^4 = 0 \quad (8.10)$$

This equation is true when

$$\frac{s^2}{n^2} = \frac{-(1 + 3k_1 + k_1k_3) \pm \sqrt{(1 - 3k_1 + k_1k_3)^2 - 4^2k_1k_3}}{2} \quad (8.11)$$

For the roots to be imaginary the following equations should hold

$$1 + 3k_1 + k_1k_3 > 0 \quad (8.12)$$

$$1 + 3k_1 + k_1k_3 > 4\sqrt{k_1k_3} \quad (8.13)$$

$$k_1k_3 > 0 \quad (8.14)$$

The satellite is stable around all three axis when conditions 8.6, 8.12, 8.13 and 8.14 are all met [Chu(2009a)].

8.2 Control

The fact that there is no or little friction in space is both an advantage as a disadvantage for spacecraft. The advantage is that less power is required for the spacecraft to move, the disadvantage is that there is nothing to stop the spacecraft from moving when it does. Every torque which is imposed on the satellite, both by external and internal sources, has to be countered to stop the spacecraft from rotating. The simplified control equations of motion for the satellite are

$$M_{c1} = J_{11}\ddot{\theta}_1 \quad (8.15)$$

$$M_{c2} = J_{22}\ddot{\theta}_2 \quad (8.16)$$

$$M_{c3} = J_{33}\ddot{\theta}_3 \quad (8.17)$$

If the satellite needs to make a manoeuvre with an angle of θ_{man} two torques need to be exerted on the satellite with a magnitude of

$$M_c = 4\theta_{man}J/(t^2) \quad (8.18)$$

where t is half the time required for making the total manoeuvre. The torques first need to be in one direction for half the time, then in the opposite direction for the other half of the time [Chu(2009c)].

Chapter 9

Sustainable Development Strategy

In this chapter the Sustainable Development Strategy is discussed in the order of production (section 9.1), operations (section 9.2) and EOL (section 9.3).

9.1 Production and Logistics

The design is aimed at a swarm of mostly identical satellites. This may allow for series production which is more efficient in terms of resources than a one-of large satellite with a lot of unique components. This also implies that the number of different spare parts could be reduced. Smaller satellites could also use smaller facilities for production and testing.

Transportation can be split up into two parts: transportation to the launch site and the launch from the surface to the final orbit in space. On both occasions the system can again profit from its small size. If the satellites are not launched all together, they can “piggyback” on another satellite’s launcher.

Spreading the swarm, i.e. piggybacking using different launchers, has several advantages. First of all, the emissions are lower than in case of a dedicated launcher. Also, if the first satellite fails before the launch of the rest of the swarm, the others can be repaired and thus less resources are wasted.

9.2 Operations

Once in orbit, the satellite’s influence on the Earth is very limited. The only real concern is the debris it leaves behind during launch and deployment, which can be dangerous to other satellites orbiting the Earth. However, the deployment mechanism, which is responsible for most of the debris, is not included in this technical feasibility study. Later studies developing the ideas from this feasibility study should take it into account, since more satellites could mean more deployment mechanisms and hence more waste. One aspect that can be dealt with is the efficient use of resources. The swarm can be designed in such a way that if one of the satellites fails a replacement satellite can be sent, whilst any remaining satellites can be reused.

9.3 End of Life

Each satellite will be at the end of its life if it cannot perform its function anymore. It is important that after the mission is over all satellites are removed from their orbit and burn up in the atmosphere so that they do not pose any danger to other satellites. Final decommissioning of the swarm will be more complex than for a regular satellite, since every individual satellite has to be decommissioned separately.

Chapter 10

Simulation

This chapter preliminarily discusses the design and workings of a software tool developed with the purpose of guiding and validating the results of the tradeoff done in the main laser swarm project, as well as demonstrating the feasibility of the concept of the laser swarm.

Generally speaking, the simulator program is divided into two parts. The first part is the simulation of the physical path of the photons in the laser pulse up to the point where they are received by the receiving satellites. This part has been documented in section 10.1.

The second part is the analysis of the received photon data, to determine terrain height and the terrain BRDF. Obtaining this data is what the software and in general this feasibility study is about. This part is described in section 10.2.

10.1 Simulation

In this section the simulation of the satellites, moving through space and sending and receiving laser pulses, is discussed. In subsection 10.1.1 the emitter and receiver satellite orbits are considered. In subsection 10.1.2 the way the Earth's surface was modeled is explained. In subsection 10.1.3 the path of the signal is examined, whereas in subsection 10.1.4 the introduction of noise into the signal is disclosed.

10.1.1 Orbit

The orbit of each satellite in the constellation is defined by means of six Keplerian elements. These define the shape of the orbit, the orientation of the orbit with respect to the center of the Earth and the position of the satellite on the orbit.

As there are a number of rotating bodies, three reference frames are used in order to facilitate the process of locating the satellites in space. The three reference frames used in the simulation are described below.

The first is True Of Date (TOD). Its X-axis points towards the direction of the vernal equinox and its Z-axis coincides with the axis of rotation of the earth. TOD takes into account nutation and precession of the earth. For practical reasons, it does not rotate with respect to the Sun.

In the second place there is Earth-Centered, Earth-Fixed (ECEF). Its X-axis points towards 0° latitude

and 0° longitude. The XY plane lies in the plane of the equator. Its origin is in the center of mass of the Earth.

Thirdly there is the PQW. The P-axis points towards the perigee of the orbit, the PQ plane lies in the plane of the orbit and the W-axis is perpendicular to the plain of the orbit. The origin of the frame is at the focal point.

The program converts between the before-mentioned reference frames for the user's convenience.

The position of the satellite is defined with respect to the TOD reference frame. Kepler's equations are solved for a certain time to determine the position. The orbit is determined for every satellite in the constellation. The orbit is assumed to be perfect, meaning that its orientation and shape do not change: perturbations are not considered.

The Earth's rotation about its own axis and around the Sun is simulated in order to provide a more realistic simulation environment. From the rotation of the Earth around the Sun, the sun vector is deduced; this is used in noise calculations.

Most of the functions are adapted to the simulator from the Java Astrodynamics Toolkit (JAT) library.

10.1.2 Earth Model

The Earth model is the digital representation of the Earth surface. It stores a Digital Elevation Model (DEM), and the scattering characteristics of the local terrain. In section 10.1.2.1, the DEM implementation will be elaborated and section 10.1.2.2 describes the way incoming radiation is scattered.

10.1.2.1 Digital Elevation Model

A Digital Elevation Model is a digital representation of a topographic surface. For the ground representation in the simulator a few tiles of the Advanced Spaceborne Thermal Emission and Reflection Radiometer (ASTER) Global Digital Elevation Model (GDEM) were used. This DEM was created using the complete history of the ASTER instrument launched on the Terra satellite. This DEM has a spatial resolution of one arc-second and a vertical accuracy of 7 – 14 meters. The elevations of the intermediate points were obtained using nearest-neighbor interpolation.

The ASTER GDEM elevations are expressed with respect to the World Geodetic System 1984 (WGS84) ellipsoid. To simplify the internal simulator, the DEM tiles were projected to the EPSG:3857 spheroid. The projection is done using the GeoTools Java toolkit [geo(2010)].

The digital elevation is used to compute the total distance (and thus the time) that the laser pulse travels. Because scattering is dependent on the terrain normal, this normal is derived from the DEM, using the two perpendicular surface gradients that can be extracted from the DEM.

10.1.2.2 Scattering Model

Scatter is the physical process where incident radiation is absorbed and reflected back towards the atmosphere. To this end a scattering model is used. This scattering model is a way to construct a BRDF. A BRDF is a distribution of the incident light over the hemisphere [Rees(2001), pages 47-49]. An example is shown in figure 10.1, page 104.

The most basic example of a BRDF is the Lambertian model [Rees(2001), pages 49-50]. This model as-

sumes a homogeneous perfectly rough surface, causing a homogeneous scattering distribution. Apart from the index of refraction of the air, the incident radiation vector and the exitant radiation vector (which are all known), use of Snell's law is needed to find Fresnel's coefficients, thereby requiring the index of refraction of the ground.

A modification that can be made to take into account the tendency of surfaces to scatter more in the direction of the surface normal, is called the Minnaert model [Rees(2001), page 50]. It causes a more elliptical BRDF. It depends on the Minnaert parameter κ .

Another important modification is the Henyey-Greenstein term. It accounts for the tendency of surfaces to back- or forwardscatter [Rees(2001), page 51]. This rotates and deforms the elliptical BRDF obtained from the Minnaert model. The Henyey-Greenstein term is parameterized by Θ . The final result is shown in figure 10.1, page 104.

This is the scattering model used in the program. Because there is no data from which all three parameters can be accurately determined, a coefficient map was made up. It does not matter much what the precise form of the BRDF used in the simulation is, so long as it can be retrieved.

With the help of the formulae from [Rees(2001), pages 43-51], the incidence vector can be taken and the number of photons radiated in a specific direction can be calculated. Note that the program does not integrate over part of the sphere: because the angle of the cone is very small, the BRDF is assumed to be constant over the cone. The error induced here is worth avoiding the computationally expensive integration.

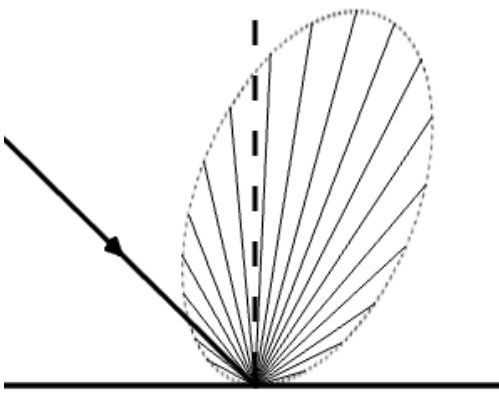


Figure 10.1: Example of a BRDF

10.1.3 Signal Path

The simulated path that the laser signal follows is visualized in figure 10.1.3 on page 104. There are three distinct phases. The first one is the travel of the signal down through the atmosphere. This is followed by the scattering on the Earth's surface. Finally the pulse has to travel back up through the atmosphere. This sequence is elaborated on in more detail below.

The signal originates from the emitter. For each pulse, the emitter position is determined from a set of Kepler elements. The energy in the pulse is found by distributing the emitter power over a constant number of pulses of a given duration.

The signal then starts to propagate through the atmosphere. The atmosphere affects the signal in several manners, but the most important one is the attenuation of the signal. Attenuation is the only disturbance

by the atmosphere taken into account. The pulse energy exponentially decays with travel distance through the atmosphere. Furthermore also the optical thickness of the atmosphere is taken into account.

Then the intersection of the pulse with the DEM is computed. As a simplification in this process, the intersection of the pulse (i.e., the ray) with a sphere is computed. The sphere has a radius of the average terrain height of the DEM tile plus the Earth radius. Then the ray-sphere intersection point coordinates are converted into latitude and longitude. These are then used to find the actual terrain elevation from the DEM and the three-dimensional position.

Then the scattering characteristics are constructed. For this, the terrain normal and the inbound laser pulse vector are used. The power of the emitted pulse is now distributed over the entire footprint area of the emitter and then scattered back using the scattering technique described in section 10.1.2.2. The backscattered energy is computed separately for every receiver satellite.

The reflected pulse now travels back through the atmosphere. More attenuation takes place along this path. The energy received by the receivers now depends on the receiver aperture. The received energy can then be converted into photons by dividing the energy received by the energy per photon.

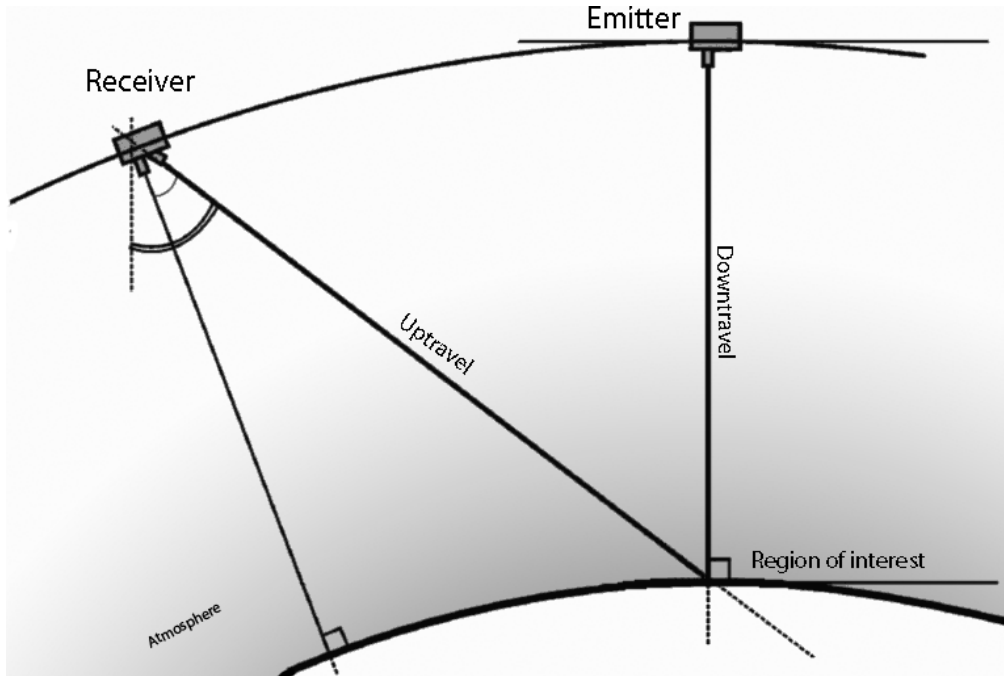


Figure 10.2: Signal path representation

10.1.4 Noise

The main source of noise in the system comes from the Earth's surface. This includes sources on the Earth such as lights along highways and reflected radiation, i.e. the Earth's albedo. The amount of radiation that is received by the receivers depends on the footprint of the receivers. This is an ellipse created by the intersection of the cone originating from the receiver with the terrain. A simplification is made in that the DEM is assumed to be a flat area with the elevation of the center point.

The amount of power emitted per square meter is dependent on the illumination of the Earth by the Sun. If the Sun illuminates the footprint, the emitted power is the scattered power of the Sun in the receiver

detection wavelength bandwidth. This power can be found by integrating Planck's law over the detection spectrum and the solid angle the Sun subtends to the receiver footprint on Earth. If the Sun does not illuminate the receiver footprint, the only contribution to noise is the Earth's greybody radiation, which is also taken into account.

While noise propagates through the atmosphere it is also attenuated. This attenuation is computed in the same way the signal attenuation is; see section 10.1.3.

10.2 Data Analysis

In this section the analysis of the received photon data taken care of in the software tool is elaborated on. The analysis consists of two parts: the terrain altitude determination and the BRDF determination. The first is expounded in subsection 10.2.1, the second in 10.2.2.

10.2.1 Altitude Determination

In order to tackle the problem of decrypting the raw data and converting it into a coherent terrain model, various statistical techniques need to be employed. The basic principle behind the altitude determination of the terrain is as following. First the time difference between generation and reception of the pulse is registered. As the position of the emitter at the time when the pulse was sent is known, just like the position of the receiver at the time the pulse was received is, the distance to ground can be determined. In theory only one emitter and one receiver are necessary to determine the altitude, but due to various uncertainties in position and noise characteristics of the received data, more receiving satellites are necessary to obtain a reliable and complete terrain representation.

In the simulator the emitter is modelled such that it records the time when the pulse was sent. The receivers are modelled such that they register the time and intensity (in photons) of the received pulse. The problem is that not all emitted pulses are registered, and sometimes noise, which does not correspond to any emitted pulse, is registered.

One of the ways to solve this problem is to use multiple receivers. The noise could be identified and removed by means of looking for a spike in the received photons for the whole swarm within a certain time range (usually twice the time it takes for a light beam to travel the orbit altitude). This data could be filtered by means of correlating the distance of the receiver to the Earth center and the time of the received pulse. Usually, the larger the distance, the larger the time difference. This method helps to eliminate outliers. Since the footprints overlap, the measured altitudes could be further smoothed out by means of a running average.

10.2.2 Bidirectional Reflection Density Function Determination

The BRDF returns the ratio of the radiance to irradiance for a given angle perpendicular to the surface. In theory, it is possible to measure it by means of the received photons of all of the receivers for a given pulse, where each received photon indicates the relative intensity. From the position of the receivers the direction of the irradiance vector can be calculated. Having the direction and intensity of the reflected radiation a segment of the BRDF for a specific incident angle could be reconstructed. By making a multiple passes over the same region, a partial BRDF for different incidence angles can be recorded. If the data is interpolated, a complete BRDF can be determined.

10.3 Simulations

In order to determine the correct sizing of various subsystems, the behavior of the swarm needs to be known. To this purpose several simulations have been ran. The first and most important one is to determine the variation of the photon count with increasing altitude. This simulation is described in section 10.3.1 on page 107. In section 10.3.2 on page 108, second simulation is discussed. This simulation determines the amount of noise photons received from the sun with respect to the number of photons from the laser emitter.

10.3.1 Variation of Photon Density with Altitude

To determine the number of photons with increasing altitude, a simulation was ran with several constellations. These constellations differ only on the constellation altitude. Each constellation exists of a single transmitter and receiver, on the same orbit. Furthermore, to reduce errors not due to the altitude effect, the scattering coefficients and elevation remain constant over the entire DEM area.

The scattering coefficients values used were 1.5 for the index of refraction, 1.3 for the Minnaert correction and -0.5 for the Henyey-Greenstein correction. The area over which the simulation ran is a rectangle stretching from (48° lat; 8° long) to (54° lat; 9° long). The laser (500 nm) that was used has 10W of lasing power, spread over 5000 pulses per second, each with a length of 1ns. The receiver satellite has an aperture of 8x8 cm (0.0064 m²) and a perfect receiver. The constellation orbital parameters are as follows:

- Semi-major axis: Earth radius + altitude (variable),
- Eccentricity: 0,
- Inclination: 90°,
- Right ascension of ascending node: 8.5°,
- Argument of perigee: 0°,
- True anomaly: 0°.

The results are shown in table 10.1 and visualized in figure 10.3. The datapoints show a clear exponential decaying trend. This trend can be approximated with the mathematical function $y = e^{-0.0052 \cdot x + 0.6558}$. The function shows a high decay rate with increasing altitude. For example moving from altitude of 500 km to 350 km doubles the number of received photons. To compensate for this effect, one would have to design the laser to have double the power, or the receiver double the aperture. This is because both of these parameters directly effect the number of received photons.

Altitude [km]	300	325	350	375	400	425	450	475	500
Average # photons	0.4249	0.3613	0.2991	0.2692	0.2483	0.2054	0.1843	0.1641	0.1483

Table 10.1: Simulation results for varying altitude

From this simulation, one can conclude that purely on the bases of received photons, a lower altitude is better. This is in direct contradiction to the drag analysis. However higher altitudes are possible, with increased laser power and/or receiver aperture area.

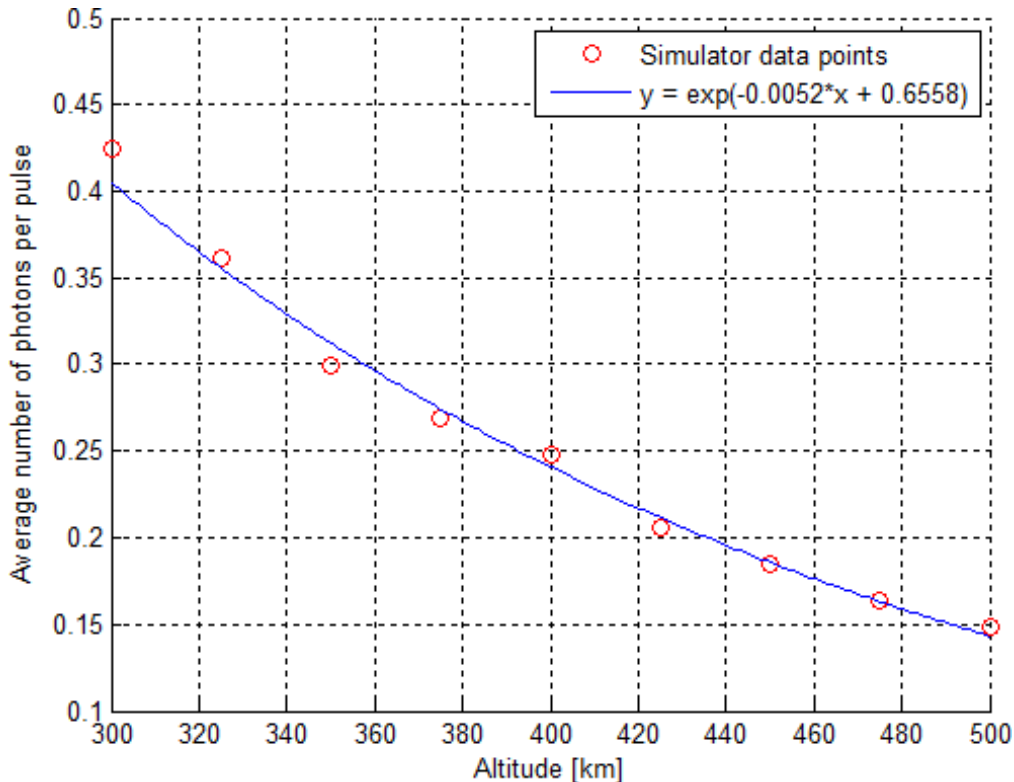


Figure 10.3: Height variation effect in the # received photons

10.3.2 Solar Photons Fraction

The goal of this simulation is to get an idea of the number of photons received due to radiation noise from the sun. This is required to get an idea of what fraction of photons is actually from the laser emitter and what fraction is noise. A single pass over an again flat area with constant scattering coefficients was simulated.

The scattering coefficients remain the same as for the previous simulation. Also the same orbit characteristics were used, only at a fixed altitude of 450 km. The emitting laser now has 33 W of lasing power. The other characteristics of the emitter remain the same. The receiver satellites have an aperture are of 20x20 cm (0.04 m^2) and are sensitive in a band of 1 nm around the center laser wavelength (500 nm). Furthermore the receiver has an optical efficiency of 90% and quantum efficiency of 40%. The results are summarized below:

- Pulses sent: 24989 (about 5s)
- Photons from pulses received: 12289 (86.5%)
- Sun noise photons received: 1930 (13.5%)
- Total photons received: 14219

From these results, one can conclude that the majority of the photons received are indeed from the transmitted laser pulses, and not from the sun. Furthermore, about every second pulse is detected by the receiver. Coupled with the swarm concept, that means that per pulse, a couple of photons are detected. This knowledge can be used to filter out the lower random sun noise photons. This means that this orbit altitude combined with the given laser power is sufficient to filter out the noise.

Bibliography

- [Mar(2008)] Ocean surface topography from space, Jul 2008. URL <http://sealevel.jpl.nasa.gov/overview/benefits.html>.
- [cub(2010)] Cubesatshop.com. online, 2010. <http://www.cubesatshop.com>.
- [del(2010)] DelfiSpace, the nanosatellite programme of the Delft University of Technology, 2010. <http://www.delfispace.nl>.
- [geo(2010)] Geotools, May 2010. URL <http://www.geotools.org/>.
- [ice(2010)] Icesat: Spacecraft, 2010. URL <http://icesat.gsfc.nasa.gov/icesat/spacecraft.php>.
- [imi(2010)] Miniature 3-axis reaction wheel & attitude determination and control system for cubesat kittm nanosatellites, April 2010. http://www.cubesatkit.com/docs/datasheet/DS_CSK_ADACS_634-00412-A.pdf.
- [lan(2005)] Chapter 2 - landsat 7 spacecraft: section 4 communication links, 2005. URL http://landsathandbook.gsfc.nasa.gov/handbook/handbook_htmls/chapter2/chapter2.html#section2.4.
- [mar(2010)] Maryland aerospace inc., April 2010. <http://www.miniadacs.com>.
- [mil(2010)] Milstar ii, 2010. URL http://www.boeing.com/defense-space/space/bss/factsheets/government/milstar_ii/milstar_ii.html.
- [spa(2010)] Spacequest, ltd., 2010. <http://www.spacequest.com/>.
- [tno(2010)] TNO. website, 2010. <http://www.tno.nl>.
- [Chow(1999)] Dr. Weng. W. Chow. *Semiconductor-Laser fundamentals*. Springer, 1999.
- [Chu(2009a)] Dr. Q.P. Chu. Spacecraft attitude dynamics and control, course notes no. 1 part 3, 2009a.
- [Chu(2009b)] Dr. Q.P. Chu. Spacecraft attitude dynamics and control, course notes no. 2 part 1, 2009b.
- [Chu(2009c)] Dr. Q.P. Chu. Spacecraft attitude dynamics and control, course notes no. 2 part 2, 2009c.
- [Cristiano Niclass and Charbon(2007)] Robert Henderson Lindsay Grant Cristiano Niclass, Marek Gersbach and Edoardo Charbon. A single photon avalanche diode implemented in 130-nm cmos technology. *IEEE Journal of selected topics in quantum electronics*, 13:863–869, 2007.
- [David Stoppa and Charbon(2009)] Justin Richardson Richard Walker Lindsay Grant Robert K. Henderson Marek Gersbach David Stoppa, Fausto Borghetti and Edoardo Charbon. A 32x32-pixel array with in-pixel photon counting and arrival time measurement in the analog domain. 2009.
- [Delfi-C3(2010)] Delfi-C3, 2010. URL http://www.delfic3.nl/index.php?option=com_content&task=view&id=25&Itemid=37.
- [Dhere()] N. G. Dhere. Solar energy materials and solar cells.

- [DutchSpace(2007)] DutchSpace, 2007. URL http://www.dutchspace.nl/pages/products/content.asp?id=324&P=2_6_4.
- [ESA-DutchSpace(2007)] ESA-DutchSpace, November 2007. URL <http://telecom.esa.int/telecom/www/object/index.cfm?fobjectid=13406>.
- [et al.(2001)] James R. Wertz et al. *Mission Geometry; Orbit and Constellation Design and Management*. Microcosm Press and Kluwer Academic Publishers, 2001.
- [et al.(2010)] J.P. Florijn et al. Laser swarm: Baseline report. Technical report, TU Delft, 2010.
- [et al.(2007)] Peter Fortescue et al., editor. *Spacecraft Systems Engineering*. John Wiley & Sons Ltd., Chichester, West Sussex, England, 3 edition, January 2007.
- [M. Gersbach and Charbon(2009)] E. Labonne J. Richardson R. Walker L. Grant R Henderson F. Borghetti D. Stoppa M. Gersbach, Y. Maruyama and E. Charbon. A parallel 32x32 time-to-digital converter array fabricated in a 130 nm imaging cmos technology. 2009.
- [McGlone(2004)] J.Chris McGlone, editor. *Manual of Photogrammetry Fifth edition*. American Society for Photogrammetry and Remote Sensing, 2004.
- [Niclass(2008)] Cristiano L. Niclass. *Single-Photon Image Sensors in CMOS: Picosecond Resolution for Three-Dimensional Imaging*. PhD thesis, cole Polytechnique Fdrale de Lausanne, 2008.
- [N.V.Yastrebova(2007)] N.V.Yastrebova. High-efficiency multi-junction solar cells: current status and future potential. *Solar Energy*, 2007.
- [Paschotta(2008)] Dr. Rdiger Paschotta. Photonics: Laser and optical physics, 2008. URL <http://www.rp-photonics.com/lasers.html>.
- [Rees(2001)] W. G. Rees. *Physical Principles of Remote Sensing*. Cambridge University Press, Cambridge, second edition, sixth printing edition, 2001. ISBN 9780521669481.
- [Robert P. Bukata(1995)] Kirill Ya. Kondratyev Robert P. Bukata, John H. Jerome. *Optical Properties and Remote Sensing of Inland and Coastal Waters*. CRC press, 1995.
- [S.Cova and F.Zappa(1996)] A.Lacaita C.Samori S.Cova, M.Ghioni and F.Zappa. Avalanche photo diodes and quenching circuits for single-photon detection, 1996. URL http://en.wikipedia.org/wiki/Single-photon_avalanche_diode.
- [Shelley Brown(2008)] Youichi Kumeuchi Shinsuke Enomoto Masatoshi Uno Hirobumi Saito Yoshitsugu Sone Daniel Abraham Gran Lindbergh Shelley Brown, Keita Ogawa. Cycle life evaluation of 3ah lixmn2o4-based lithium-ion secondary cells for low-earth-orbit satellites. *Journal of Power Sources*, 2008.
- [solar energy GmbH(2010)] Azurospace solar energy GmbH, 2010.
- [SPECTROLAB()] INC SPECTROLAB. 28.3% ultra triple junction (utj) solar cells datasheet.
- [Wertz(2006)] Wiley J. Larson & James R. Wertz, editor. *Space Mission Analysis And Design*. Microcosm Press and Springer, El Segundo, CA (Microcosm Press) & New York, NY (Springer), 3 edition, 2006.

Appendix A

Design Option Diagrams

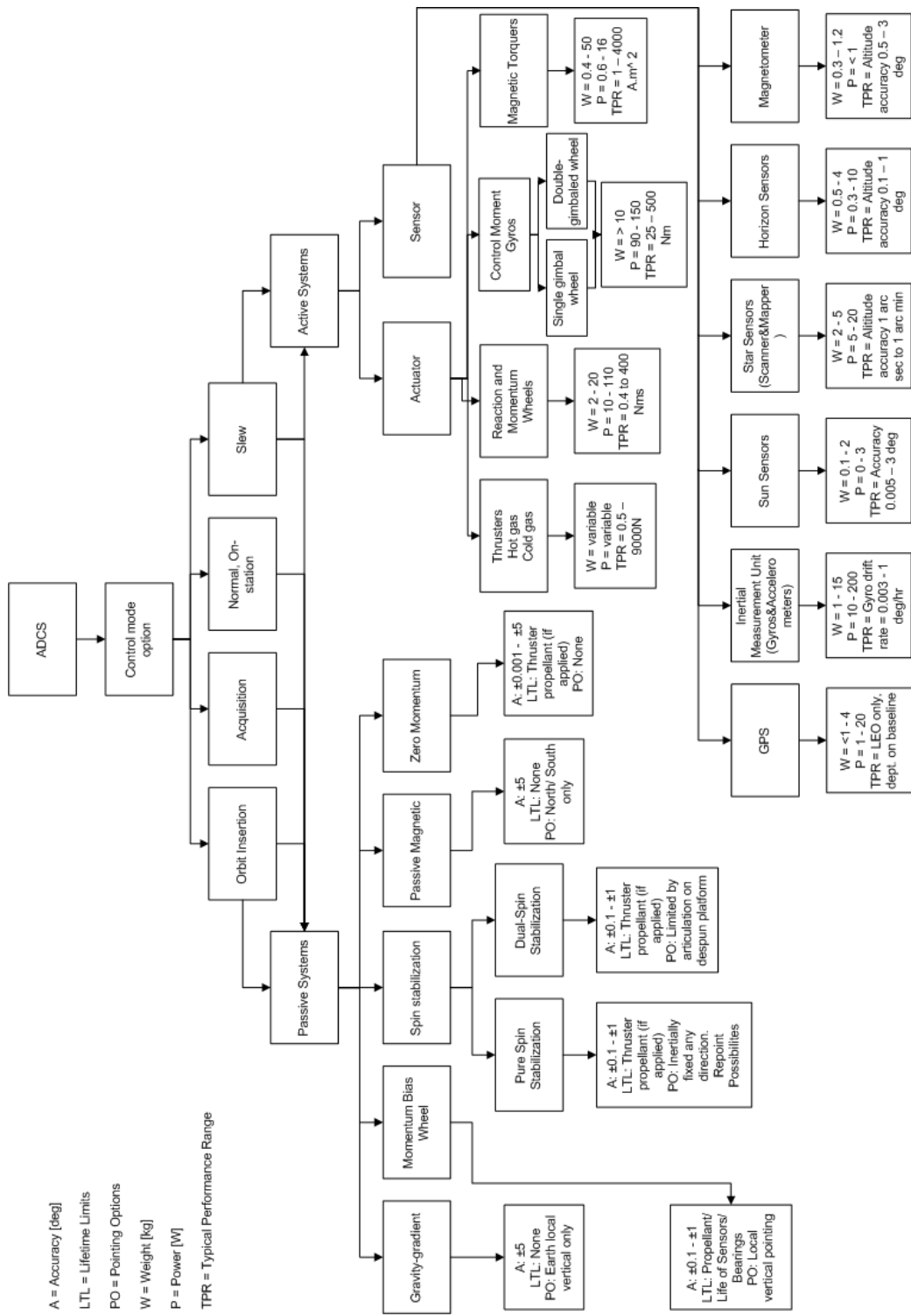


Figure A.1: Design option tree for the ADCS

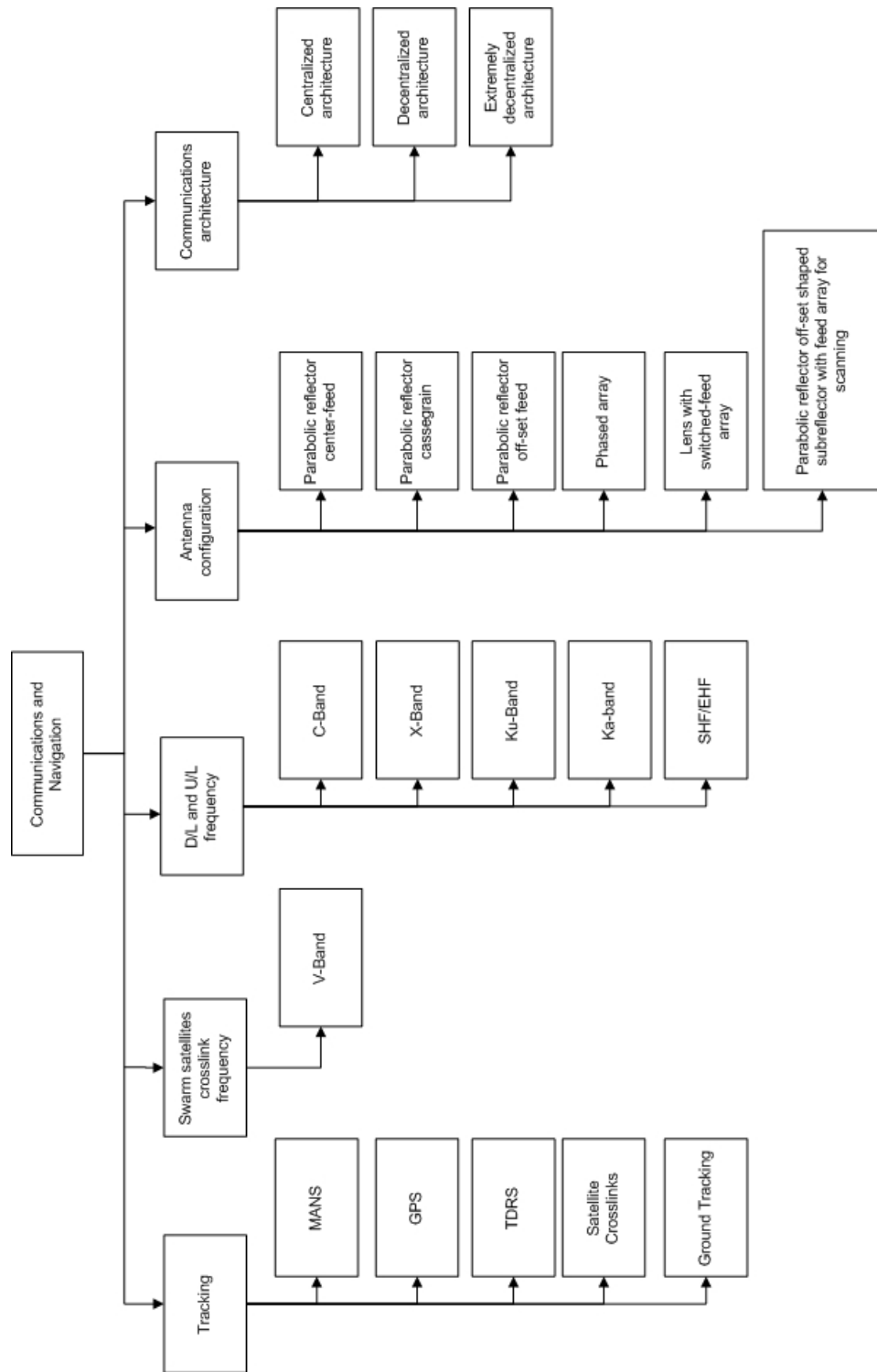


Figure A.2: Design option tree for the communication systems

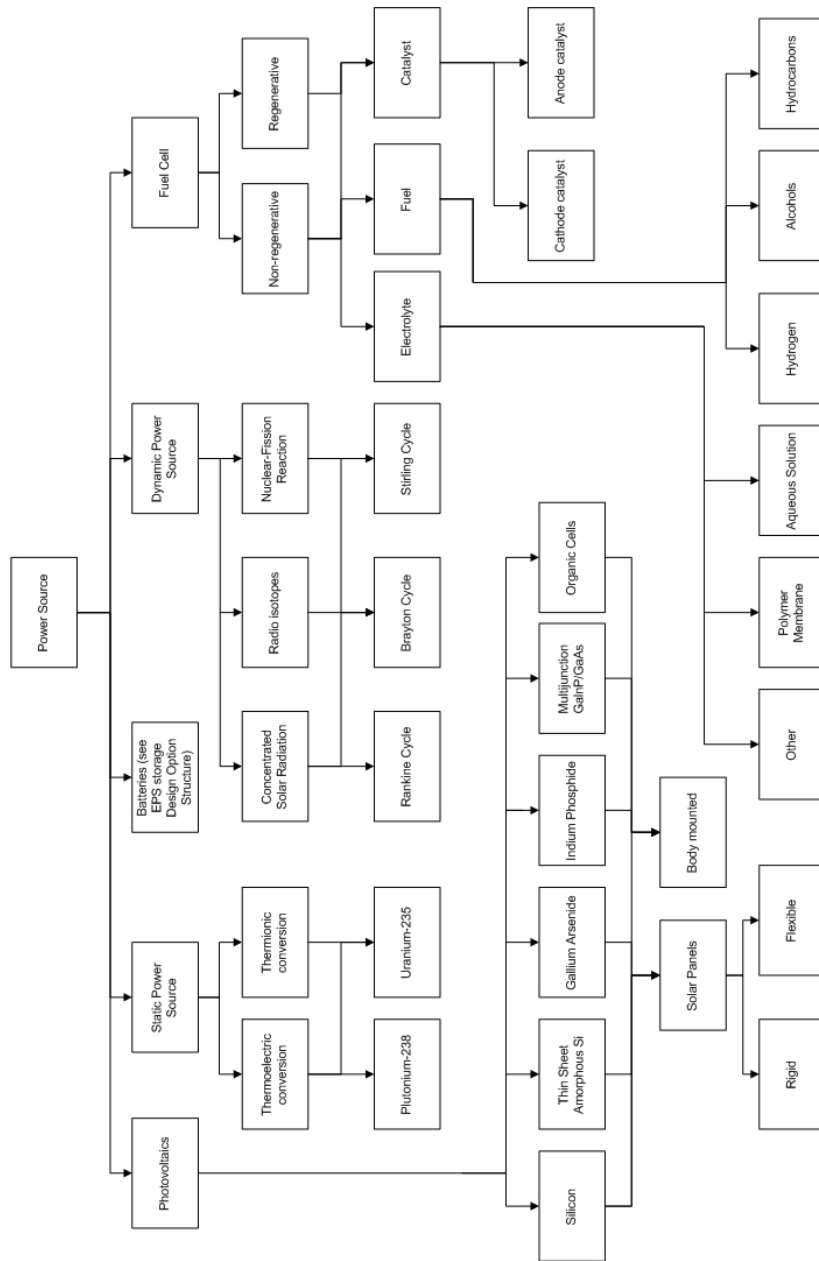


Figure A.3: Design option tree for the power source

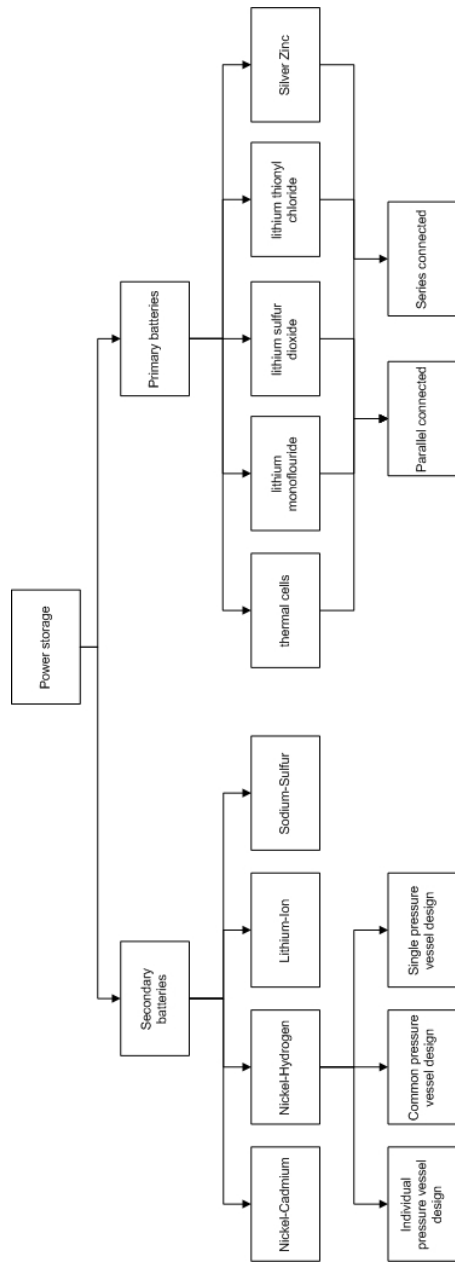


Figure A.4: Design option tree for the power storage

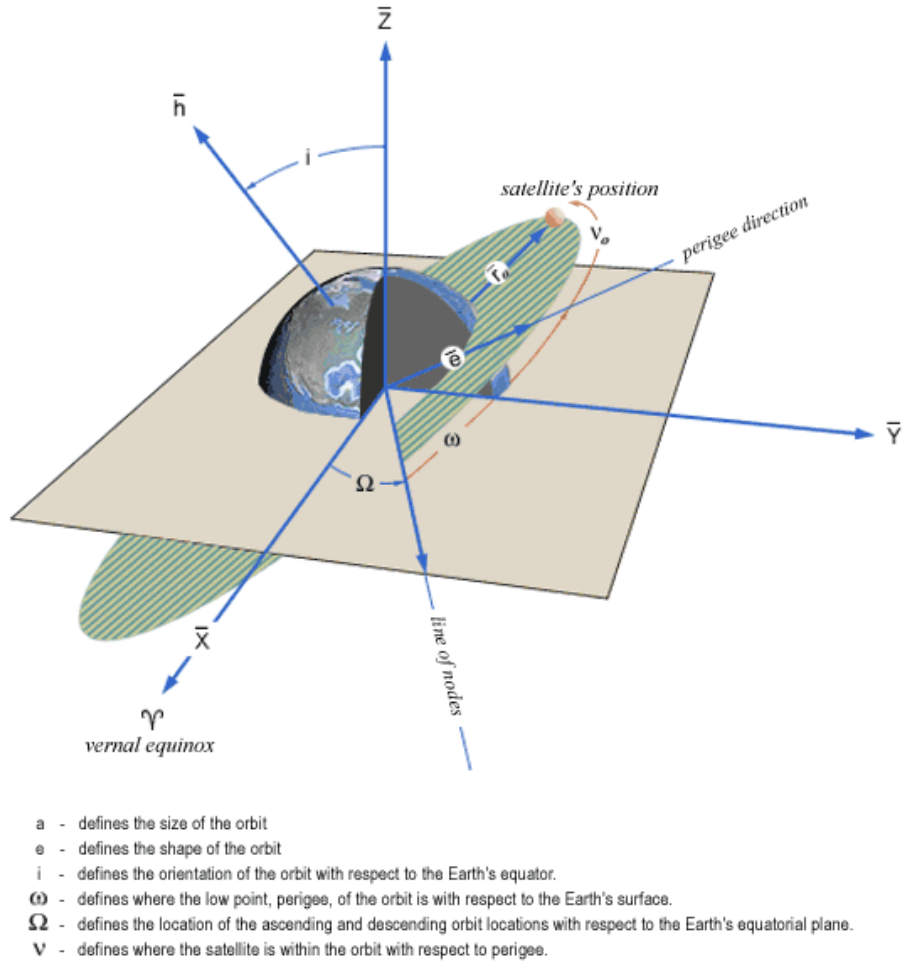


Figure A.5: Definitions of the inclination i , the right ascension of the ascending node Ω , the argument of perigee ω and the true anomaly ν . source: <http://reentrynews.aero.org>

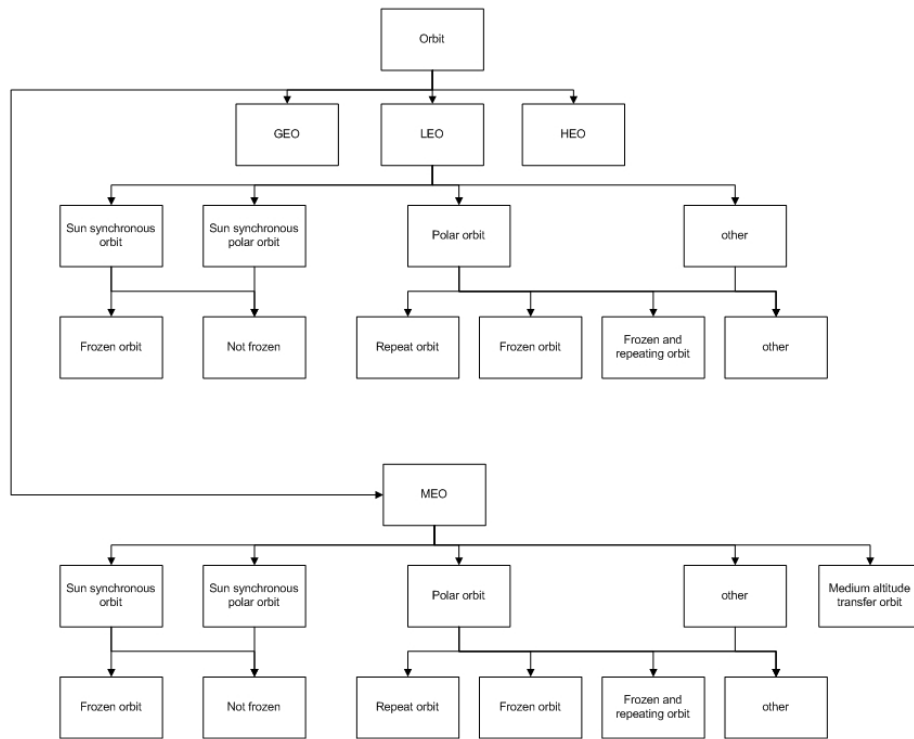


Figure A.6: Design option tree for the orbit architecture of LEO and MEO

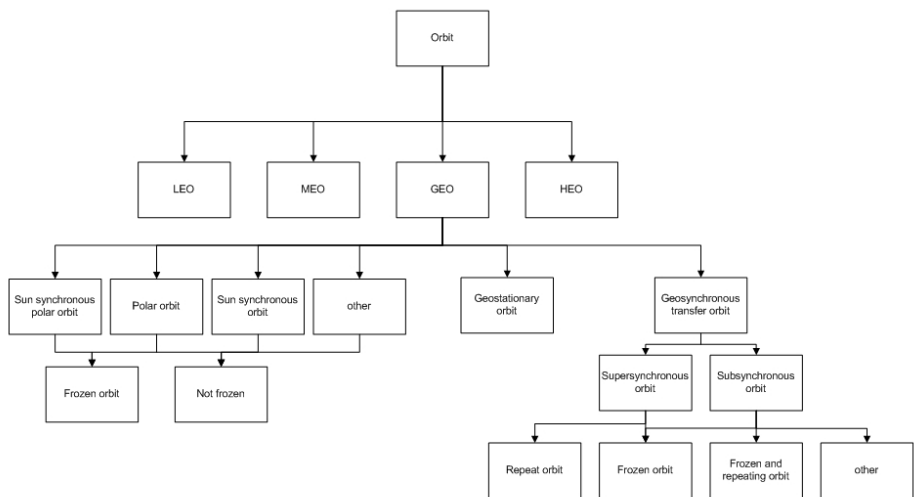


Figure A.7: Design option tree for the orbit architecture of GEO

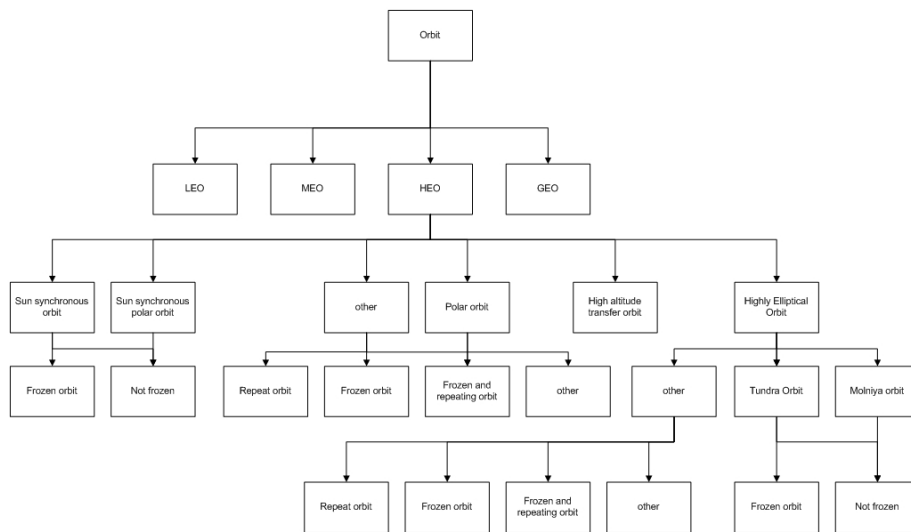


Figure A.8: Design option tree for the orbit architecture of HEO

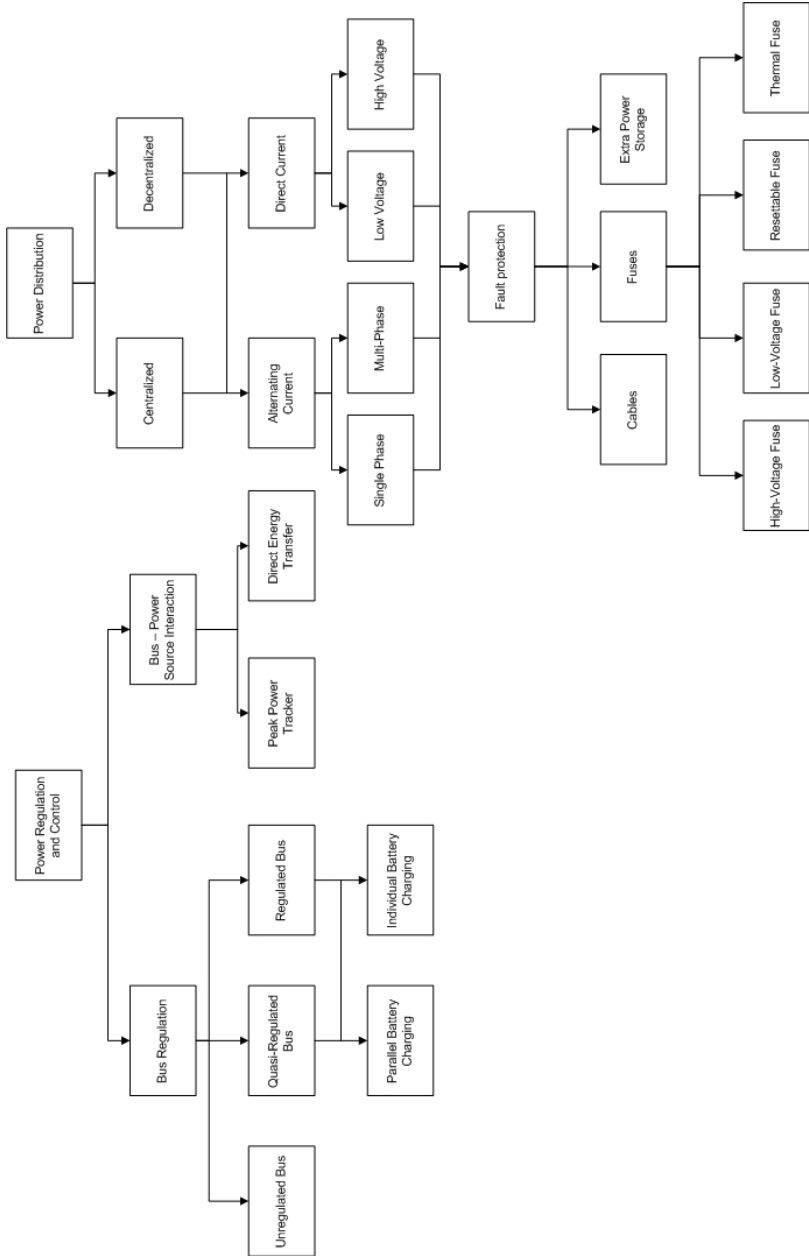
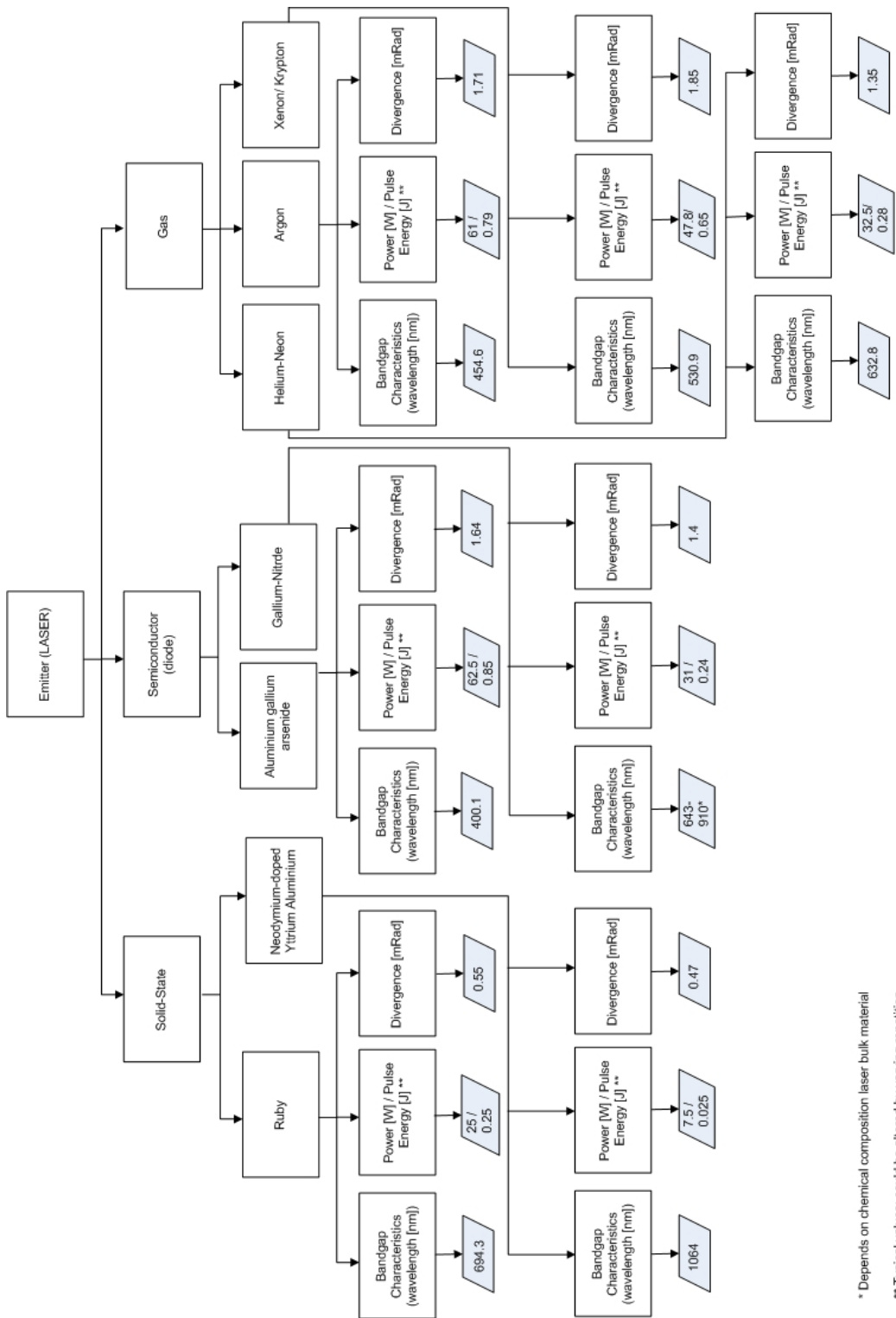


Figure A.9: Design option tree for the distribution and regulation and control of the EPS



* Depends on chemical composition laser bulk material

** Typical values; could be altered by varying repetition rate, external electron excitation or input power variation

Figure A.10: Design option tree of laser emitter. Numbers indicate typical values.

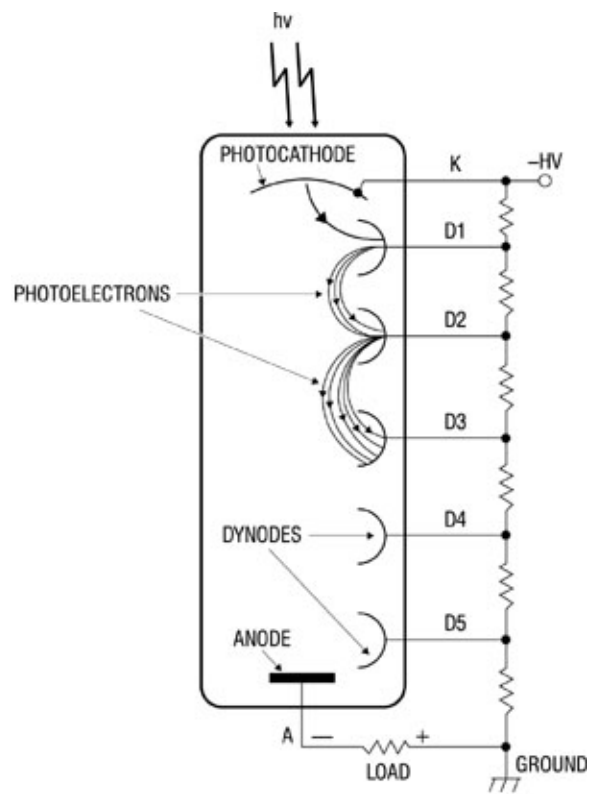


Figure A.11: Photomultiplier tube configuration and working mechanism

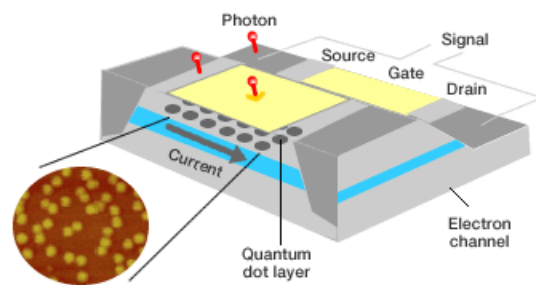


Figure A.12: Single photon detection using quantum dot configuration

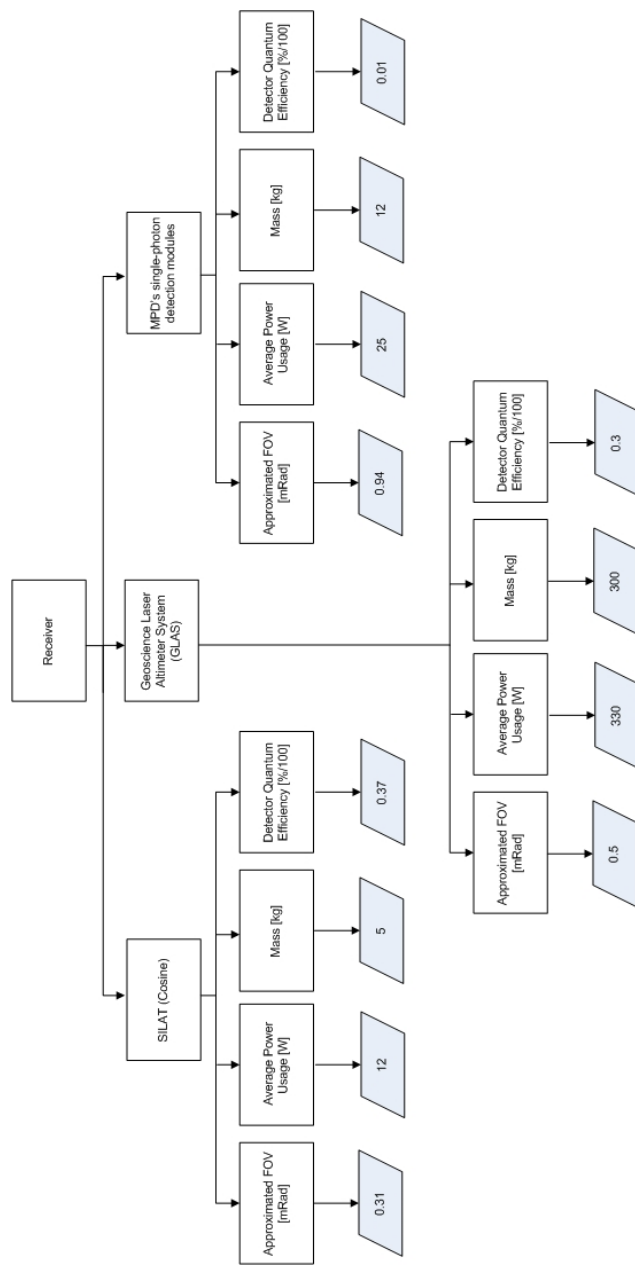


Figure A.13: Design option tree for laser receiver. Numbers represent typical values.

Appendix B

Subsystem Budget Overview

	ADCS	Communications	ORP	OEP	EPS	Optics	Structural & Thermal	Total
power [W] E:	8.0	45.4	0.0	100.0	50.0	0.0	0.0	203
R:	4.0	2.0	0.1	0.0	1.0	0.0	0.0	7
mass [kg] E:	15.0	21.0	0.0	45.0	10.0	0.1	27.3	118
R:	5.0	1.1	0.1	0.0	1.0	1.0	2.5	11
volume [m^3] E:	0.002	0.300	0.000	0.015	0.000	0.001	0.000	
R:	0.027	0.000	0.000	0.000	0.000	0.010	0.000	
h x w x l [cm] E:	50x30x30	30.5x33x7.4	-	100x15x10	$2m^2$	20x5x5	0	Frontal Area [m^2] 2.5
R:	8x8x10	-	2x2x1	-	$0.2m^2$	20x20x40	0	0.24

Appendix C

Gantt Chart